

**KINEMATICS OF THE ANTERIOR CRUCIATE LIGAMENT (ACL) AND ACL
GRAFT**

by

Junjun Zhu

B.S., Mechanical Engineering, Shanghai Jiao Tong University, 2010

M.S., Mechanical Engineering, Carnegie Mellon University, 2012

Submitted to the Graduate Faculty of
the Swanson School of Engineering in partial fulfillment
of the requirements for the degree of
Doctor of Philosophy

University of Pittsburgh

2018

UNIVERSITY OF PITTSBURGH
SWANSON SCHOOL OF ENGINEERING

This dissertation was presented

by

Junjun Zhu

It was defended on

December 11, 2017

and approved by

Mark C. Miller, Ph.D., Associate Professor, Department of Bioengineering

William S. Slaughter, Ph.D., Associate Professor, Department of Mechanical Engineering

Qing-Ming Wang, Ph.D., Professor, Department of Mechanical Engineering

Dissertation Director: Patrick Smolinski, Ph.D., Associate Professor, Department of

Mechanical Engineering

Copyright © by Junjun Zhu

2018

KINEMATICS OF THE ANTERIOR CRUCIATE LIGAMENT (ACL) AND ACL GRAFT

Junjun Zhu, Ph.D.

University of Pittsburgh, 2018

The anterior cruciate ligament (ACL) is one of the four main ligaments of the knee and is the most important ligament for knee's stability. ACL injury has an annual incidence of more than 200,000 cases with approximately 100,000 of these knees having ACL reconstruction annually in the United States alone. However, the behaviors of the ACL and the graft in knees were still debated. There is still no golden standard in choosing appropriate reconstruction techniques, such as the position and orientation of the graft. Tunnel enlargement and graft failure could happen after reconstruction if the ACL graft was improperly placed. To have better knowledge of the behavior of the intact ACL during flexion-extension and under external loads, this dissertation measured the strain of two bundles of the ACL by using two different measurement methods. This dissertation also measured graft position in femoral tunnel during knee motions and under different external loadings. This graft position information provides insight into ACL graft behavior and function and may be important for determining appropriate rehabilitation time. Last, a finite element (FE) model was constructed and used to simulate the graft behavior in reconstructed knees with boundary and loading conditions from corresponding cadaveric experiments. Geometry of the tibia and femur were obtained from CT imaging. An isotropic hyperelastic material was used to model the cylindrical graft. Three-dimensional joint kinematics were obtained via a six-degree-of-freedom robotic manipulator and were used for input into the

computational model. Graft stress, tension as well as the location of the graft in the tunnel were calculated after the kinematics were applied.

TABLE OF CONTENTS

PREFACE.....	XVI
1.0 INTRODUCTION	1
1.1 THE ANTERIOR CRUCIATE LIGAMENT (ACL) AND ACL INJURY	1
1.2 ANATOMY AND BIOMECHANICS.....	2
1.3 TREATMENT AND ACL RECONSTRUCTION	6
2.0 FINITE ELEMENT MODELING OF ACL.....	11
3.0 OBJECTIVE AND SPECIFIC AIMS.....	19
3.1 SPECIFIC AIM 1: MEASURE STRAINS IN ANTEROMEDIAL AND POSTEROLATERAL BUNDLES OF THE ACL UNDER DIFFERENT KNEE LOADING CONDITIONS.....	20
3.2 SPECIFIC AIM 2: MEASURE ACL GRAFT POSITION IN TUNNEL UNDER VARIOUS KNEE MOTIONS AND LOADINGS	21
3.3 SPECIFIC AIM 3: DEVELOP A FINITE ELEMENT MODEL OF THE GRAFT AND TUNNEL FOR SINGLE BUNDLE ACL RECONSTRUCTION	21
3.4 SUMMARY.....	22
4.0 DETERMINE STRAINS IN AM AND PL BUNDLES UNDER DIFFERENT LOADING CONDITIONS.....	24
4.1 BACKGROUND AND SIGNIFICANCE.....	24
4.2 METHODS	27
4.2.1 Specimen preparation and Robotic testing	27
4.2.2 Strain measurement and analysis.....	29

4.2.2.1	Digital Image Correlation (DIC) Measurement	29
4.2.2.2	Measurement of Strain with Markers.....	34
4.3	RESULTS AND DISCUSSION.....	37
4.3.1	Kinematics and In-Situ Force	37
4.3.2	Strain in AM and PL Bundles with DIC.....	40
4.3.2.1	Strain during knee flexion.....	41
4.3.2.2	Strain Under Anterior Tibial (AT) load	46
4.3.2.3	Strain Under Internal Rotational (IR) load	49
4.3.2.4	Strain Under External Rotational (ER) load	49
4.3.2.5	Strain Under Valgus Rotational (VAL) load	50
4.3.3	Strain in AM and PL Bundles with Markers	52
4.4	CONCLUSION.....	59
5.0	MEASUREMENT OF ACL GRAFT POSITION IN TUNNEL UNDER VARIOUS KNEE MOTIONS AND LOADINGS.....	61
5.1	BACKGROUND AND SIGNIFICANCE.....	61
5.2	METHODS	63
5.2.1	Specimen Preparation	64
5.2.2	Robotic Testing.....	65
5.2.3	Geometric Scanning and Analysis.....	66
5.3	RESULTS AND DISCUSSION.....	70
5.3.1	Kinematics and In-Situ Force	71
5.3.2	Shift of the graft during flexion/extension and under external loadings	76
5.3.3	Percentage of tunnel area at the aperture filled by the graft	83
5.3.4	Percentage of tunnel boundary at the aperture in contact with the graft	86

5.3.5	Angular Position of contact area during flexion/extension and under external loadings	88
5.4	CONCLUSION.....	91
6.0	FINITE ELEMENT MODEL OF THE GRAFT AND TUNNEL FOR SINGLE BUNDLE ACL RECONSTRUCTION	93
6.1	BACKGROUND AND SIGNIFICANCE.....	94
6.2	METHODS	95
6.2.1	Constitutive model of the ACL graft.....	96
6.2.2	Transformations between the local coordinate system and global coordinate system	97
6.2.3	Geometry	100
6.2.4	Boundary and initial conditions.....	102
6.2.4.1	Analysis 1: Application of initial graft tension.....	103
6.2.4.2	Analysis 2: Application of Tibial Displacement.....	104
6.2.5	Model and experimental comparison of results.....	106
6.3	RESULTS AND DISCUSSION.....	107
6.3.1	Graft Position.....	107
6.3.2	Graft-Tunnel Contact Position.....	114
6.3.3	Graft force.....	116
6.3.4	Frictional Coefficient.....	119
6.3.5	Mesh Sensitivity Analysis	122
6.3.6	Graft Initial Tension	125
6.3.7	Tunnel to Tunnel Distance	128
6.4	CONCLUSION.....	131
7.0	SUMMARY.....	133

APPENDIX A.....	135
APPENDIX B.....	138
BIBLIOGRAPHY.....	144

LIST OF TABLES

<i>Table 1. Previous studies on ACL material property & model.....</i>	<i>15</i>
<i>Table 2. Previous studies on finite element modeling of ACL.....</i>	<i>17</i>
<i>Table 3: Tibia displacement and rotation under external loads</i>	<i>38</i>
<i>Table 4: ACL in-situ force under external loads</i>	<i>38</i>
<i>Table 5: Longitudinal strain of AM bundle under external loads, calculated from DIC and laser scanning measurement (Sample F170840R)</i>	<i>58</i>
<i>Table 6: Tibia displacement and rotation under external loads in intact, ACL deficient and ACL reconstructed knee (* indicates statistically significance compared to intact states).....</i>	<i>72</i>
<i>Table 7: In-situ force in intact ACL and graft under external loads</i>	<i>73</i>
<i>Table 8: Magnitude of graft shift with mean \pm standard deviation for each external loading condition and flexion/extension (F/E).....</i>	<i>77</i>
<i>Table 9: Percentage of femoral tunnel outline contact with graft for each external loading condition and flexion/extension (F/E).....</i>	<i>87</i>
<i>Table 10: Angular position change of graft in femoral tunnel for each external loading condition and flexion/extension (F/E).....</i>	<i>90</i>
<i>Table 11: Correlation coefficient between tunnel to tunnel distance and graft end constraint force as well as the maximum von-Mises stress with different initial tension and frictional coefficient.....</i>	<i>129</i>

LIST OF FIGURES

Figure 1: Anatomy of human knee (www.Medicinenet.com)	1
Figure 2: Anterior view of a left knee depicting the anteromedial (AM) bundle and posterolateral (PM) bundle of the ACL (Ziegler et al.)	4
Figure 3: Mean length change patterns for the three ACL bundles during flexion in neutral rotation. AMB anteromedial bundle, IB intermediate bundle, and PLB posterolateral bundle (Amis and Dawkins, 1991)	5
Figure 4: double-bundle(DB) and single-bundle(SB) ACL reconstruction (www.arthrex.com) 10	
Figure 5: A typical stress-strain plot of uniaxial loading of ACL along the fiber direction (Robi, 2013)	12
Figure 6: Schematic of proposed methodology	19
Figure 7: Flowchart of testing and DIC strain measurement.....	30
Figure 8: Dissected and prepared sample with random speckle pattern.....	31
Figure 9: The placement of cameras for measuring the strain of AM and PL bundles on a representative right knee model and the cameras calibration.	32
Figure 10: a) Camera setup and robotic testing with femur fixed to the base and tibia connected to the robot; b) Image of sample from reference camera; c) longitudinal strain distribution in the ACL with camera coordinate system; d) defining local coordinate system based on orientation of bundles; e) longitudinal stain based on new coordinate system	34
Figure 11: Flowchart of ACL strain measurement with markers and laser scanning.....	35
Figure 12: a). Dissected knee with beads on ACL; b). Laser scan of the ACL with beads; c) highlighted bead in front and side view; d) element determined by three marker centroids.....	36
Figure 13: Average anterior tibial translation (ATT) under 89 N anterior tibial load (n=6)	39

Figure 14: Average rotation angles under external rotational load (n=6).....	39
Figure 15: Average in-situ force (n=6) of the ACL under external loads	40
Figure 16: a) images of six intact ACL samples from reference camera; b) longitudinal strain distribution in the six ACLs with anatomical coordinate system	41
Figure 17: Longitudinal strain (mean±sd) of AM and PL bundles during flexion using DIC measurement	43
Figure 18: Transverse strain (mean±sd) of AM and PL bundles during flexion	44
Figure 19: Shear strain (mean±sd) of AM and PL bundle during flexion extension.....	46
Figure 20: Longitudinal strain of the AM and PL bundles under anterior tibial load	47
Figure 21: Transverse strain of AM and PL bundle under anterior knee load	48
Figure 22: Shear strain of AM and PL bundle under anterior tibial loading	48
Figure 23: Strain of AM and PL bundle under internal torque.....	49
Figure 24: Strain of AM and PL bundle under external rotation torque.....	50
Figure 25: Strain of AM and PL bundle under valgus rotation torque	51
Figure 26: Strain of a) AM and b) PL bundle under anterior tibial load calculated from and scanning comparing to the DIC measurement results.....	54
Figure 27: Strain of AM and PL bundle under internal rotation load, calculated from markers and scanning	55
Figure 28: Strain of AM and PL bundle under external rotation loads, calculated from markers and scanning.....	55
Figure 29: Strain of AM and PL bundle under valgus rotation loads, calculated from markers and scanning	56
Figure 30: Flowchart of studying graft position in tunnel under various knee motions and loadings.....	64
Figure 31: (a) Dissected femur with single-bundle ACL reconstruction; (b) Scan of the sample with ACL graft; (c) Femur geometry from CT scan; (d) Scan of the sample with ACL graft removed and (e) Combination of two scans	67

Figure 32: a) Scan of the lateral condyle and the fitted femoral tunnel; b) Standardized plane that is perpendicular to the femoral tunnel.	68
Figure 33: Left: The intercept curve between the femoral tunnel cylinder and the trimmed surface was defined as the outline of the graft at the aperture; Right: Outline of the graft at the standardized plane of the femoral tunnel with (yellow) and without (red) AT load.	69
Figure 34: Graft centroid position change, percentage of the femoral tunnel been filled by the graft, percentage of contact region and the rotation of the contact region (vertical axis: superior direction based on femur).	70
Figure 35: Tibia displacement and rotation of specimens with intact knee, ACL deficient knee and ACL reconstructed knee under: A) anterior tibial translation, B) posterior tibial translation, C) internal rotation, D) external rotation and E) valgus rotation.....	74
Figure 36: In-situ force in intact ACL and graft under: A) anterior tibial translation, B) posterior tibial translation, C) internal rotation, D) external rotation and E) valgus rotation0.....	75
Figure 37: Magnitude of graft shift in femoral tunnel under passive flexion and external loading.	76
Figure 38: Change in graft centroid position under anterior tibial loading (89 N) and flexion extension.	78
Figure 39: Graft shift under external rotational torque (5 Nm) and flexion extension.....	79
Figure 40: Graft shift under internal rotational torque (5 Nm) and flexion extension.	80
Figure 41: Graft position shift under posterior tibial load (89 N) and flexion-extension.....	81
Figure 42: Graft position under valgus load (7 Nm) and flexion extension.	82
Figure 43: Percentage of femoral tunnel aperture filled by graft under external loadings and knee flexion	84
Figure 44: Femoral tunnel filled by graft under (a) knee flexion and (b) AT load (Sample 14_0900L).....	85
Figure 45: Percentage of graft contact area with external load and flexion/extension.....	86
Figure 46: Contact region angular location compared to neutral position at different under external loadings.	89
Figure 47: Contact region change in angular position as compared to the full extension position.	90

Figure 48: Percent graft-bone contact and mid-point angle during (a) passive flexion-extension and (b) under anterior tibial load.	91
Figure 49: Placement of registration screws and geometry of femur and tibia from CT scan	98
Figure 50: Local coordinate system (i' , j' , k') defined with respect to the global reference frame (i , j , k).....	99
Figure 51: femoral and tibia tunnel in the FE model	101
Figure 52: Geometry of graft represented by two portions determined by tibial and femoral tunnel and a third portion treated as a cylinder connecting the two portions	102
Figure 53: Two steps of analysis used in the finite element model.....	103
Figure 54: Boundary conditions used in analysis 1 for the calculation graft deformation due to initial tensioning.....	104
Figure 55: Boundary conditions used in analysis 2 for modeling the knee motion and external loads.....	106
Figure 56: Graft shift under anterior tibial (AT) load with respect to the position without external load at different knee flexion angles.....	108
Figure 57: Shift of graft center under posterior tibial (PT) load with respect to the position without external load at different knee flexion angles.....	109
Figure 58: Shift of graft center under internal rotation (IR) load with respect to the position without external load at different knee flexion angles.....	110
Figure 59: Shift of graft center under external rotation (ER) load with respect to the position without external load at different knee flexion angles.....	111
Figure 60: Shift of graft center under valgus rotation (VAL) load with respect to the position without external load at different knee flexion angles.....	112
Figure 61: Graft shift in flexion with respect to the position without external load at full extension	113
Figure 62: Graft-tunnel contact angular position change in the femoral tunnel based on left knee model during: (a) flexion; (b) anterior tibia (AT) load; (c) posterior tibia (AT) load; (d) internal rotational (IR) load; (e) external rotational (ER) load; (f) valgus rotational (VAL) load.....	115
Figure 63: Coordinate at the mid-section of the graft with z axis in the direction of the graft's long axis.....	117

Figure 64: Graft force during passive knee flexion from full extension (FE) to 90° knee flexion.	117
Figure 65: Graft force under external loads under different flexion angles	119
Figure 66: Graft force with two frictional coefficients (0.2 and 0.8) between graft and femoral tunnel.....	120
Figure 67: Maximum von-Mises stress in graft during knee flexion in the FE model with frictional coefficient 0.2 and 0.8.....	121
Figure 68: Location of maximum von-Mises stress in the ACL graft at 90° knee flexion.....	122
Figure 69: Two different sizes of elements were tested in this study: a) 100% (maximum edge lengths 2.7e-3m) and b) 85% edge lengths.....	123
Figure 70: Graft end constraint force during knee flexion for the model and with 85% element size	124
Figure 71: Maximum von-Mises stress in graft during knee flexion for the model and with 85% element size.....	124
Figure 72: Graft force during flexion with 40 and 60 N initial tension.....	125
Figure 73: Maximum von-Mises stress in the graft during flexion with 40 and 60 N initial tension	126
Figure 74: Calculated distance between femoral and tibial tunnel during flexion extension.....	129

PREFACE

First and foremost, I would like to thank my advisor, Dr. Patrick Smolinski, for his guidance and encouragement through these years. I am grateful for the opportunity you provided me to develop into a confident and resourceful researcher. Thank you for your faith in me; you have been an excellent mentor as well as friend.

I am deeply thankful to the members in my PhD thesis committee: Dr. Mark Miller, Dr. Qing-Ming Wang and Dr. William Slaughter for their interest in my research as well as their valuable time, energy, and helpful guidance and insightful suggestions towards refinement of the research work.

I would also like to thank the members of my research group for their overwhelming support and assistance in this work. The extensive help for experiment setup, data collection from Brandon Marshall cannot be separated from this research. I thankfully acknowledge contribution of Dr. Xin Tang and Dr. Weimin Zhu for their support with the surgical aspects of this study. I would also like to thank Monica Linde for her guidance and advice in all aspects of this research.

Finally, but most importantly, I would like to thank my family and friends for their continual support. I could not have done this without you and this degree is for all of us.

1.0 INTRODUCTION

1.1 THE ANTERIOR CRUCIATE LIGAMENT (ACL) AND ACL INJURY

The anterior cruciate ligament (ACL) is one of the four main ligaments of the knee (Figure 1). Its primary role is to prevent anteroposterior displacement of the tibia on the femur, with a secondary role of providing rotational stability. The ACL provides about 85% of the restraining force to anterior tibial displacement at 30 degrees and 90 degrees of knee flexion and is frequently subjected to high mechanical stress [41].

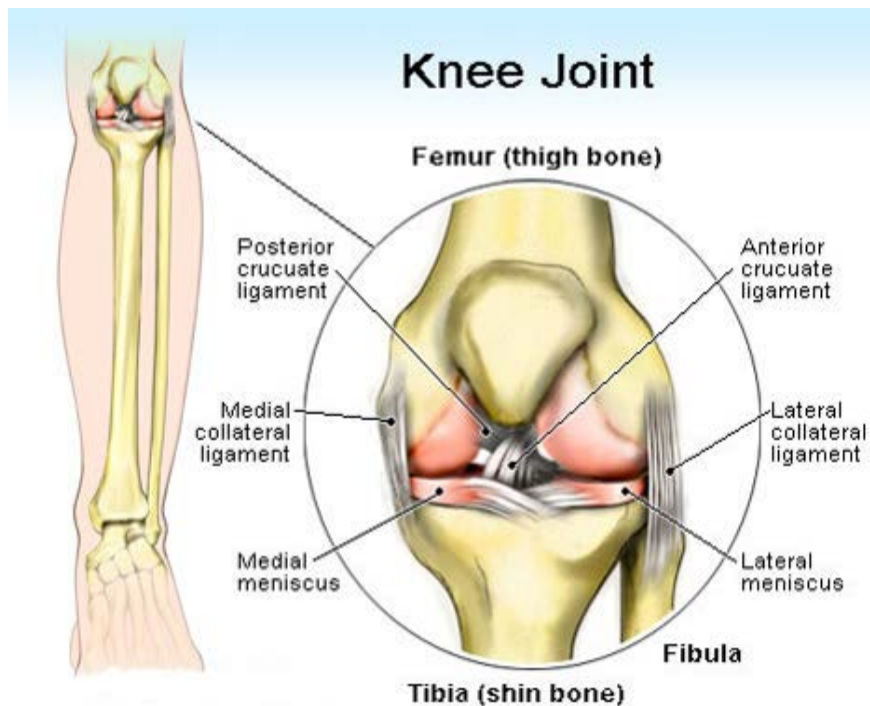


Figure 1: Anatomy of human knee (www.Medicinenet.com)

ACL injuries most commonly occur during sports that involve sudden stops, jumping or sharp changes in direction-such as basketball, soccer, football, tennis and skiing. Although many studies have been done by researchers, the mechanisms that lead to ACL injury and proper reconstruction techniques are still not clear. The incidence of ACL rupture in males and females are also different. A study by Arendt et al. showed significantly higher ACL injury rates in female players in collegiate basketball and soccer compared to male players. Non-contact mechanisms were the primary cause of ACL injury in both sports. Possible factors for the higher rate of ACL injuries among women may be extrinsic (body movement, muscular strength, shoe-surface interface, and skill level) or intrinsic (joint laxity, limb alignment, notch dimensions, and ligament size) [9]. While some studies have focused on finding risk factors of ACL injury and how to prevent ACL injury during activities, there are still between 100,000 and 200,000 ACL ruptures per year in the United States. Resulting national estimates of the incidence of ACL reconstruction vary between 60,000 and 175,000, with the annual cost of treatment is over two billion dollars [79].

1.2 ANATOMY AND BIOMECHANICS

The ACL mainly consists of a well-organized parallel bundles of collagen [191]. The ACL originates from the medial surface of the lateral femoral condyle posteriorly in the intercondylar notch and attached medially to the anterior intercondylar area of the tibia and partly blending with the anterior of the lateral meniscus. ACL ascends posterolaterally, twisting and fanning out to attach to the posteromedial aspect of the lateral femoral condyle (Figure 2). The length of the

ligament is about 31 to 38 mm and having an average width 10 to 12 mm [66, 127, 168]. Amis et al. divided the ACL into three functional bundles (anteromedial, intermediate, and posterolateral) and studied their contributions to resisting external loads in cadaver knees [6]. Changes in the bundles' length during flexion and extension were also measured (Figure 3). They found that the posterolateral bundle was stretched in extension while the anteromedial in flexion. Also, multiple studies suggested that the ACL can be divided into two functional and anatomic distinct bundles: the anteromedial (AM) and the posterolateral (PL) bundle (Figure 2) [195]. This classification is based on their tibial insertion sites, and this division can be achieved by the varying orientation and tensioning patterns of the fibers during knee range of motion [25]. The AM fibers originate on the most proximal part of the femoral origin and insert on the anteromedial aspect of the tibial insertion site. The PL fibers originate on the most distal aspect of the femoral origin and insert on the posterolateral aspect of the tibial insertion site [190].

The ACL is the main static stabilizer preventing anterior translation of the tibia on the femur and accounts for up to 86 % of the total force resisting anterior loading of the tibia. At different stages of knee flexion, distinct portions of ACL appear to act to stabilize the knee joint. The AM bundle becomes taut at 90 degrees of flexion, and PM bundle becomes tight at full extension[114]. The ACL also plays a lesser role in resisting internal and external tibial rotation. The ultimate load of the femur-ACL-tibia complex was found in Woo et al. study to be approximately 2160 ± 157 N when tested in its anatomical orientation, which is less than the maximum force that occurs in vigorous athletic activities[181]. Laboratory studies have determined load-elongation curve of a bone-ligament-bone complex by a uniaxial tensile test. The stress-strain relationship can also be obtained, from which the modulus, tensile strength,

ultimate strain and strain energy density can be measured to represent the mechanical properties of the tissue [99, 114].

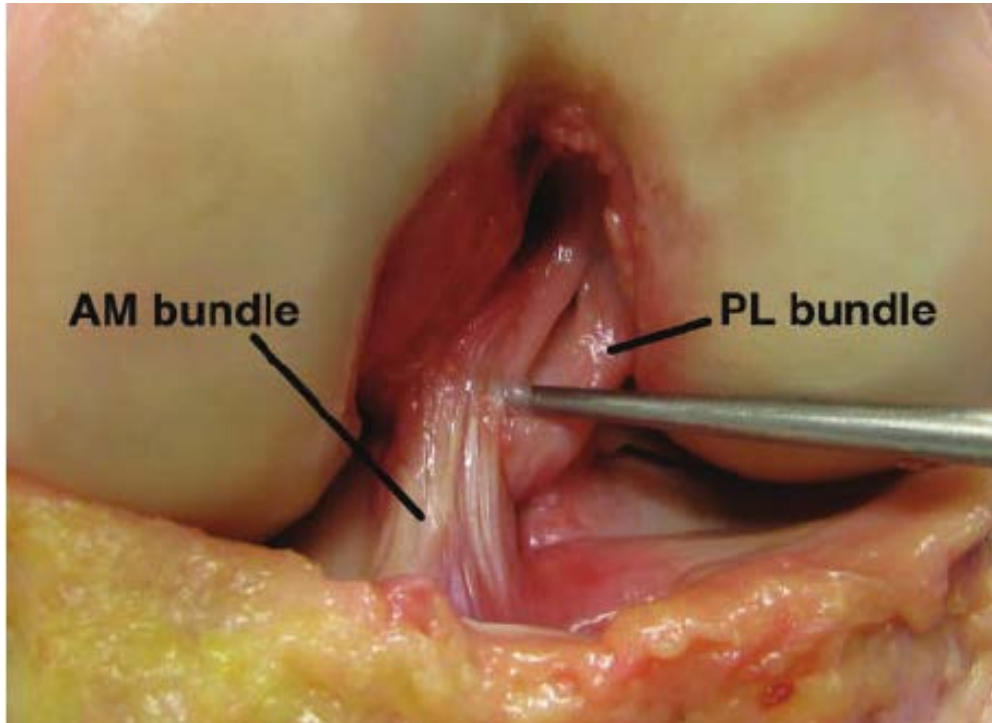


Figure 2: Anterior view of a left knee depicting the anteromedial (AM) bundle and posterolateral (PM) bundle of the ACL (Ziegler et al.)

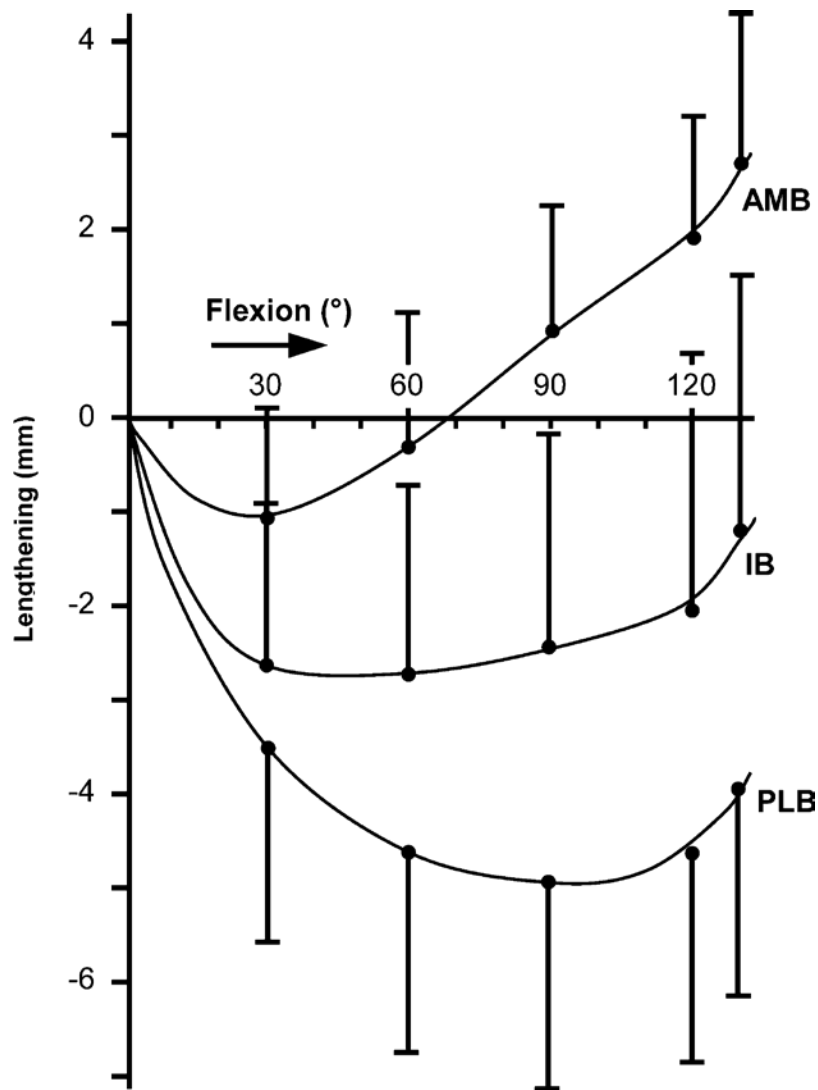


Figure 3: Mean length change patterns for the three ACL bundles during flexion in neutral rotation. AMB anteromedial bundle, IB intermediate bundle, and PLB posterolateral bundle (Amis and Dawkins, 1991)

1.3 TREATMENT AND ACL RECONSTRUCTION

Because the ACL is often permanent stretched during injury, the tissue usually cannot be repaired. Those who are not very active may choose non-operative treatment, such as strengthening program, since the injury is not likely to interfere with their daily activities. Active, athletic people are more likely to opt for surgery, so that the knee can be repaired and rehabilitated and they can return to their activities. To surgically repair the ACL and restore knee stability, the ligament must be reconstructed. Grafts choices, tunnel placement, initial tension, fixation angle are among those essential factors that need to be considered in surgery. During the past forty years, there has been an extensive evolution of the surgical procedures for repair or reconstruction of the ACL. The ultimate aim of an ACL reconstruction is to restore the function of the intact ACL. In the 1970s, a trend towards repairing ACL was started by surgeons who thought the ACL performed an important function. Repair of the ACL with augmentation using autografts was altered in the 1970s and early 1980s by completely replacing the torn ligament with autografts and occasionally allografts [35, 129]. In 1990s, transtibial technique was suggested, which is non-anatomic, but quick technique. With this method the femoral tunnel drilled with offset guide through the tibial tunnel. Some researchers found that the non-anatomic transtibial techniques resulted in high percentage of osteoarthritis(OA)[22, 56, 167]. Numerous experiments and numerical studies have been done and there are several surgical variables in ACL reconstruction that relate to the result. Among them, reconstruction technique (double-bundle or single-bundle technique), graft choice, initial tension and tunnel placement are thought to be the most critical surgical variables.

The complex anatomy and the biomechanical function of the ACL have been well described by numerous authors. When trying to restore the intact ACL function, there are two

classifications of ACL reconstruction in general: single bundle reconstruction (SB), where the torn or injured ACL is replaced by a single graft, and double bundle (DB) ACL reconstruction, where the torn or injured ACL is replaced by two grafts (Figure 4). However, there is still controversial about which technique better restores intact ACL behavior. Until recently, SB ACL reconstruction was the primary method used by surgeons. However, some biomechanical studies have shown that SB reconstruction can effectively restore the anterior laxity associated with a deficient ACL, but is ineffective in restoring rotational laxity associated with a combined rotary load of internal and valgus torque [30]. Double-bundle (DB) ACL reconstruction replaces the two functional bundles of the ACL with two grafts. It is believed that the addition of a second graft mimics the behavior of the more posterior and lateral PL bundle of the native ACL, thereby increasing rotational stability [183]. Woo et al. believed that some of the failures after ACL reconstruction occurred because single bundle ACL reconstruction was insufficient to control combined internal and valgus torques applied to the knee [180]. Several investigators have reported improved ability to restore knee function after double bundle ACL reconstruction technique was used [6, 112, 119, 155, 186]. Despite these findings, Radford et al. in their study concluded that two femoral attachment sites were not superior to a single site in a sheep model of ACL reconstruction, probably because of the more complex surgery [146]. Likewise, Hamada et al, comparing two case series, found no evidence that using a bi-socket ACL reconstruction in humans improved results compared with a single-socket technique[68]. Adachi and colleagues also found no evidence that a two tunnel hamstring autograft better restored normal knee laxity than a single-tunnel procedure [1].

The ideal graft should reproduce the complex anatomy of the native ACL, provide the same biomechanical properties of the native ACL, permit secure fixation, promote rapid biologic

incorporation to allow for accelerated rehabilitation, and minimize donor site morbidity. Although many different types of grafts, both autogenous and allogenic, have allowed athletes to return to their sport, no single graft choice meets all of the above criteria [60, 126, 163]. Commonly used autogenous grafts include bone-patella-tendon-bone (BPTB), quadrupled hamstring tendon and quadriceps tendon with or without bone. Allograft options include BPTB, hamstring tendon, Achilles tendon, and anterior or posterior tibialis tendon. The advantages of using a BPTB graft are lower rate of graft failure, sufficient strength, a natural tissue insertion to the bone and the bone plug to bone tunnel fixation. A disadvantage is donor site morbidity. Advantages of a hamstring graft includes adequate strength and little donor site morbidity. But higher rate of graft failure and increased knee laxity come are disadvantages [53, 59, 65]. Autogenous tissue for ACL reconstruction has been associated with knee pain, decreased range of motion and weakness [12, 59]. It also leads to longer recovery and rehabilitation time. Allograft concerns include risk of disease transmission, bacterial infection, and the possibility of immunogenic response by the host [40]. There are also concerns with altering graft mechanical properties by sterilization and storage procedures. The advantage of an allograft is decreased operative time, lower incidence of arthrofibrosis and preservation of extensor or flexor mechanisms [15, 74, 175]. Both autograft and allograft techniques have successful short-term results, but five-year follow-ups yield instability and pain [52].

Most surgeons would agree that the initial tension applied to an ACL graft at the time of fixation has a direct effect on outcome [5, 61, 69, 85, 116, 189]. An under-tensioned graft may result in abnormal knee laxity and an unstable knee, and an over-tensioned graft may lead to graft failure, fixation failure, or a restricted range of knee motion. Graft tensioning at the time of fixation involves consideration of the knee's flexion angle during tensioning and the magnitude

of tension applied to the graft. Both variables interact and have a direct effect on knee biomechanics.

Tunnel placement could also affect ACL surgical outcome. Misplacement of the tunnels, which is not precisely defined, can result in decreased range of knee motion or increased anterior tibial translations (ATT) and knee instability[5]. However, the best tunnel placement still remains controversial [21, 100, 120, 192]. The ACL has a complex, 3-dimensional attachment to bone. The femoral insertion of the ACL does not insert on a flat area that is aligned to an anatomical plane, instead, it is located on a curved surface, with the wall of the femoral notch becoming the roof of the femoral notch. In addition, the tissue fans out at the insertion sites. Femoral tunnel widening, an increase in the tunnel size after reconstruction, is a complication of ACL reconstruction [3, 50, 83, 176]. Mechanical explanations for the widening include the “windshield wiper” effect as the graft moves along the tunnel edge during knee motion [101]. Also, in ACL reconstruction with a soft tissue graft, a space is frequently observed between the posterior aspect of the femoral tunnel wall and the placed graft at the tunnel. This may be attributable to a size difference between the graft and the tunnel and graft deformity. Nonetheless, a correlation between tunnel widening and any single factor has not been demonstrated. Studies suggest that even though the femoral tunnel center is positioned in the center of the ACL footprint, the centroid of the graft may be deviated from the footprint center due to graft deformation and graft shift [121, 124, 162]. However, no biomechanical study has described the graft shift phenomenon.

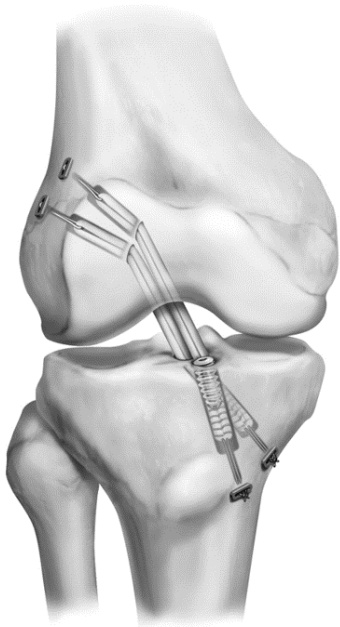


Figure 4: double-bundle(DB) and single-bundle(SB) ACL reconstruction (www.arthrex.com)

2.0 FINITE ELEMENT MODELING OF ACL

The finite element (FE) method has been widely used in the field of biomechanics as it allows for detailed analysis of the joint and tissue behavior under complex, clinically relevant loading conditions. There are a few essential components in finite element model analysis, which remain the same through all problems: model geometries, material properties, initial, boundary, and loading conditions. Models of the ACL can include complicated three-dimensional geometry, nonlinear and/or inhomogeneous material properties, and complex initial, boundary and loading conditions. The FE method has been a tool for analyzing the stress and strains outcomes of ACL related reconstructions [10, 13, 18, 48, 91, 107, 135, 149]. A number of items must be considered to apply the FE method correctly in the modeling of ACL.

Three-dimensional continuum models have been developed to represent the material behavior and the role of ligaments through constitutive equations. Constitutive equations are used to describe the stress-strain behavior of materials through specification of the dependence of stress on variables, such as the deformation. Applications range from very simple (e.g. linear beams and springs) to complex models (e.g., anisotropic hyperelastic 3D materials, or biphasic formulations). The accurate description of the three-dimensional mechanical behavior of ligaments remains a challenge. Researchers have tried to describe the stress-strain response of ACL by experimental tests and mathematically developing material models that fit the experimental data [26, 64, 75, 142, 143, 177]. A typical stress-strain plot of uniaxial loading of

ACL along the long axis is shown in Figure 5 [153]. The stress-strain curve for ligaments possesses a toe region for uniaxial loading. One theory to explain the toe region is the sequential recruitment of collagen fibers. As the ligament is stretched, additional fibers are recruited to bear load and when a critical stretch is reached all fibers are recruited and the stress-strain behavior becomes linear [38].

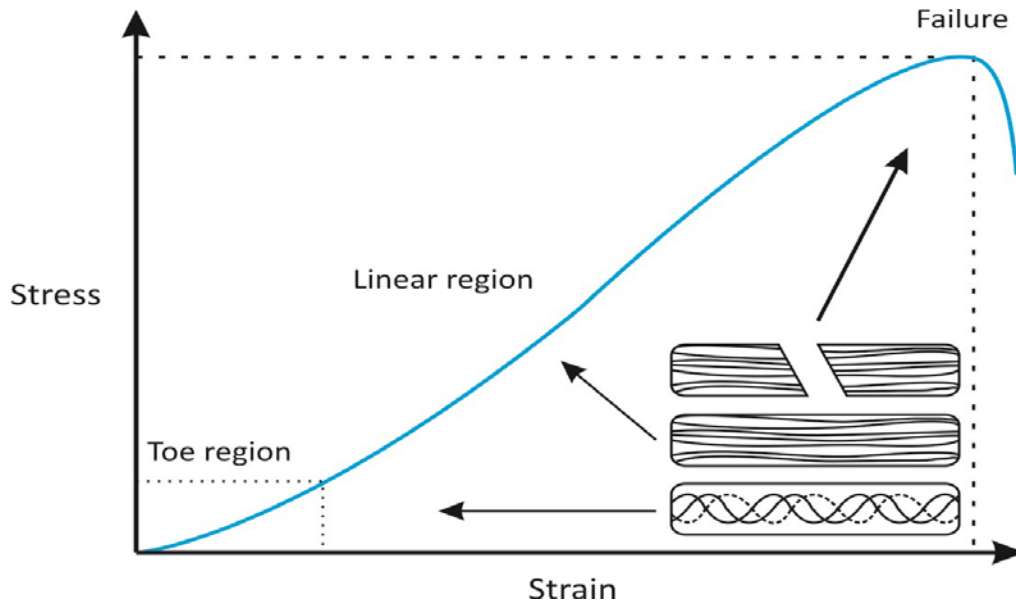


Figure 5: A typical stress-strain plot of uniaxial loading of ACL along the fiber direction (Robi, 2013)

Table 1 gives a list of studies that focused on characterizing the ACL material properties and developing models. Butler et.al [26] measured the ACL axial surface stain and described the stress and strain response. They first proposed an equation for describing the nonlinear stress-strain curve of the ACL. Weiss et. al [177] mathematically developed an ACL model by assuming the ACL as a incompressible, isotropic and hyperplastic material. Based on previous work, Pioletti and coworkers [142–144] developed a hyper-elastic, incompressible, and

viscoelastic isotropic law. In this formulation, the elastic part is based on the isotropic Veronda–Westmann [174] material law and the novelty is mainly the viscous behavior. Veronda proposed an elastic potential that fits the non-linear elastic stress-strain curve of the ACL.

$$W_e = \alpha \exp[\beta(I_1 - 3)] + C_1(I_2 - 3) \quad 2-1$$

α , β and C_1 are elastic parameters. I_1, I_2 are the invariants of the right Cauchy-Green strain tensor.

Another constitutive model which is more complex but more realistic in describing ACL and graft behavior, is also widely used [75, 134]. It describes an incompressible, fiber-reinforced material able to simulate large displacements. This material model was designed to fit the response of the biological soft tissues, especially ligaments, based on experimental data. The ground substance matrix of the tissue is modelled with neo-Hookean material which is incompressible isotropic hyperelastic. With this model, the strain energy is expressed as

$$\Psi_m = C_1(I_1 - 3) \quad 2-2$$

and the stress-stretch curve of pseudo fibers is given by:

$$\sigma = \begin{cases} 0 & \text{if } \lambda < 1 \\ C_2(e^{C_3(\lambda-1)} - 1) & \text{if } 1 \leq \lambda < \lambda^* \\ C_4\lambda + C_5 & \text{if } \lambda^* \leq \lambda \end{cases} \quad 2-3$$

$$C_5 = C_2(e^{C_3(\lambda^*-1)} - 1) - C_4\lambda^* \quad 2-4$$

where λ is the stretch along the fiber direction, and C_1 through C_5 and λ^* are material constants, which are to be determined through material testing [27, 151, 181].

The Holzapfel–Gasser–Ogden (HGO) model [64, 78] was initially developed to describe the elastic properties of arterial tissue, but is now used for modelling a variety of anisotropic hyper-elastic fiber reinforced materials. When the incompressibility condition is adopted the

strain energy Ψ of the HGO model is a function of one isotropic and two anisotropic deformation invariants:

$$\bar{\Psi}(\bar{\mathbf{C}}, \mathbf{a}_{01}, \mathbf{a}_{02}) = \bar{\Psi}_{iso}(\bar{\mathbf{C}}) + \bar{\Psi}_{aniso}(\bar{\mathbf{C}}, \mathbf{a}_{01}, \mathbf{a}_{02}) \quad 2-5$$

$$\bar{\Psi}_{iso}(\bar{\mathbf{C}}) = \frac{c}{2}(I_1 - 3) \quad 2-6$$

$$\bar{\Psi}_{aniso}(I_4, I_6) = \frac{k_1}{2k_2} \sum_{i=4,6} \{\exp[k_2(I_i - 1)^2] - 1\} \quad 2-7$$

where $c, k_1, k_2 > 0$ are material parameters, I_1 through I_6 are invariants, defined by

$I_1 = tr \mathbf{C}$, $I_4 = \mathbf{M}_4 \cdot (\mathbf{C}\mathbf{M}_4)$ and $I_6 = \mathbf{M}_6 \cdot (\mathbf{C}\mathbf{M}_6)$. where $\mathbf{C} = \mathbf{F}^T \mathbf{F}$ is the right Cauchy–Green tensor, where \mathbf{F} is the deformation gradient tensor, and $\mathbf{M}_4, \mathbf{M}_6$ are unit vectors pointing in the direction of the tissue's fibers before any deformation has taken place. This model provides the anisotropy property and “exponential-shaped” stress–strain curve common to many biological materials. However, as it is a phenomenological model, the parameters c, k_1 and k_2 cannot be directly linked to measurable quantities. These parameters are chosen to fit the experimental data and can be obtained by curve fitting to experimental data.

Table 1. Previous studies on ACL material property & model

Author (year)	Type	Material	Parameters
Butler (1990)	Experimental	ACL (1. measure axial surface strain 2. describe stress-strain response)	Yes
Weiss (1996)	Mathematical	Soft tissues (incompressible, isotropic hyperelasticity)	No
Pioletti (1997)	Experimental & mathematical	Ligament and tendon -isotropy, incompressible (Veronda and Westmann, 1970)	Yes
Pioletti (1998)	Experimental	ACL - (Veronda and Westmann, 1970)	Yes
Hirokawa (2000)	Mathematical	ACL: ground substance (Mooney-Rivlin material, Oden, 1972) + fibers	No
Gasser (2006)	Mathematical	Criss-crossed fibrous soft tissues (hyperelastic, anisotropic)	No

In the finite element study of the ACL, implementation of material models and properties has been performed for decades, a wide range of element types and material models has been used to represent knee ligaments, ranging from elastic one-dimensional elements [18, 105] to complex hyperelastic three-dimensional structures with anatomically realistic shapes [94, 136].

Table 2 shows a list of finite element modelling studies of the ACL including the sources of the ACL and bone geometry as well as the material model used.

Song et al. modelled the ACL as incompressible hyper-elastic homogeneous isotropic material [142] to calculate force and stress distribution within the AM and PL bundles [169]. The geometry of ACL was modelled as a cylinder that joined the insertion sites. Kinematics from robotic system with anterior tibial load of 134N was applied as the boundary conditions. Initial in situ strain of the AM and PL bundles was assumed to be 3%.

Limbert et.al [107] modelled the ACL as a neo-Hookean incompressible isotropic hyper-elastic ground matrix, plus a fiber reinforced composite. Both the geometry and applied kinematics were obtained by digital measurements. Simulations of passive knee flexion were performed with and without an initial stretch of 1.043, force and stress distribution within the ligament were then assessed.

In the Park et. al[134] study, the finite element method was implemented to assess ACL-bone impingement. The ligament surface was obtained by using a digitizing probe. The geometry of the femur and the tibia was measured by using a laser scanner (LPX-250, Roland Corp., rotary). In their model, the ACL was modeled as a composite structure consisting of pseudo fibers embedded in an isotropic hyperelastic incompressible neo-Hookean material matrix as described by Hirokawa [75]. Material parameters were determined by their previous material testing[151]. Displacement boundary conditions was measured tibiofemoral kinematics by tracking markers when the knee was manually flexed.

In the Bae et. al finite element study, contact pressures between graft and bone and maximum principal stresses in the grafts were calculated. The geometry of bone was taken from CT images. The graft was modeled as cylinder and considered as a hybrid hyperelastic material model with neo-Hookean ground matrix and graft collagen fiber data from literature [13]. An Initial tension of 44 N was applied to the graft to simulate the clinical process.

Table 2. Previous studies on finite element modeling of ACL

Author (year)	Geometry(Bone/Ligament)	ACL Property
Bendjaballah (1997)	CT	Nonlinear stress strain data from literature (Butler, 1986, Race,1994)
Pioletti (1998)	MRI	isotropy, incompressible, hyper-elastic (Veronda, 1970, Pioletti 1997)
Li (1999)	MRI	Stress strain data from (Blankevoort et al., 1991, Andriacchi et al., 1983; Butler et al, 1986; Wismans et al, 1980)
Song (2004)	MRI	Incompressible hyperelastic homogeneous and isotropic (Veronda and Westmann, 1970, Pioletti et al., 1998).
Limbirt (2004)	Laser scanner	incompressible isotropic hyperelastic potential -neo-Hookean fiber reinforced composites (Pioletti et al., 1997, Bates & Watts 1998.)
Ramaniraka (2005)	CT & MRI	nonlinear hyperelastic (Pioletti et al., 1998; Pioletti and Rakotomanana, 2000)
Pena (2006)	MRI	Graft tissue matrix -neo-Hookean (Weiss et al., 1996 and Pena et. al, 2005) +Graft collagen fiber (Butler et al. 1990)
Park (2010)	Laser scanner & digitizing probe	Isotropic hyperelastic ground substance matrix -neo-Hookean + Pseudo fibers (Weiss et al., 1996, Ren et al., 2010)
Kiapour (2014)	CT & MRI	anisotropic hyperelastic -Holzapfel-Gasser-Ogden (Gasser et al. 2006, Butler et al. 1990)
Bae (2015)	CT	neo-Hookean (Weiss et al., 1996 and Pena et. al, 2005) + graft collagen fiber (Suggs et al. 2003)

In addition to the non-linear elastic response, ligaments exhibit time and history dependent visco-elastic properties that arise from the interaction between the water and the ground substance matrix. There have been numerous experimental investigations into the viscoelastic properties of ligaments, as well as attempts to characterize these properties with models [135, 142]. The results of experimental studies have concluded that the material response of ligament is relative insensitive to strain rate over several decades of variation [142, 168]. In addition, ligaments reach a pre-conditioned state after repeated loadings, and there is minimal amount of hysteresis (Weiss 2001). Therefore, in a lot of finite element modeling of ligaments, the inclusion of viscoelastic properties was neglected, and the focus was on the non-linear elastic response.

For the bones in the FE knee model, the geometries were often obtained through CT scanning or MR imaging. Human bone properties have been well studied experimentally [24, 33, 115, 154, 188, 196]. Zysset et al. measured the elastic properties of bone by a nanoindentation technique with a custom irrigation system was used for simultaneously measuring force and displacement of a diamond tip pressed 500 nm into the moist bone tissue [196]. The measured elastic moduli ranged from 6.9 ± 4.3 GPa in trabecular bone and up to 25.0 ± 4.3 GPa in cortical bone. However, when the bone was involved in finite element studies together with soft tissues, it is usually considered as rigid due to its small strain under loading.

3.0 OBJECTIVE AND SPECIFIC AIMS

The objective of this dissertation is three-fold: (1) to measure the strain in the AM and PL bundle of the ACL to provide more information of intact ACL behavior under different knee motions and loads; (2) to measure the position of the ACL graft in tunnel in reconstructed knees under different knee motions and loads; and (3) to develop a finite element model capable of assessing the graft movement in the tunnel; and assess the strain and stress of the graft under different knee loading conditions. To this end, three specific aims are proposed. They are summarized in the following sections and illustrated in Figure 6.

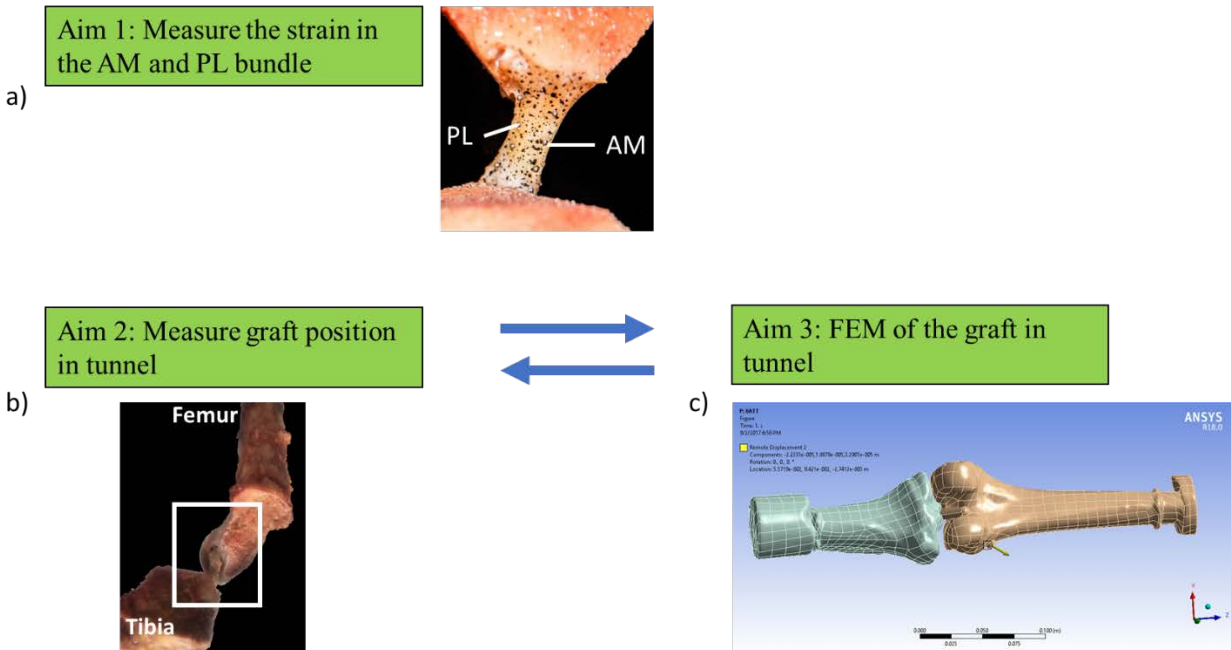


Figure 6: Schematic of proposed methodology

3.1 SPECIFIC AIM 1: MEASURE STRAINS IN ANTEROMEDIAL AND POSTEROLATERAL BUNDLES OF THE ACL UNDER DIFFERENT KNEE LOADING CONDITIONS

The first aim of the study is to measure the strains in AM and PL bundles during knee flexion-extension and under external loads. Multiple researchers have stated that the ACL consists of two major fiber bundles, namely the anteromedial and posterolateral bundles[30, 46, 47, 139, 145]. Observations that are made that when the knee is extended are that the PL bundle is tight, and the AM bundle is moderately lax. As the knee is flexed, the femoral attachment of the ACL has a more horizontal orientation; causing the AM bundle to under tension and the PL bundle to relax[114, 190]. Although, there is some degree of variability for the femoral origin of the AM and PL bundle, the AM bundle is generally located proximal and anterior in the femoral ACL origin, high and deep in the notch when the knee is flexed at 90° degrees and the PL bundle starts in the distal and posterior aspect of the femoral ACL origin, shallow and low when the knee is flexed at 90 degrees. At the tibial insertion, the ACL fans out to form the foot region. The AM bundle insertion is in the anterior part of the tibial ACL footprint, while the PL bundle in the posterior part[34, 139]. While the AM bundle is the primary restraint against anterior tibial translation, the PL bundle tends to stabilize the knee near full extension, particularly against rotatory loads[140]. With this anatomical knowledge, more information about the strain in these two bundles under different loading conditions with non-contact measurement can provide a better understanding about the intact ACL behavior, injury mechanisms, and with assist anatomical reconstruction of ACL.

3.2 SPECIFIC AIM 2: MEASURE ACL GRAFT POSITION IN TUNNEL UNDER VARIOUS KNEE MOTIONS AND LOADINGS

The second aim of the study is to measure the graft position in femoral tunnel during flexion-extension and under external loads. Femoral tunnel widening is a complication of ACL reconstruction[36, 50]. Studies imply that biological as well as mechanical factors can play a role in enlargement [1,2]. Mechanical factors that can contribute to tunnel enlargement include stress deprivation of bone within the tunnel wall, improper tunnel placement, aggressive rehabilitation and so called the “bungee effects” and “windshield wiper effects” as the graft moves inside the tunnel during knee motion[101]. There are also debates about graft tunnel position and the amount of the insertion site that should be reconstructed. Studies suggest that even though the femoral tunnel is positioned in the center of the footprint, the centroid of the graft may be deviated from the footprint due to the graft shift[121, 124]. Some studies have suggested altering tunnel position because certain regions of the ACL insertion site carry a greater percentage of the load since the graft is not centered in the tunnel[62, 89, 122]. Nonetheless, a correlation between graft position change and knee motion has not been demonstrated. Further study of ACL graft function could afford a better understanding of abnormal as well as normal graft function.

3.3 SPECIFIC AIM 3: DEVELOP A FINITE ELEMENT MODEL OF THE GRAFT AND TUNNEL FOR SINGLE BUNDLE ACL RECONSTRUCTION

The third aim of the study is to model the reconstructed knee with finite element method and calculate the position and force of the graft during flexion-extension and under external loads.

The finite element method has been a tool to analyze the stress and strains outcomes of ACL related reconstructions[13, 95, 135, 136]. Anatomic ACL reconstruction is a popular approach for single-bundle ACL reconstruction[117, 186, 187]. The effects of different tunnel position and graft fixation have been explored extensively in experiments, however, little work has been done in modeling these differences. In this part, finite element method will be used to model the ACL graft in single-bundle anterior cruciate ligament reconstruction. A geometric model of the anatomical reconstruction will be fabricated with CT images of a reconstructed knee joint model and virtual surgical operations. The position of the graft in the femoral and the tibial tunnel, the tunnel-tunnel lengths, the graft tension and the contact pressures will be calculated and evaluated with different external loadings and flexion angles.

3.4 SUMMARY

The first specific aim, characterizing the strains in the AM and PL bundle under loading, has been partially addressed in previous work by others[114, 190]. However, many of these studies have used strain gauge transducer in their tests. In addition to containing a more comprehensive description of behavior of AM and PL bundle, this work presents a novel non-contact measurement method that are capable of quantifying strain distributions in two bundles of ACL to characterize the behavior of the ACL. Chapter 4 outlines the experimental design of robotic testing, surgical procedure and strain measurement of intact ACL, and analysis of the strain of AM and PL bundles.

The experimental design for the ACL reconstruction and graft shift in tunnel are given in Chapter 5. Anatomical single-bundle ACL reconstruction will be done using a hamstring graft, to

provide more insight into the graft position change in the reconstructed knees. The results of the analysis are used to assess the overall graft position in femoral tunnel during flexion extension and under various external loadings, with respect to a coordinate system that setup based on anatomical landmarks.

The finite element model formulation of the ACL reconstruction is given in Chapter 6 along with a description of the material properties and implement of the model. To understand the mechanical behavior of the ACL graft in tunnel is currently not possible in clinic and the finite element method can give a more detailed knowledge about the ACL graft in the tunnel. The objective of this work is to develop a hyper-elastic, finite deformation finite element model, to study the stress and strain of ACL graft in reconstructed knees.

In the current research, the following hypotheses will be addressed: (1) AM and PL bundle possess different patterns of strains under different knee motions; (2) The ACL graft changes position in the tunnel with knee motion; and (3) FE modeling can predict strain outcome of experiment describe experiment. Ultimately, the information gained from this research will lead to an improved approach towards intact ACL behavior, their risk of tear and the clinical management of ACL reconstruction.

4.0 DETERMINE STRAINS IN AM AND PL BUNDLES UNDER DIFFERENT LOADING CONDITIONS

The three-dimensional (3D) deformation of the anterior cruciate ligament (ACL) of the knee can play an important role in the understanding of the biomechanics of ACL injury. This chapter describes the experimental study to determine strains in AM and PL bundles under different loading conditions. Previously, several techniques have been utilized to measure the strain of the two bundles of the ACL, including MRI, strain gauge, etc. Given that that the ACL has a complex three-dimensional shape with local changes in two bundles, the assessment of ACL strains is difficult. This chapter outlines the experiment setup and methods that were developed to measure the strains in AM and PL bundle of the ACL. This work advances previous strain measurements by including surface strain changes of two bundles.

4.1 BACKGROUND AND SIGNIFICANCE

Many ACL injuries do not involve direct physical contact at the time of injury [8, 43, 54]. Multiple studies have shown that the cause of ACL ruptures include an axial impulsive loading of the knee joint combined with a valgus knee moment, often combined with internal or external tibial rotation [23, 96, 152]. The foundation for the current hypothesis, that AM and PL bundle of the native ACL possess different patterns of strains under different knee motions, lies in the

analysis of native ACL under various loadings. Information on the strains in the bundles is useful in establishing clinical criteria for reconstruction and rehabilitation of the ACL. Therefore, the measurement of strain of the AM and PL bundles can provide important information is of clinical value.

Early measurements of strain in vivo used the Hall effect strain transducer (HEST) to measure the displacement behavior of the ACL and calculate its strain response, Renström et al. measured ACL strain during simulated hamstring activity and quadriceps activity using a HEST[152]. Access to the ACL was gained through a medial parapatellar incision. The transducer was firmly sutured of its attachments to the lower portion of the AM bundle of the ACL. After the transducer was attached, the capsule was then repaired with sutures. By applying quadriceps and hamstring loads using a servo-hydraulic testing system (MTS), the mean passive normal strain pattern was measured.

More recent studies have used a differential variable reluctance transducer (DVRT) to measure strain. Cerulli et al. measured ACL strain in vivo during rapid deceleration. A DVRT was calibrated and surgically implanted in the antero-medial band of the intact ACL[28]. The subject the hopped as quickly as possible from a distance of 1.5 m to the target, landing with the instrumented left leg and stopping in the landed position. The results showed an average peak strain of the ACL during the instrumented Lachman test of $2.00 \pm 0.17\%$. The average peak strain of the ACL during the rapid deceleration task was $5.47 \pm 0.28\%$. They also concluded that the DVRT technique may be used in further sport-specific movements to gain insight into movement patterns associated with ACL injury mechanisms. The primary advantage of using the DVRT in comparison to the HEST is that it has enhanced accuracy, improved precision, and its calibration does not need to be performed at the working temperature of the sensor. In the Beynnon et al.

literature review, they chose the use of the DVRT over the HEST because it has substantially better performance characteristics and possible capability of minimizing the variability in the study[19].

However, pointwise measurements, such as the ones provided by strain gauges, sometimes are not sufficient to fully measure ACL regional strain in an experiment. Full-field measurements through visualization of strain gradients and concentrations produces a more complete description of the behavior of biological specimens during tests. Also, contactless measurements enable the measurement of strain without disturbing the local mechanical response of the material. Ellis et al. used reflective markers in their study of measuring MCL strain under loads[48]. A digital motion analysis system consisting of two high-resolution digital cameras and digital motion analysis software was used to record MCL strain in the measurement regions and joint kinematics simultaneously.

Digital image correlation (DIC) is an alternate method of noncontact strain measurement. It based on the analysis of sets of images of the marked surface of the specimen in the undeformed (reference) and deformed states. DIC can be implemented both in a two-dimensional (2D-DIC, with a single camera) and a three-dimensional (3D-DIC, using two or more cameras) situations. With this the imaging processing defines unique correlation areas known as macro-image facets, typically 15–30 pixels square, across the entire imaging area. Each facet is a measurement point that can be thought of as an extensometer point and strain rosette. These facets are tracked in successive images. Through interpolation and the overlap of adjacent facets, sub-pixel accuracy is obtained in terms of displacement from which the strains can subsequently be calculated. A matching algorithm is used to match the facets between the reference and deformed states. The displacement field is then computed. Subsequently, the strain field is

obtained by derivation [159, 160]. Many new algorithms and methods have been proposed and developed for large displacements and rotations, so that the DIC can be applied to more applications [58, 110, 132, 194]. The DIC technique can be used for many tests including tensile, torsion, bending and combined loading for both static and dynamics applications.

For an optimal use of DIC, the surface of interest must have a random pattern, which deforms together with the specimen surface. Palanca et al. concluded in their study that to ensure accuracy and precision of the computed displacements and strains, the speckle pattern should meet some requirements [131]: 1). random distribution, to make each area of the surface of the specimen univocally identifiable; 2). High contrast, to allow the image correlation algorithm works effectively; 3). Speckle/background ratio of 50:50, to avoid regions that cannot be properly recognized; 4). The size of the speckle dots (in relation to the specimen size), in order to optimally exploit the resolution of the camera [17, 39, 102, 108, 133, 160].

4.2 METHODS

4.2.1 Specimen preparation and Robotic testing

With institutional approval, six intact fresh frozen cadaver knees were used in this study. Samples were frozen at -20 C°, and thawed the night before testing at room temperature. The knees were inspected arthroscopically before testing for any tissue abnormalities or arthritis. The tibia and femur were cut 15 cm from the joint line and the ends of femur and tibia were potted in epoxy [157].

For the biomechanical testing, a 6 degree of freedom (DOF) robotic (CASPAR Stäubli RX90 Orto MAQUET, Germany) and a universal force sensor (UFS) (Model 4015; JR3 Inc., Woodland, CA) system were used. The robot has an end-effector position repeatability of ± 0.02 mm translation and $\pm 0.02^\circ$ rotation. The UFS has accuracy of ± 0.2 N for force and ± 0.1 N·m for moments according to the manufacturer [87, 90, 157]. The potted tibia and femur were placed upside down with tibial cylinder connected to the robotic arm and the femoral cylinder was fixed to a stationary base. The passive path of flexion-extension of the intact knee joint was determined by the robotic testing system by minimizing all external forces and moments applied to the joint throughout the range of flexion from full extension to 90° flexion with 0.5° increments. The positions were accepted if the external loading less than 0.5 N for forces and 0.25 N·m for moments [42].

The knee joints were tested under the loading conditions: (1) an 89.0-N anterior tibial (AT) load (simulated KT1000 test) to test anterior tibial translation (ATT) (mm) [150], (2) a 5.0-Nm internal tibial torque to test internal rotation (IR) (degrees), (3) a 5.0-Nm external tibial torque to test external rotation (ER) (degrees) [90] and (4) a 7.0-Nm lateral bending moment to test valgus rotation (degrees). The anterior tibial load was applied at full extension (FE), 15° , 30° , 45° , 60° and 90° flexion, and internal/external and valgus rotational loads were applied at full extension (FE), 15° and 30° of knee flexion [87]. After robotic testing, all muscles, the PCL, and the menisci were removed, and a portion of condyles were removed to allow visualization of the ACL. In all specimens, the same surgeon performed the dissection. The previous passive paths under loads and flexion were then replayed by the robotic system so that the dissected knee's position was the same as that of the intact knee.

4.2.2 Strain measurement and analysis

4.2.2.1 Digital Image Correlation (DIC) Measurement

The procedure for DIC measurement of the ACL strain is shown in Figure 7. DIC is an optical method for strain measurement that uses image recognition to analyze and compare digital images acquired from a marked surface. It is a three-dimensional, full-field, non-contact optical technique to measure contour, deformation, vibration and strain. It can measure arbitrary displacements and strains from 50 microstrain to 2000% strain and above, for specimen sizes ranging from <1mm to >10m. By tracing a randomly applied high contrast speckle pattern, displacement and strain in the specimen can be calculated from the images. With the use of the two cameras taking images of the same object at an angle, photogrammetric principles can be used to calculate the precise 3D coordinates of points on the surface. In this way, a high-resolution three-dimensional maps of strain magnitude, gradient and distribution can be obtained [111].

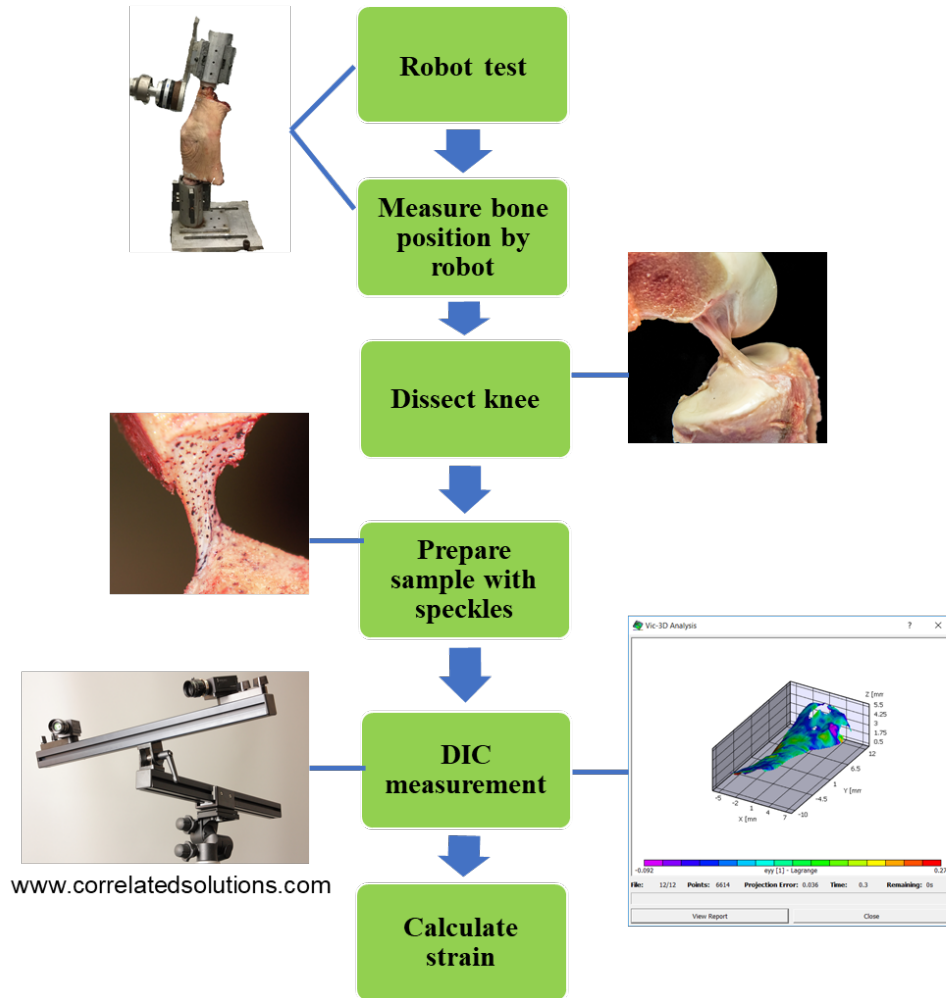


Figure 7: Flowchart of testing and DIC strain measurement.

Prior to the testing, the ACL was prepared with random black speckle pattern using an alcohol-based black ink (Figure 8). The speckle pattern was manually applied by carefully flicking a soft toothbrush dipped with the ink. The speckle size and density were controlled by adjusting the distance of the toothbrush from the specimen. The deformation of the ACL during movement was recorded through a three-dimensional DIC system with two charge-coupled device (CCD) cameras (Point Grey, Gras-20S4M-C) with a resolution of 1624 x 1224 pixels and pixel size of 4.4 μm .

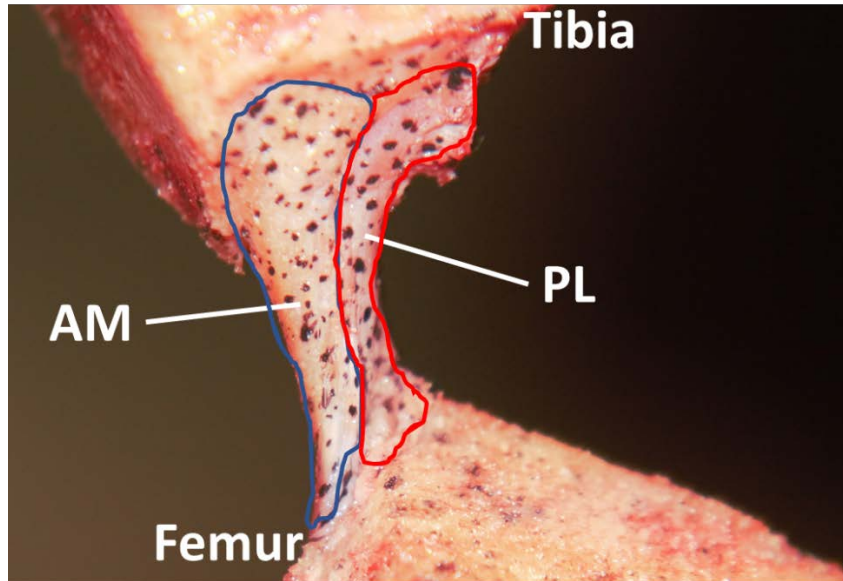


Figure 8: Dissected and prepared sample with random speckle pattern.

To assess strain in the different bundles of the ACL, the AM and PL bundles were first identified. For the identification of the different regions of the ACL (AM vs. PL), the description from previous studies was utilized [45, 47, 70, 72, 114, 170, 191]. Harner et al. found that the divisions into AM and PL bundles can be consistently performed during arthroscopic surgery in intact ACL. The AM and PL bundle and their insertions were found to be consistent and reproducible from specimen to specimen [70]. The line of separation between the AM and PL components ran anterior to posterior, separating a proximal and distal region on the femur. On the tibia, the line of separation runs anterior to posterior, separating the ACL into an anterior and posterior (Figure 8) [70]. The insertions sites of the AM and PL bundles of the ACL was determined for each specimen by single surgeon. After dissection and speckle preparation, the specimen was put back on the experimental test set up. Based on the location of two bundles, the cameras were then placed anteromedially when measuring AM bundle and were moved to posterolateral position for measuring PL bundle (Figure 9). Cameras were placed at positions to

keep the regions of interest in full view of the cameras throughout the entire flexion range. Between different samples, the position of cameras had to be adjusted slightly due to the variations in each sample such as knee size, ACL rotation and position in robot. However, before measurement, the relative position of the cameras with respect to each other and to the target was calibrated using a high-precision 11 mm × 7 mm calibration pad (Figure 9). Calibration precisely calculates the cameras' intrinsic and extrinsic parameters while triangulating the cameras' positions and removing lens distortions. This removes any measurement bias and defines a three-dimensional coordinate system on the specimen's surface. All samples were calibrated with same cameras and calibration pad. Due to cameras' limited range of focal length, they were placed approximately same distance away from the specimen for each sample.

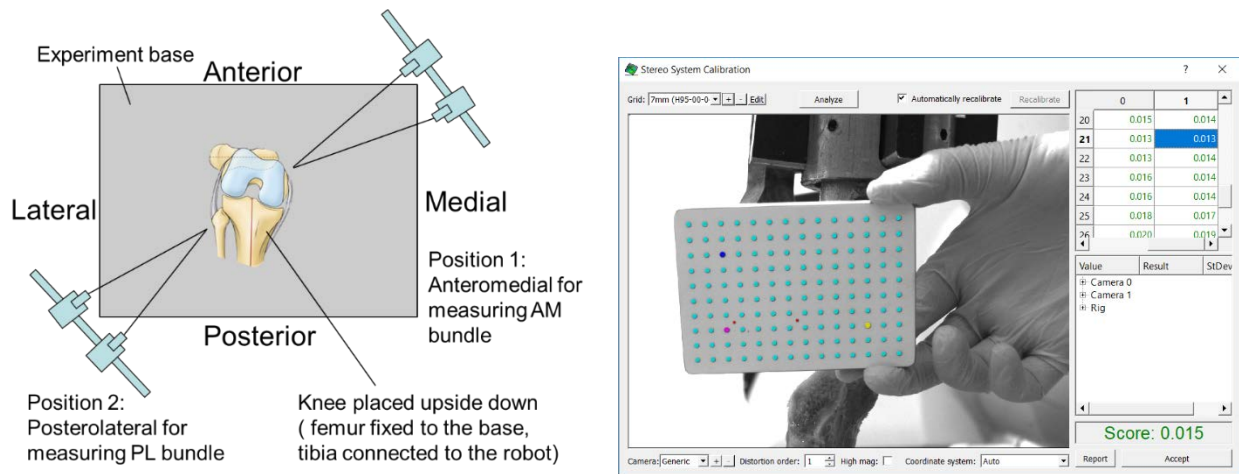


Figure 9: The placement of cameras for measuring the strain of AM and PL bundles on a representative right knee model and the cameras calibration.

For measuring AM and PL bundles' strain during flexion/extension, images were taken at 3° intervals where the knee was brought from full extension (approximately 0°) to 90° of flexion. Under external loads, images were taken at 0.5mm intervals for translation loads (AT, PT), and

0.5° intervals for rotational loads (IR, ER, VAL). A software package (VIC3D, Correlated Solutions Inc., Columbia, SC) was used to analyze the strain at each flexion angle and loadings using the camera images (Figure 10). The tissue was kept hydrated throughout testing by with 0.9% saline. Outline of the AM or PL bundle was selected in the camera images. The longitudinal strain was defined as the strain along AM or PL bundle's longitudinal axis, which was defined from camera images in the software (VIC3D, Correlated Solutions Inc., Columbia, SC) by selecting the direction that along the direction of stretched fibers under anterior tibial load (Figure 10). Transverse strain was the strain along an axis perpendicular to the longitudinal axis in the measuring plane. And the shear strain was defined as strain along an axis angulated at 45° to the longitudinal and transverse axis. As strains were calculated with respect to the reference image, in measuring strain during knee flexion the reference images were taken at full extension position. While in measuring strains of two bundles under external loads, reference images were taken at a given flexion angle without any external loads.

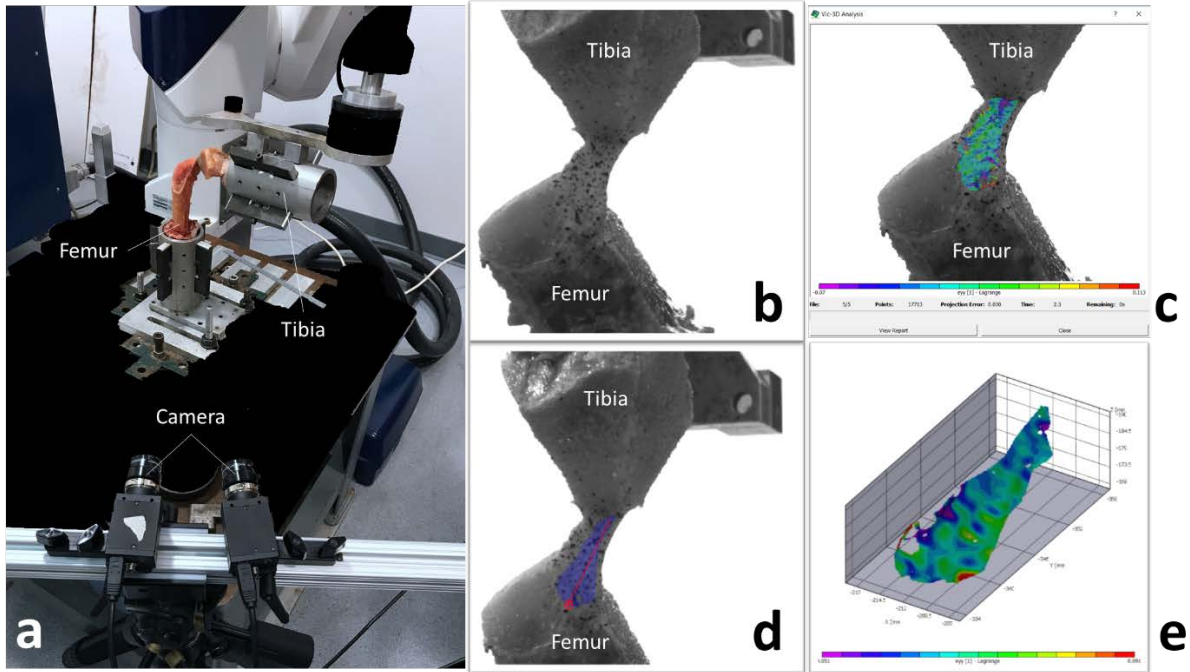


Figure 10: a) Camera setup and robotic testing with femur fixed to the base and tibia connected to the robot; b) Image of sample from reference camera; c) longitudinal strain distribution in the ACL with camera coordinate system; d) defining local coordinate system based on orientation of bundles; e) longitudinal strain based on new coordinate system

4.2.2.2 Measurement of Strain with Markers

Flowchart of ACL strain measurement with bead markers and laser scanning is shown in Figure 11. Robotic testing steps similar to with the DIC measurement were applied. After dissection, 1-mm diameter stainless steel beads were attached to the AM and PL bundle as markers for laser scanning. Beads were placed along fibers of the AM and PL bundles. Due to the size of the ACL, each bundle had two columns of beads, and each column had 4-5 beads. The robot then replayed the intact knee kinematics that were measured in previous steps for the different knee loadings. A laser scanner (FARO Technologies, Lake Mary, FL, US) was calibrated and used to scan the position of markers in unloaded and loaded positions at full extension, 15°, 30°, 45°, 60° and 90°

flexion. The scanner was mounted on a metal plate and screwed to the testing platform. A tool coordinate system was defined by the anatomical position of the knee, with its x, y, z coordinates corresponding to medial-lateral, superior-proximal, anterior-posterior direction with respect to the femur.

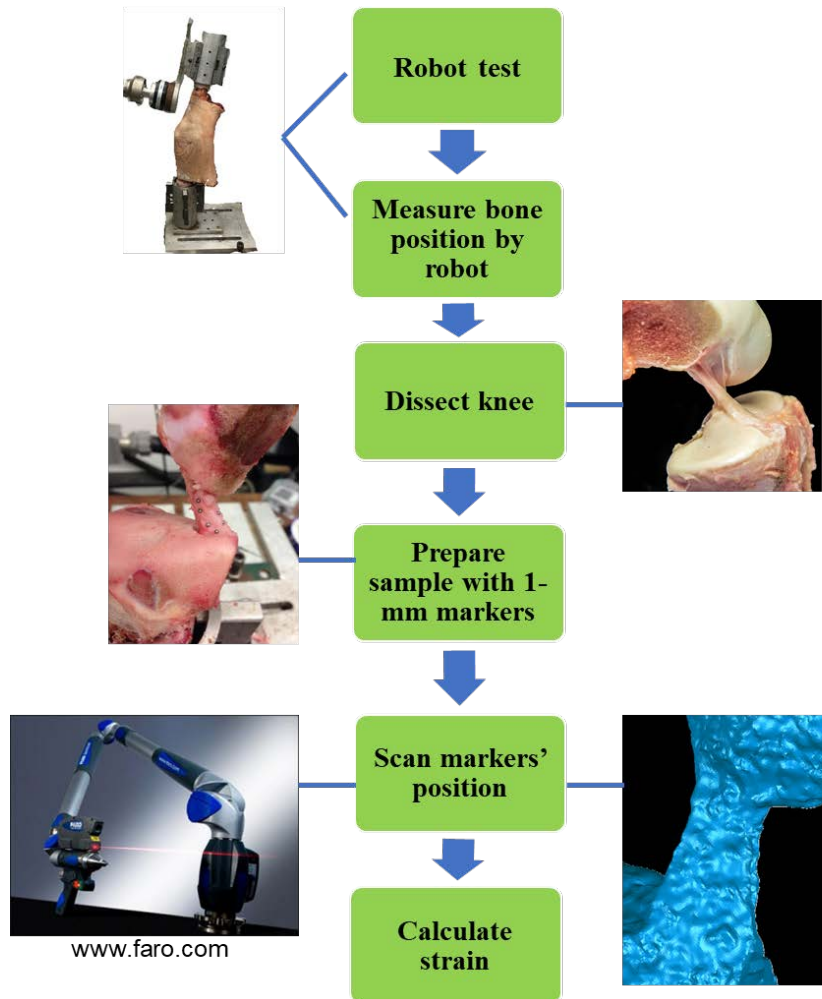


Figure 11: Flowchart of ACL strain measurement with markers and laser scanning

The scanning result was processed in software (Geomagic, Research Triangle Park, North Carolina). Each marker was selected manually from the scanned geometry, and the centroid of marker was calculated by the software (Figure 12). Every three markers that were next to each other are formed as an element to calculate the local strain (Figure 12d). A local material

coordinate was assigned to each element with one axis parallel to the bundle fiber orientation. Lagrangian finite strain will be used due to large deformation of AM and PL bundle. The Green-Lagrangian strain tensor is as follow:

$$E_{ij} = \frac{1}{2} \left[\frac{\partial u_i}{\partial X_j} + \frac{\partial u_j}{\partial X_i} + \frac{\partial u_k}{\partial X_i} \frac{\partial u_k}{\partial X_j} \right]$$

4-1

Where the i, j, k denotes the three axes of the coordinate.

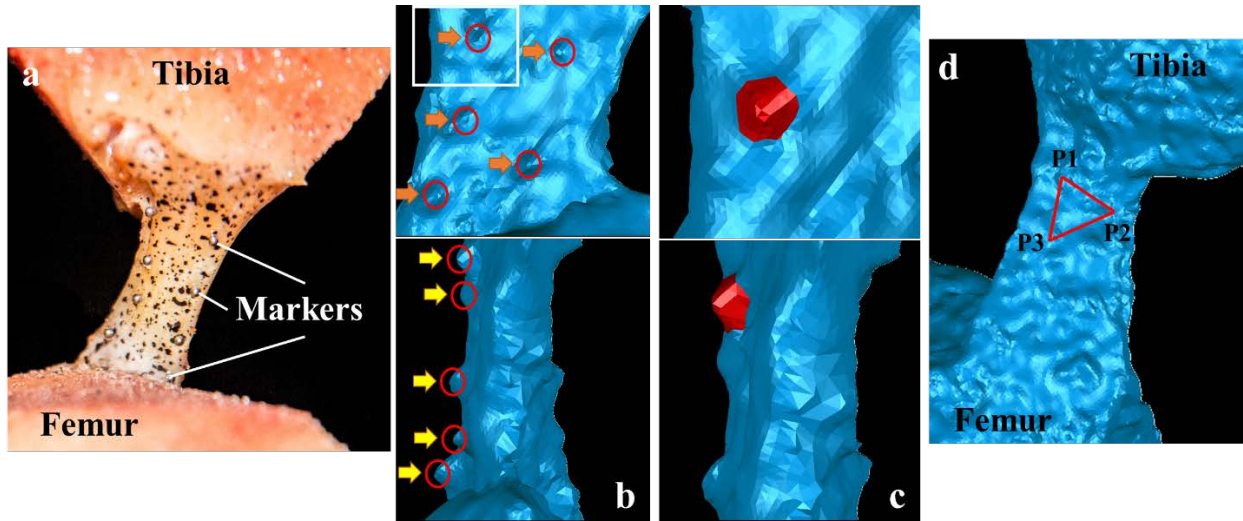


Figure 12: a). Dissected knee with beads on ACL; b). Laser scan of the ACL with beads; c) highlighted bead in front and side view; d) element determined by three marker centroids

$$E_{ij} = \frac{1}{2} \left[\frac{\partial u_i}{\partial X_j} + \frac{\partial u_j}{\partial X_i} + \frac{\partial u_k}{\partial X_i} \frac{\partial u_k}{\partial X_j} \right]$$

4-1

In 3-D, it can be explicitly expressed as:

$$E_{xx} = \frac{\partial u}{\partial X} + \frac{1}{2} \left[\left(\frac{\partial u}{\partial X} \right)^2 + \left(\frac{\partial v}{\partial X} \right)^2 + \left(\frac{\partial w}{\partial X} \right)^2 \right]$$

$$\begin{aligned}
E_{yy} &= \frac{\partial v}{\partial Y} + \frac{1}{2} \left[\left(\frac{\partial u}{\partial Y} \right)^2 + \left(\frac{\partial v}{\partial Y} \right)^2 + \left(\frac{\partial w}{\partial Y} \right)^2 \right] \\
E_{zz} &= \frac{\partial w}{\partial Z} + \frac{1}{2} \left[\left(\frac{\partial u}{\partial Z} \right)^2 + \left(\frac{\partial v}{\partial Z} \right)^2 + \left(\frac{\partial w}{\partial Z} \right)^2 \right] \\
E_{xy} &= \frac{1}{2} \left(\frac{\partial u}{\partial Y} + \frac{\partial v}{\partial X} \right) + \frac{1}{2} \left[\frac{\partial u}{\partial X} \frac{\partial u}{\partial Y} + \frac{\partial v}{\partial X} \frac{\partial v}{\partial Y} + \frac{\partial w}{\partial X} \frac{\partial w}{\partial Y} \right] \\
E_{xz} &= \frac{1}{2} \left(\frac{\partial u}{\partial Z} + \frac{\partial w}{\partial X} \right) + \frac{1}{2} \left[\frac{\partial u}{\partial X} \frac{\partial u}{\partial Z} + \frac{\partial v}{\partial X} \frac{\partial v}{\partial Z} + \frac{\partial w}{\partial X} \frac{\partial w}{\partial Z} \right] \\
E_{yz} &= \frac{1}{2} \left(\frac{\partial v}{\partial Z} + \frac{\partial w}{\partial Y} \right) + \frac{1}{2} \left[\frac{\partial u}{\partial Y} \frac{\partial u}{\partial Z} + \frac{\partial v}{\partial Y} \frac{\partial v}{\partial Z} + \frac{\partial w}{\partial Y} \frac{\partial w}{\partial Z} \right]
\end{aligned}$$

Where the u , v , w are the displacements in three axes. And the calculation was implemented in MATLAB (Appendix 0)

4.3 RESULTS AND DISCUSSION

4.3.1 Kinematics and In-Situ Force

The kinematics and in-situ force for all six samples were measured by robotic system. The results are reported in *Table 3* and *Table 4*. The magnitude and trends of tibial displacement under 89N anterior tibial load, the rotation angle under external loads at different flexion angle as well as the corresponding in-situ force were similar to previous studies[7, 88, 164, 185].

Table 3: Tibia displacement and rotation under external loads

	ATT (mm)	IR (degree)	ER (degree)	VAL (degree)
0	5.16±0.80	11.88±3.92	12.04±2.18	2.42±0.61
15	6.96±0.92	18.83±1.47	17.00±3.91	3.58±0.89
30	7.88±1.25	21.58±2.19	18.58±5.28	3.92±1.24
45	7.54±1.90	N/A	N/A	N/A
60	6.54±1.99	N/A	N/A	N/A
90	5.75±1.94	N/A	N/A	N/A

Table 4: ACL in-situ force under external loads

	ATT (N)	IR (N)	ER (N)	VAL (N)
0	88.65±32.26	30.50±18.18	19.56±15.92	14.06±7.48
15	94.94±22.82	31.58±16.11	8.40±6.23	9.76±4.53
30	93.87±15.44	23.48±13.95	5.59±3.03	7.35±5.99
45	84.92±15.07	N/A	N/A	N/A
60	75.97±14.35	N/A	N/A	N/A
90	72.85±16.01	N/A	N/A	N/A

The average anterior displacement under AT load increase with flexion angle from full extension to 30°, and then decrease from 30° to 90° knee flexion, with maximum value of 7.86 mm (Figure 13). The average rotation angle under internal/external/valgus rotation all increase with flexion angle from full extension to 30° flexion, with maximum rotation angle 21.58°, 18.58°, 3.92° accordingly (Figure 14).

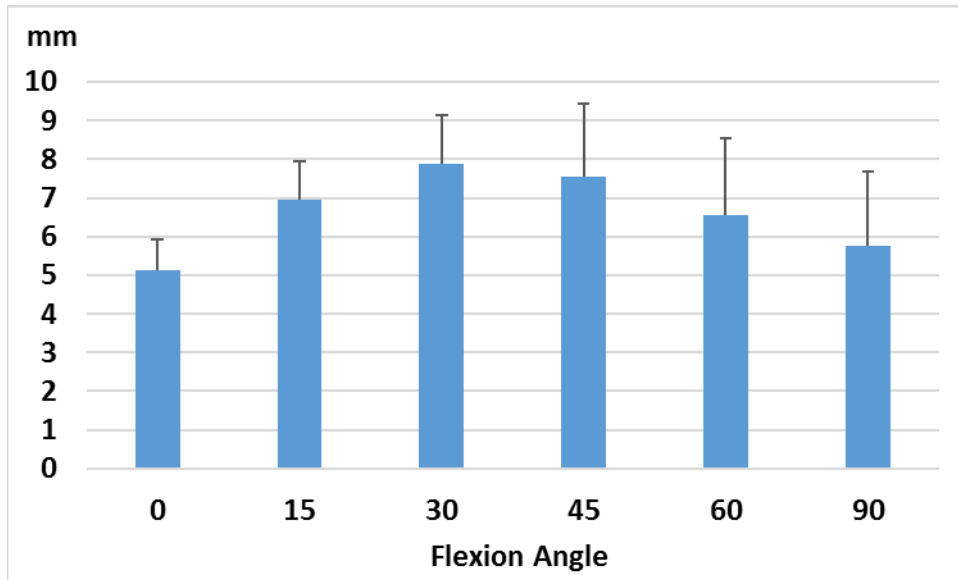


Figure 13: Average anterior tibial translation (ATT) under 89 N anterior tibial load (n=6)

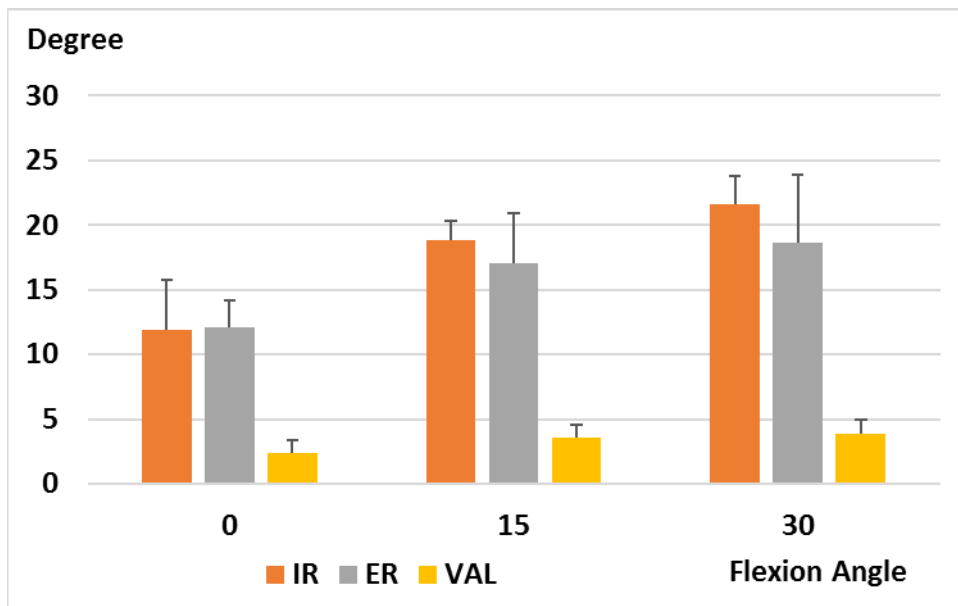


Figure 14: Average rotation angles under external rotational load (n=6)

In-situ force of the ACL under external loads are plotted in Figure 15. From results, average in-situ force under AT loading are much higher than those under rotational loads at all measured flexion angles. The average ACL in-situ force under AT load ranges from 72.85N to 94.94N. And average in-situ force of ACL under external loads are all less than 35N. Compared

with 89N anterior tibial load applied, the calculated in-situ force in the ACL shows that the ACL is the primary constraint of anterior tibial translation, and also provided a secondary restraint for knee rotational stability.

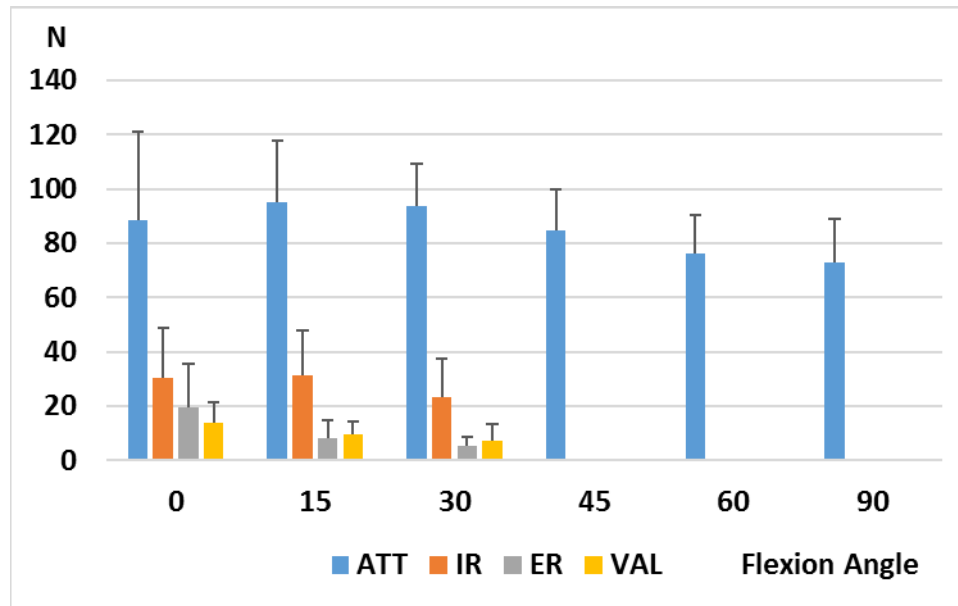


Figure 15: Average in-situ force (n=6) of the ACL under external loads

4.3.2 Strain in AM and PL Bundles with DIC

Longitudinal, transverse and shear strains of the two bundles during knee flexion and under external loads were calculated from the series of images. Figure 16 shows an example of longitudinal strain in the PL bundle under AT load. Based on DIC strain measurement results, the averaged strains in AM or PL bundles at all flexion angles are reported.

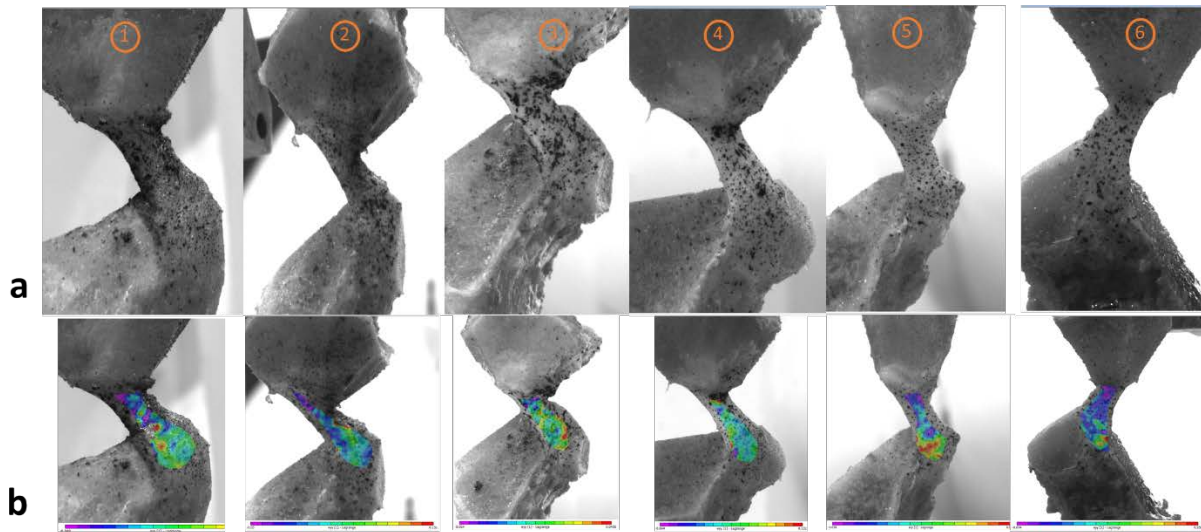


Figure 16: a) images of six intact ACL samples from reference camera; b) longitudinal strain distribution in the six ACLs with anatomical coordinate system

4.3.2.1 Strain during knee flexion

Longitudinal strains of the two bundles during knee flexion are shown in Figure 17. During flexion, the AM bundle slightly reduced strain from full extension to about 45° flexion, and then it was stretched with knee flexed from 45° to 90° flexion. The maximum strain occurred at 90° flexion angle with a value of 0.031. The PL bundle reduced strain with increase of flexion angle and started to stretch beyond 60° flexion angle. At 60° flexion angle, PL bundle had maximum longitudinal strain of 0.068.

The results showed PL bundle had the maximum length at full extension, while the AM bundle had the maximum length at 90° flexion angle. These results agree with previous studies that focused on the behavior of two bundles of ACL during flexion extension [6, 45, 77]. Hollis et al. showed that the AM bundle lengthens and under tension in flexion, while the PL bundle shortens and becomes slack. According to their study, the AM bundle length increases by 1.9

mm (5%) at 30° of knee flexion, and by 4 mm (12%) at 90°. Conversely, the PL bundle decreases by 3.2 mm (14%) when the knee is passively flexed from 0 to 30°, and by 7.1 mm (32%) at 90° of knee flexion[77]. Our study shows that the longitudinal strain of AM bundle decreased slightly by 0.8% at 30° flexion and increased to its maximum value 3.2% at 90° flexion. For PL bundle, the longitudinal strain decreased by 4.3% from full extension to 30° knee flexion and 4.9 % at 90° of knee flexion, while its maximum occurred at 60° of knee flexion as 6.8%.

The general pattern of longitudinal strain of two bundles in this study agrees with previous observations correlated with length changing of AM and PL bundles by Amis and Dawkins[6]. In contrast to Hollis et al. study, Amis and Dawkins found that the AM bundle initially shortens until 30° of flexion, and then gradually elongates until it reaches maximal length at 120°. They also found that internal rotation lengthens the ACL a slightly more than external rotation. This also matches result of this study, most noticeably at 30° of flexion with a longitudinal strain of 7.5% in AM bundle under internal rotation and 4.6% in AM bundle under external load. Compared to the magnitude of longitudinal strain in two bundles under AT load, tibial rotation torques of 5 Nm do not cause significant ACL elongation. This again suggests that ACL mainly constrains the anterior posterior translation, the rotational stability is resisted by a combination of other soft tissue such as capsular shearing, slanting collateral ligament action, joint surface, and meniscal geometry, while the ACL play only played a secondary role[4, 125].

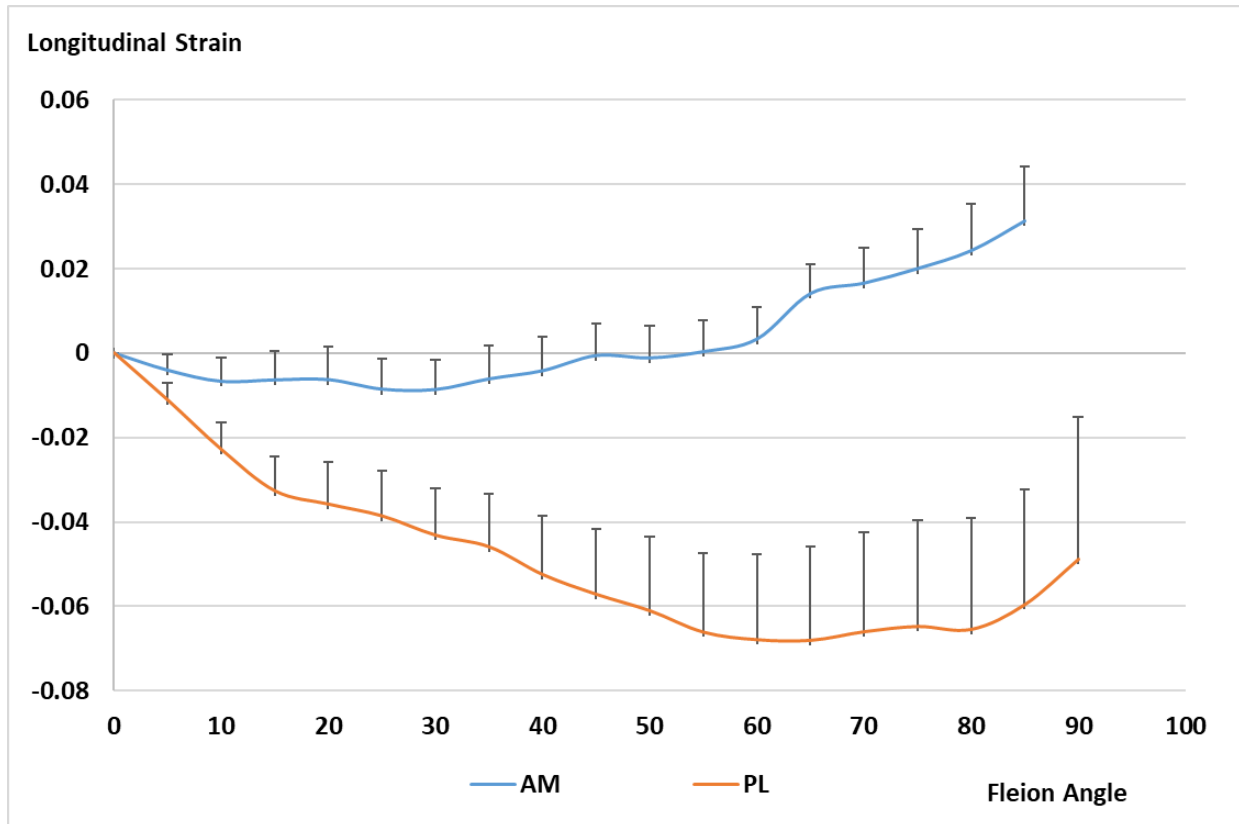


Figure 17: Longitudinal strain (mean±sd) of AM and PL bundles during flexion using DIC measurement

Transverse strains of the two bundles during knee flexion are shown in Figure 18. During flexion from full extension, PL bundle's transverse strain increase with flexion angle. It has a maximum transverse strain at 65° flexion angle with a value of 0.026. The transverse strain of AM bundle has mild change at low flexion angles (full extension to 40°), and then decreases rapidly from 40° flexion angle to 90° flexion angle with its maximum value of -0.029 at 90° flexion angle.

Another finding in this study related to the so called the “stress-free” state of the ACL. Multiple studies have shown that the ACL has no stress-free state at any flexion[107, 137, 143, 169]. However, the value of the magnitude of stress (or strain) is unknown because there was no information of the resultant force of the ACL at various angles of flexion. Therefore, in FE

analyses of the ACL, it is often performed without prestressing the ACL[63, 134, 193], or some assumptions initial stress have to be made[107, 137]. In this study, the longitudinal and transverse strain results of the AM bundle during flexion show that the AM bundle became stretched in longitudinal direction while its transverse strain starts to decrease around 35°~40° knee flexion angle. Soft tissues are often considered being able to only carry tension but not compression load. These findings suggest that the “stress-free” state of the AM bundle might be around 35°~40° knee flexion. However, the PL bundle does not show a trend regarding to a “stress-free” state. The observed “stress-free” state of AM bundle may provide information for finite element analysis of the ACL, and also provide information for surgical reconstruction.

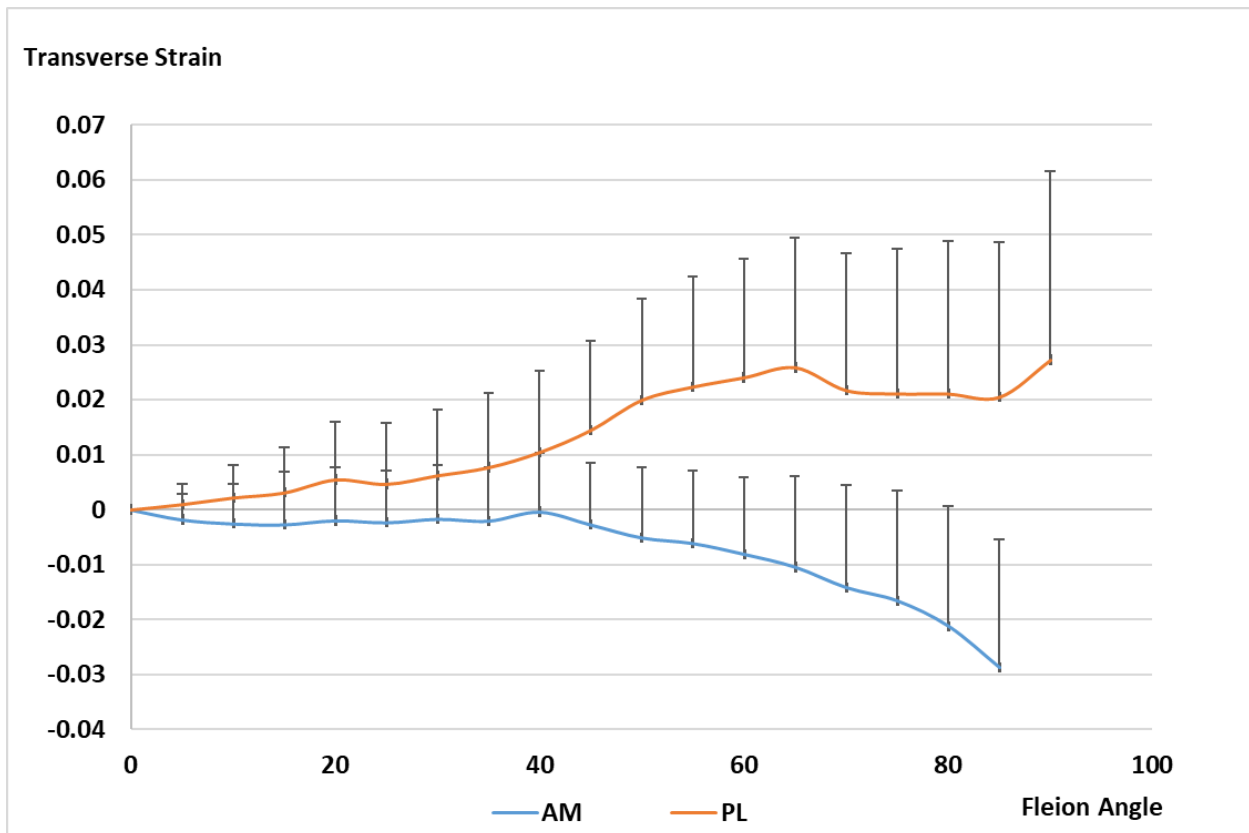


Figure 18: Transverse strain (mean±sd) of AM and PL bundles during flexion

Shear strains of the two bundles during knee flexion are shown in Figure 19. Shear strain in the PL bundle increases from full extension to about 40° flexion, with maximum shear strain of 0.011, and then decreases with increased flexion angle. Shear strain of AM bundle increases with flexion angle and reaches the maximum at 65° with a value of -0.026. Positive shear strain means that the angle of the between the +x and +y-axes due to external loads to decrease, while negative shear strain implies that the angle to increase.

In the early study by Duthon et al., it was found the two bundles of ACL are not isometric with the main change being lengthening of the AM bundle and shortening of the PL bundle during flexion, but experience different patterns of length changes during passive knee flexion [45]. They also found during flexion, there is a slight lateral rotation of the ligament as a whole around its longitudinal axis, and the AM bundle begins to spiral around the rest of the ligament. This relative movement of one bundle upon the other is due to the orientation of the bony attachments of the ACL. This observation was found in this study with DIC measurement. The AM bundle had a large shear strain when the knee flexed close to 90° while the PL bundle had a small shear strain. Together with plot of longitudinal strain, it suggests that the AM bundle may twist itself at the same time elongate when the knee flexed to 90° flexion.

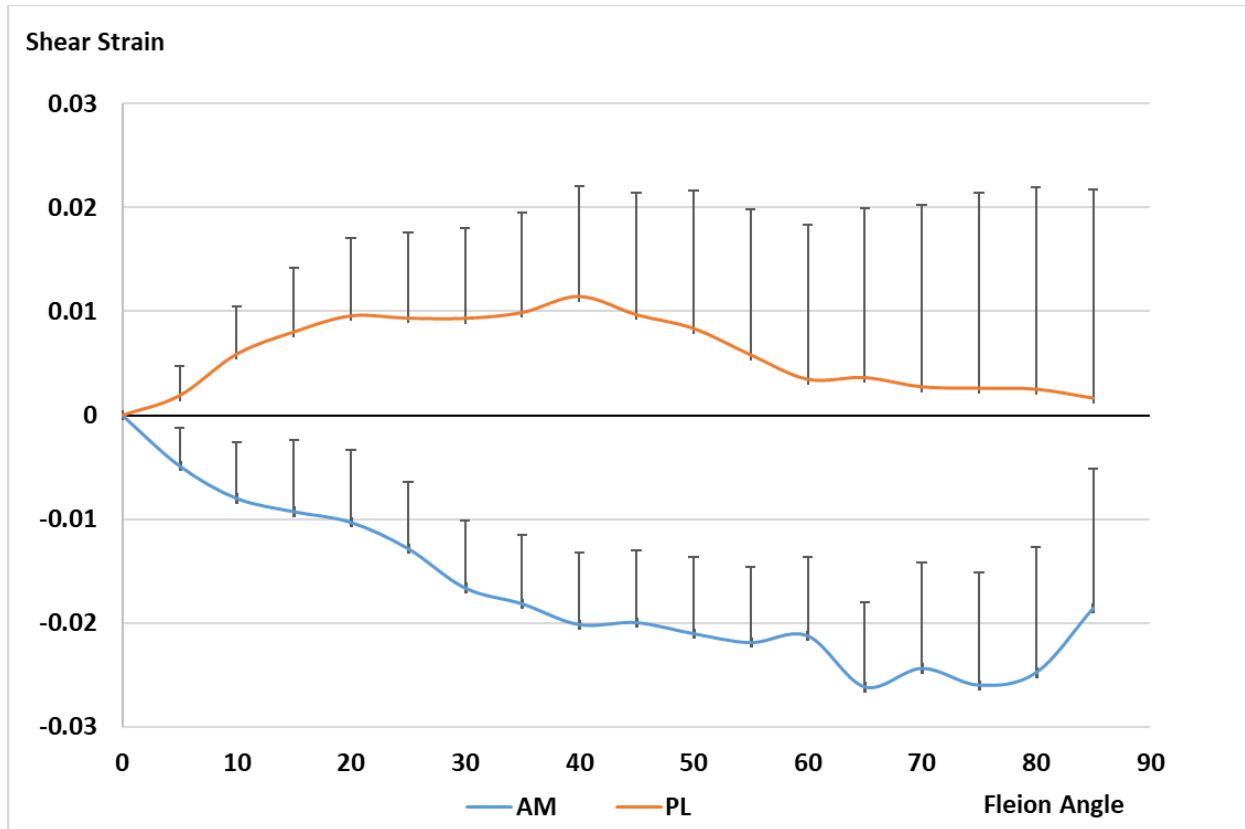


Figure 19: Shear strain (mean±sd) of AM and PL bundle during flexion extension

4.3.2.2 Strain Under Anterior Tibial (AT) load

The longitudinal strains of the AM and PL bundle under AT load are shown in Figure 20. Under AT load, the trend of average longitudinal strain for AM bundle at measured flexion angles matches the trend of in-situ force of ACL, with maximum longitudinal strain 0.097 at 30° knee flexion. The average longitudinal strain for PL bundle increases with flexion angle from full extension and has the maximum value of 0.16 at 60° knee flexion. Statistical significance was found between PL and AM bundle at full extension, 60° and 90° knee flexion.

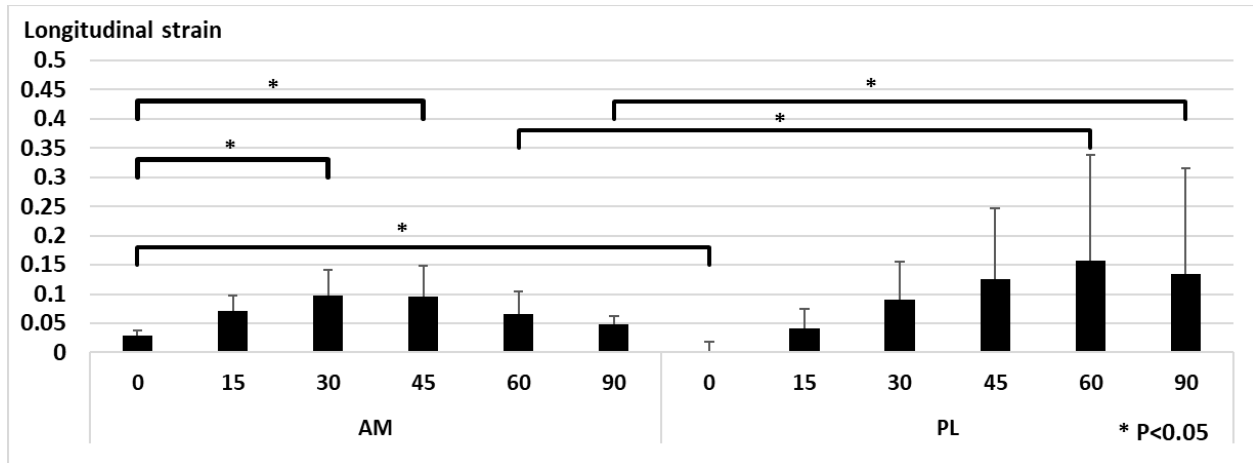


Figure 20: Longitudinal strain of the AM and PL bundles under anterior tibial load

The transverse strains of the AM and PL bundles under anterior knee loading are shown in Figure 21. There was no statistical significance found between AM and PL bundles at the measured flexion angles. However, trends can be seen that the transverse strain of both bundles are larger at low flexion angles. With increased flexion angle, the transverse strain increases to an average value of -0.002 for AM bundle and -0.005 for PL bundle both at 60° knee flexion. This result shows both AM and PL bundle have larger contraction in transverse direction under AT load at low flexion angle. While at high flexion angle, very small transverse strain in transverse direction. It may be explained that the AM and/or PL bundle is under tension at high flexion angle without external load.

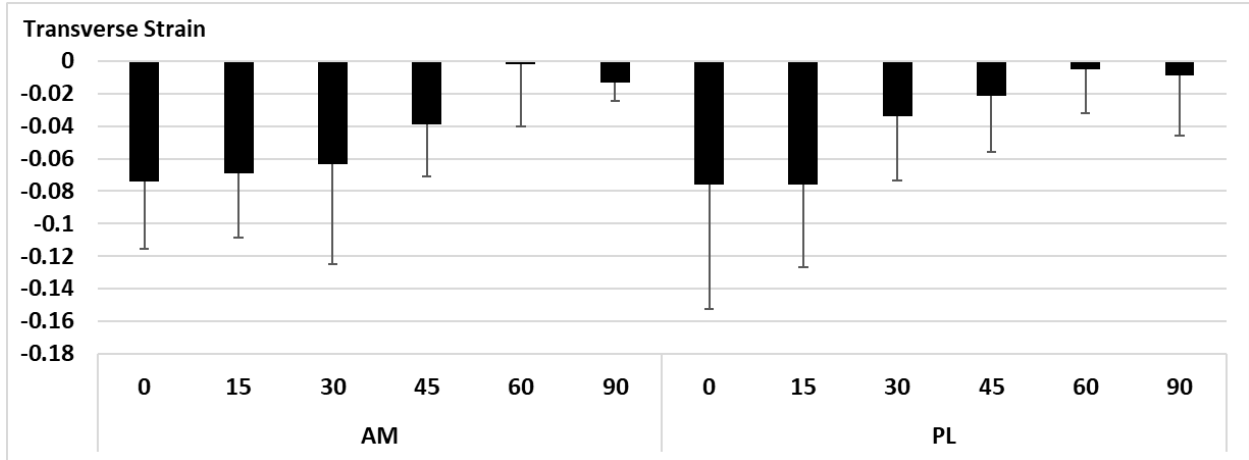


Figure 21: Transverse strain of AM and PL bundle under anterior knee load

The shear strains in the AM and PL bundles is given in Figure 22. The average shear strain of AM bundle increases with flexion angle, while the shear strain of PL bundle decreases from 0° to 30° knee flexion and increases from 30° to 90° knee flexion. Statistical significances were found between AM and PL bundles under valgus load at 15° and 30° knee flexion, under external load at 30° knee flexion and under anterior tibia load at 45° knee flexion.

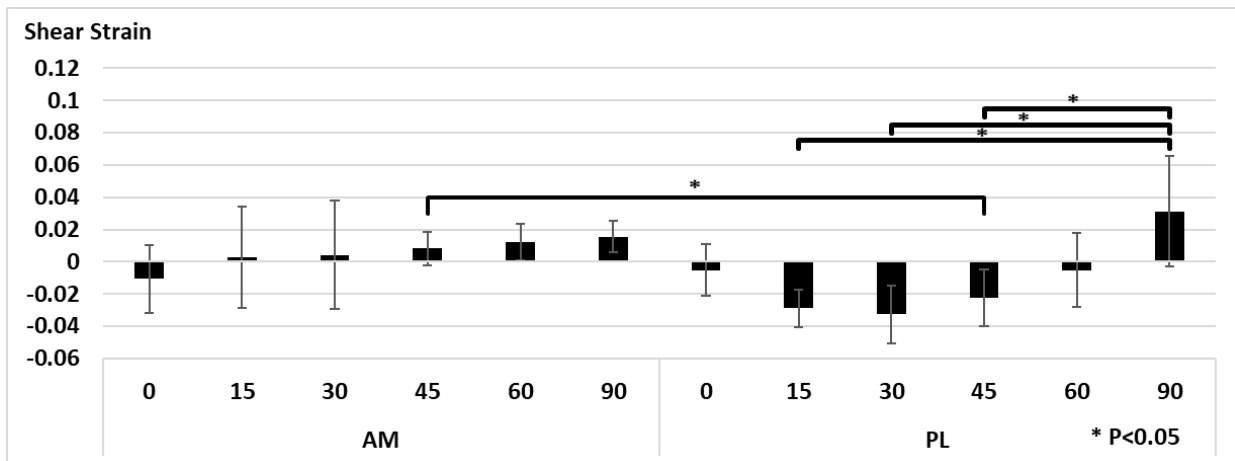


Figure 22: Shear strain of AM and PL bundle under anterior tibial loading

4.3.2.3 Strain Under Internal Rotational (IR) load

Under internal rotational torque, no significance was found for the longitudinal, transverse or shear strain between AM and PL bundle (Figure 23). Both bundles have similar trend need figure number. The longitudinal strain for both bundles increase with flexion angle. The transverse strain under internal load for both AM and PL bundle first increase with flexion and have maximum transverse strain at 15° knee flexion, and it decreases with knee flexion angle from 15° to 30° knee flexion. Small shear strain occurred in both AM and PL bundles when the knee was under internal rotation.

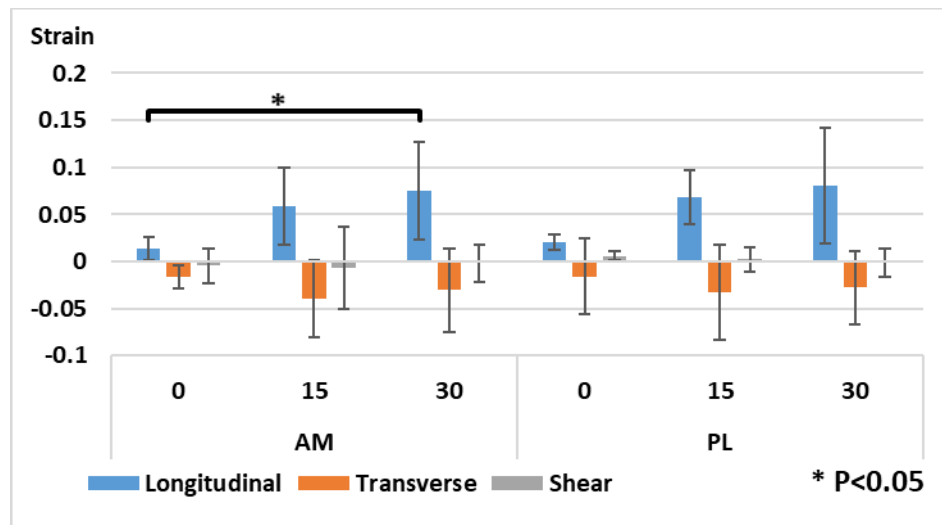


Figure 23: Strain of AM and PL bundle under internal torque

4.3.2.4 Strain Under External Rotational (ER) load

Under external rotational torque, statistical significance was found for shear strain between AM and PL bundle at 30° knee flexion(Figure 24). The longitudinal strain in both AM

and PL bundles increased with flexion angle, with maximum value of 0.046 in AM bundle and 0.027 in PL bundle. The transverse strain under external load for both bundles have a maximum at 15° knee flexion. Unlike strain behavior under internal rotation, shear strain under external torque caused the AM bundle to have a maximum value of 0.01 at 30° knee flexion and the PL bundle to have a maximum value of -0.015 at 30° knee flexion

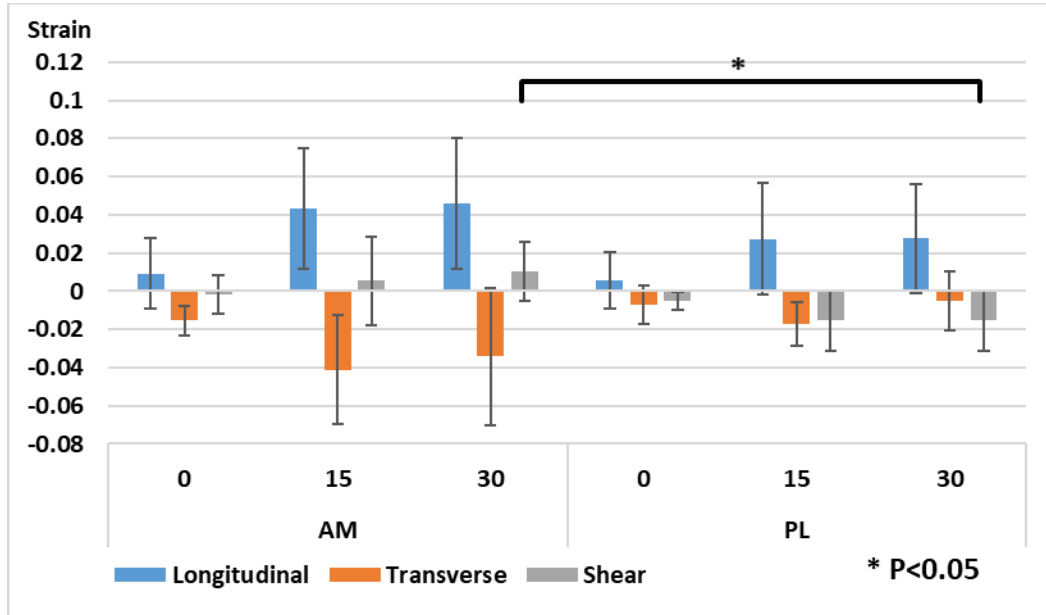


Figure 24: Strain of AM and PL bundle under external rotation torque

4.3.2.5 Strain Under Valgus Rotational (VAL) load

Under a valgus rotational torque, the AM bundle has maximum longitudinal strain at 15° knee flexion while the PL bundle has maximum at 30° knee flexion (Figure 25). The transverse strain of AM bundle decreases with flexion angle, with a maximum of -0.012 at full extension. While the transverse strain of PL bundle decreases from full extension to 15° knee flexion and increases from 15° to 30° knee flexion. Significances were found in shear strain between AM and PL bundles at 15° and 30° knee flexion.

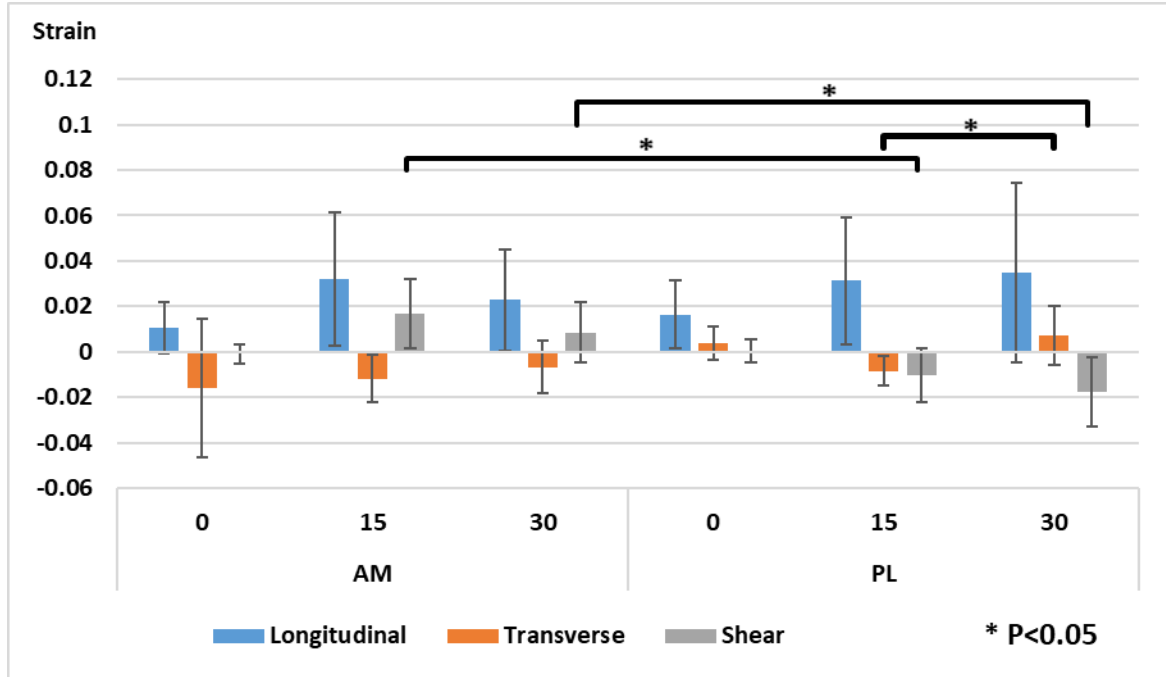


Figure 25: Strain of AM and PL bundle under valgus rotation torque

The strain measurements show the two bundles respond differently to external knee loadings, such as anterior tibia load and rotational tibial torques. When under 89 N anterior load at full extension, 15°, 30°, 45°, 60° and 90° flexion, the average longitudinal strain of both bundles trend to increase with flexion angle from full extension to 45° of knee flexion. However, from 45° to 90° of knee flexion, the longitudinal strain of AM bundle decreases while PL bundle's strain still increases, and the maximum longitudinal strain occurred at high flexion angle. However, the trends show that the longitudinal strain for both bundles increased with flexion angle. None of rotation torques (IR, ER, VAL) cause significant ACL elongation or shortening. These behaviors of two bundles under external loads are important for understanding ACL injury and improving ACL reconstruction techniques.

The search for an ‘isometric point’, about which the femoral origin may rotate with the ligament (graft) length remaining constant, is still in debate in ACL reconstruction. It has been popular to place the femoral tunnel at the so-called 11 o’clock position for the right knee (or 1 o’clock position for the left knee), in order to replicate the origin of the AM bundle of the ACL[156]. A point at the superior corner of the femoral attachment was chosen by Melhorn and Henning[113] and Penner et al[138]. But other tunnel positions have been advocated. Odensten and Gillquist [128] chose a site at the center of the attachment. Loh et al. found that a more lateral graft placement, which is anatomically closer to the femoral insertion of the PL bundle more effectively resists rotatory loads when compared with the AM bundle position as evidenced by smaller ATT and higher in situ force in the graft[109]. Our strain measurement results of two bundles show that the AM bundle has smaller mean longitudinal strain than that of the PL bundle. From the longitudinal strain result during flexion, the PL bundle continuously decreased from full extension to high flexion angle while the AM bundle decreased slightly from full extension to 45° flexion and then increased thereafter. This suggests that in single bundle ACL reconstruction the graft might be fixed at low flexion angle, achieving minimum graft length between tunnel so that the graft could be effectively tight for most knee flexion angles.

4.3.3 Strain in AM and PL Bundles with Markers

Sample F170840R (right knee, 30 years old) was measured with the bead markers and laser scan method. Longitudinal, transverse and shear strain were also calculated to compare with the result from DIC measurement.

Under AT load, calculated longitudinal strain of AM and PL bundles gave large values at full extension as 0.10 and 0.12 (Figure 26). Compared to the result from DIC measurement, the

maximum longitudinal strain of AM bundle is 0.1 at 30° flexion and the maximum longitudinal strain of PL bundle is 0.16 at 60° flexion. The transverse and shear strain of the AM and PL bundles are also shown to have significant larger values compared to the results from DIC measurement. The maximum transverse strain of AM bundle under AT load was 0.41 at full extension, and 0.66 at 45° for PL bundle. Maximum shear strain of AM bundle under AT load was 0.13 at 45°, and 0.09 at 90° for PL bundle.

Under other external loads (IR, ER, VAL), the calculated longitudinal, transverse and shear strain of AM and PL bundles are shown in Figure 27, Figure 28 and Figure 29. The maximum longitudinal strain of AM and PL bundle under external rotation load and valgus rotation load were both at full knee extension, while under internal rotation load, it occurred at 30° knee flexion.

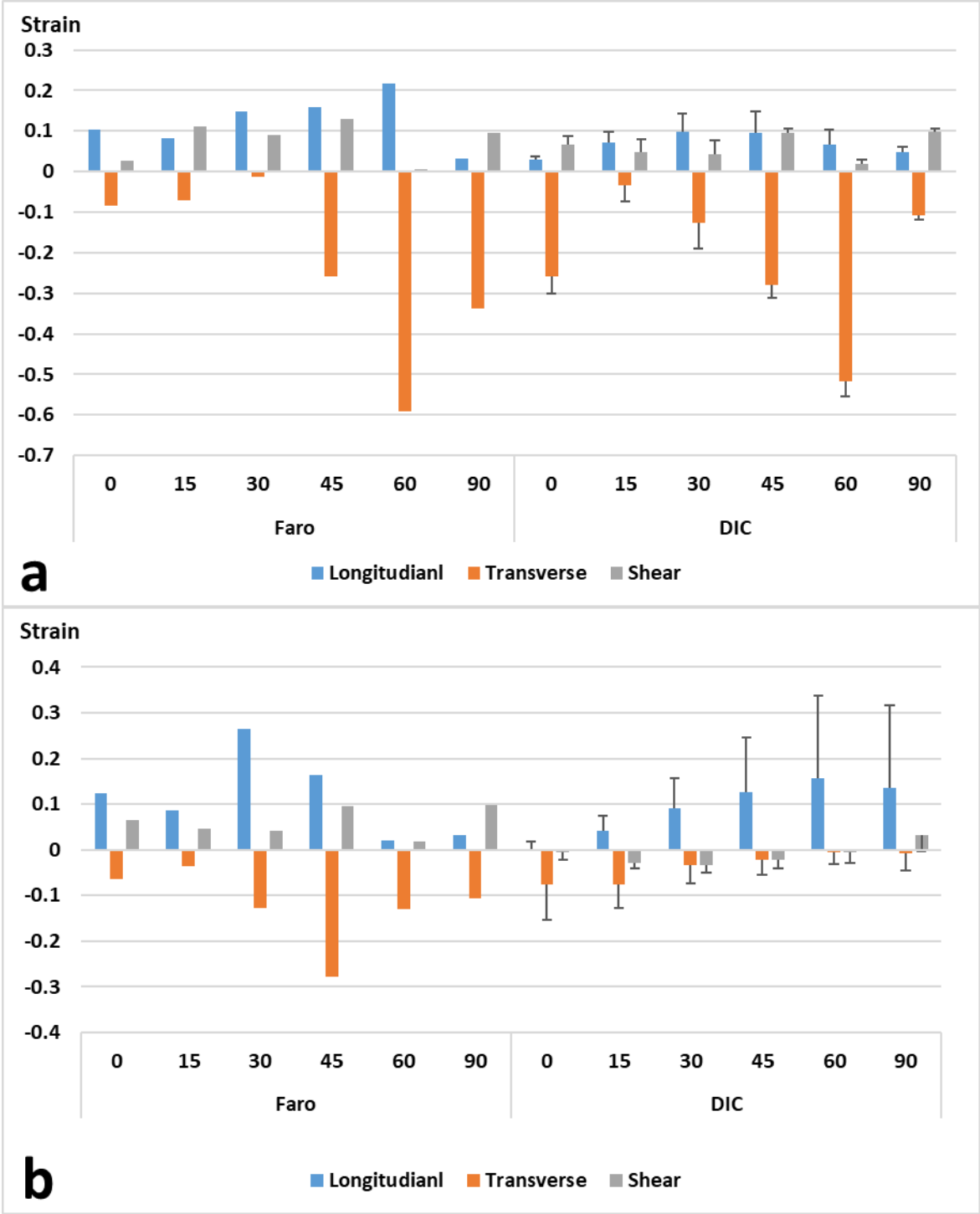


Figure 26: Strain of a) AM and b) PL bundle under anterior tibial load calculated from and scanning comparing to the DIC measurement results

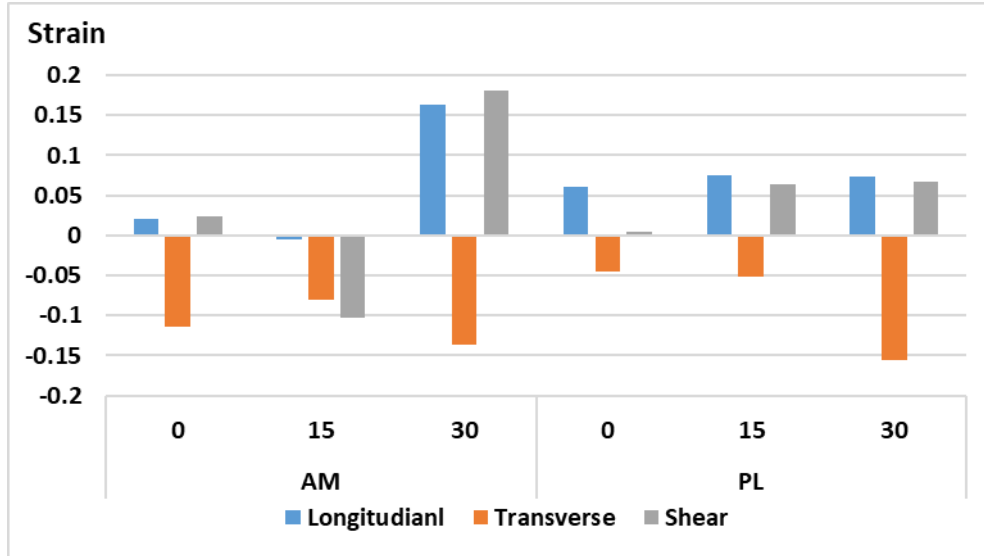


Figure 27: Strain of AM and PL bundle under internal rotation load, calculated from markers and scanning

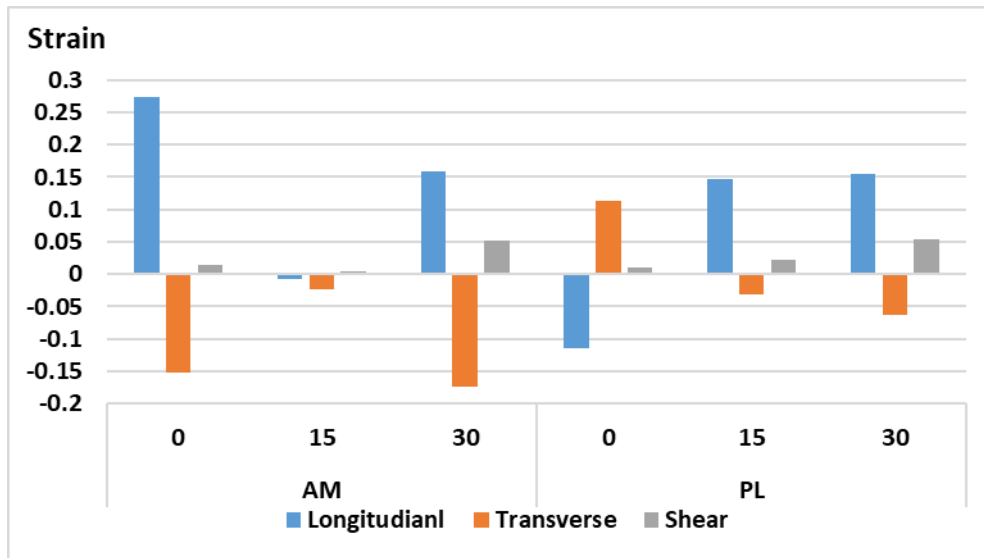


Figure 28: Strain of AM and PL bundle under external rotation loads, calculated from markers and scanning

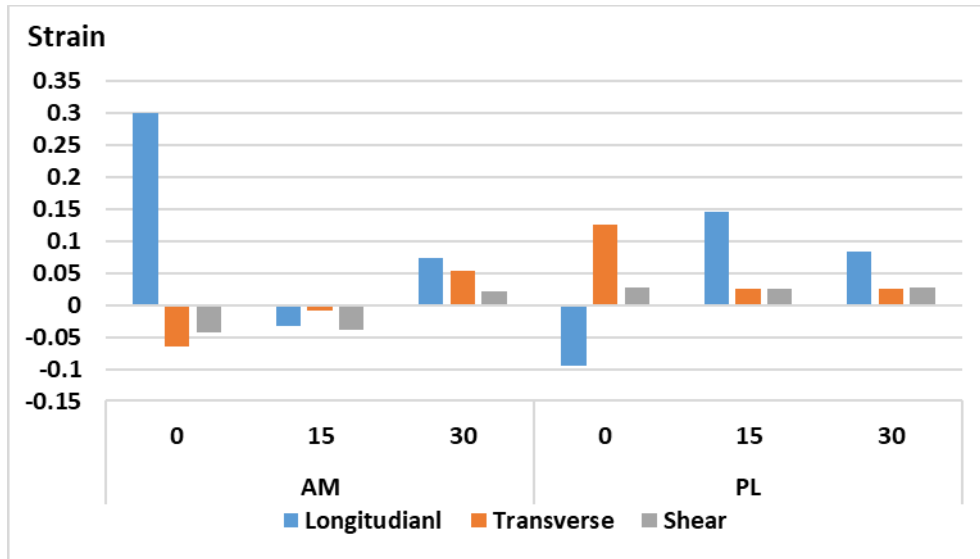


Figure 29: Strain of AM and PL bundle under valgus rotation loads, calculated from markers and scanning

Two methods were used in to measure the strain of the AM and PL bundles under external loads. The method with the bead markers does not match the result of DIC measurement. Especially at full extension, the bead marker measurement had the largest longitudinal strain for AM bundle under AT, ER (Figure 28) and valgus rotation (Figure 29) load at full extension, which is does not seem reasonable in that the knee had the smallest displacement or rotation under external load at full extension. *Table 5* gives the longitudinal strain of AM bundle under external loads of one sample (Sample F170840R), calculated from both DIC and laser scanning measurement. The bead and laser scanning had greater values of longitudinal strain, seemingly inaccurate when compared to DIC measurement. This might be caused by the limited scanning angle. This means to have a accurate measurement of the marker, the markers need to be scanned all angles. With limited scanning angle, the position of the marker may be affected. From 15° to 60° knee flexion, marker measurement shows similar trend in longitudinal strain with the DIC measurement. However the strain values are greater than the

ones from DIC measurement. This may be caused by several reasons. The first reason is that the size of the marker is relatively big compared to the size of the ACL. The laser scanner may not be able to access the full range of scanning angle for a good quality scanning. Second is that more of the error could have been introduced in laser scan measures. Manually selecting and determining centroid of the marker from scanned image could introduce inaccuracies. And also markers may be in contact with other soft tissue during knee loading or motion and change its relative position on the ACL.

Strain measurement with markers has been proved to be successful in measuring soft tissue strains by some researchers[48, 67, 141, 161, 182]. Ellis et al. used 21 markers with 2.38 mm diameter on MCL defined 18 regions for strain measurement under valgus with camera tracking system. The MCL is a broad, flat, membranous band compared to ACL, situated on the medial side of the knee joint[48]. So, it is relatively easy to have a big view angle for the bead markers. Wren et al. measured the mechanical properties of the human Achilles tendon with 10 1-mm diameter beads. Beads were glued at intervals (1-1.5 cm) along the length of the tendon to serve as visual markers. The sample was load axially with different strain rates[182]. Due to small size of the ACL, the beads were glued in one column and only axial loading was applied and only strain in loading direction can be measured. Screen et al. measured local strain within tendon matrix with cell nuclei as biological markers. During both loading and unloading of the tissue, samples were strained in a custom-designed rig, allowing real-time visualization of cell nuclei, on a confocal microscope[161]. Although the strains recorded are strongly dependent on the associations between the cells and the surrounding collagen matrix, their study shows that the marker size should be adjust based on different size of object to provide an accurate analysis of local strains of soft tissues. Future work could consider using smaller size markers to reduce the

error in the step of determining markers' position in the laser scan and take advantage of other faster and effective (real-time) motion analysis systems.

Table 5: Longitudinal strain of AM bundle under external loads, calculated from DIC and laser scanning measurement (Sample F170840R)

		ATT	IR	ER	VAL
0	DIC	0.03	0.03	0.00	0.03
	Laser	0.10	0.02	0.27	0.30
15	DIC	0.10	0.08	0.04	0.08
	Laser	0.08	0.00	-0.01	-0.03
30	DIC	0.11	0.08	0.04	0.04
	Laser	0.15	0.16	0.16	0.07
45	DIC	0.07	N/A	N/A	N/A
	Laser	0.16	N/A	N/A	N/A
60	DIC	0.07	N/A	N/A	N/A
	Laser	0.22	N/A	N/A	N/A
90	DIC	0.07	N/A	N/A	N/A
	Laser	0.03	N/A	N/A	N/A

4.4 CONCLUSION

In this study two methods were used to measure the strains of the two bundles of the ACL at the different flexion angles and external loadings. Longitudinal, transverse and shear strain are measured by using the DIC technique and compared with laser scanning measurements based on surface markers. Statistical analysis was done using one-way ANOVA with significance at $p < 0.05$. Statistical analyses were performed to: (i). compare the strain of AM and PL bundle at different flexion angle and external loadings; (ii). compare the strain between different flexion angle and external loadings. The data demonstrated that the two bundles of the intact ACL possess different strain patterns under flexion and external loads. The PL bundle has higher longitudinal strain under anterior load at high flexion angle, while the AM bundle has higher longitudinal strain at relatively low flexion angles. Though rotational loads do not cause significant ACL longitudinal strain, internal rotation caused a larger longitudinal strain in both bundles of the ACL than under external rotation.

The main contributions of this study include:

(1). The DIC technique was used to measure the strain in AM and PL bundles in an experimental setup which applied anterior tibial load and internal/external/valgus moments to the knee. The experiment setup allows the knee to be tested in an anatomical position, in order to provide more appropriate results. Only a limited number of studies can be found in measuring the strain behavior of AM and PL bundles under external load. This study provides the experimental design and measurement technique for more sophisticated studies.

(2). The DIC measurements show that AM and PL bundles are not isometric during knee flexion-extension and possess different patterns of strain, the main differences being increase in longitudinal strain of the AM bundle and decrease in longitudinal strain of the of the PL bundle

during flexion. The strain of AM and PL bundles can be correlated with their length changing as the knee flexed. There are reports of isolated ruptures of the AM or PL bundle[139]. The different behavior of two bundles during flexion/extension and under external can help explain the cause of individual ACL bundle ruptures by relating the strain behavior of two bundles to the external loads.

There are some limitations in this study. First, since the ACL has a complex shape, in the current project surgeon inspection was used to identify the AM and PL bundles.. To reduce this error in the study, all samples were dissected, prepared and bundle insertions sites marked by a single surgeon. Secondly, the fibres of the ligament are twisted to a varying degree as the knee flexes due to relative rotation of the attachments. Thus the straight line presumption that the AM and PL bundle are straight fibers connecting insertion sites when determining the longitudinal axis of the bundles is not accurate. Third, although a three-dimensional measurement method was used, the range and angle of capturing by the cameras is still limited. Through evaluation, the cameras were placed with the largest viewing angle to the AM and PL bundle. Last, there might be thickness change in the direction that is perpendicular to the measuring surface (z-direction) occurred in the ACL. Since soft tissue such as ligament is nearly compressible, thickness change could cause a result in the measuring plane that AM or PL bundle with a large longitudinal strain but small transverse and shear strain at the same flexion angle. However, in the current experimental setup with two cameras, this change in z-direction (or thickness) was not able to be viewed or measured.

5.0 MEASUREMENT OF ACL GRAFT POSITION IN TUNNEL UNDER VARIOUS KNEE MOTIONS AND LOADINGS

5.1 BACKGROUND AND SIGNIFICANCE

The motivation for the current hypothesis, that the ACL graft shifts and rotates in the femoral tunnel during knee flexion-extension and under external loadings, is the tunnel enlargement phenomenon and concepts as the “bungee cord” and “windshield” wiper effects in ACL reconstruction. It has been suggested that mechanical effects may be cause of tunnel enlargement graft motion in the tunnel may be related to this. Graft motion or shift and varying graft-tunnel contact could cause stress concentrations and tunnel enlargement.

Recent studies have shown that in ACL reconstruction, a space is frequently observed at the tunnel aperture[61]. This is mainly attributable to graft deformation. Studies have suggested that even though the femoral tunnel is positioned in the center of the footprint, the centroid of the graft may be deviated from the footprint due to the graft shift[61]. Also, the graft may shift its position under external loadings. Quantitative data on graft position in the tunnel with knee flexion and loading is not available.

Femoral tunnel enlargement after ACL reconstruction has been noticed clinically. While early reports suggested that bone tunnel enlargement is mainly the result of an immune response to allograft tissue, more recent studies imply that other biological as well as mechanical factors

may play a more important role[162]. Biological factors associated with tunnel enlargement include immune response against allografts, inflammatory response, cell necrosis due to toxic products in the tunnel, and heat necrosis as a response to drilling [49, 75]. Mechanical factors contributing to tunnel enlargement could include stress deprivation of bone within the tunnel wall, graft-tunnel motion, improper tunnel placement, and aggressive rehabilitation[80, 177].

Jagodzinski et al. used MRI to calculate force components of the graft for the femoral tunnel in the sagittal direction as well as coronal plane. By determining the angle between graft and the tunnels, vector analysis was used to calculate the direction and magnitude of the perpendicular component of the force between the bone tunnel and the graft at the entrance of the bone tunnel. The differences in force components calculated in this study corresponds with the amount and location of tunnel enlargement in the radiographic planes and provided evidence that biomechanical forces play a key role in postoperative tunnel expansion[81].

Fujii et al. measured the semitendinosus tendon graft shift, defined as the distance between the center of the simulated tunnel and the center of the graft on the 2-dimensional coordinate, at the tunnel aperture with graft bending using a simulated femoral bone tunnel. The semitendinosus tendon was harvested, folded and verified to be 7.0 mm. A custom-made aluminum fixture, with 7.0-mm-diameter hole was used as a simulated femoral bone tunnel. The distal end of the graft was tensioned with 30 N at an angle of 15°, 30°, 45°, 60°, 75° that reproduced the graft bending angle during knee range of motion. The results showed that the graft shift significantly increased when the graft bending angle was increased. The largest shift was observed when the graft bending angle was 75° in all specimens, and the value was 1.10 mm \pm 0.12. [61].

Lee et al. evaluated and compared the graft filling area and graft position within the femoral tunnel aperture in two ACL reconstruction techniques using MRI. They found that grafts did not fill the entire tunnel aperture area, and the centers of the grafts differed slightly from the centers of the tunnel apertures. The eccentric graft positioning in the tunnel with shift in a particular direction in each technique might suggest the necessity of an underreamed femoral tunnel [101].

In a clinical MRI study by Onodera et al. on double-bundle ACL reconstruction, two different MRI protocols were used to measure the shift of grafts in the tunnels. In the first method, the graft location was evaluated on an inclined sagittal multiplanar reconstruction (MPR) image taken using a standard T2-weighted protocol. The second method used a pure axial MPR image using a VISTA (volume isotropic turbo spin echo acquisition) protocol. They concluded that the grafts were not shifted anteriorly in the femoral tunnel 1 year after anatomic double-bundle ACL reconstruction. The PL graft was located approximately at the center of the tunnel outlet, while the AM graft was slightly but significantly shifted posteriorly and proximally [128].

5.2 METHODS

Six human cadaver knees were used in this study for measuring the ACL graft position in femoral tunnel under knee flexion and external loads. The protocol used in this study, along with the methodology for testing each specimen, can be described in three parts: 1) specimen preparation; 2) robotic testing and 3) geometric scanning and analysis. All cadaveric knee

specimens underwent arthroscopic check by an orthopedic surgeon to ensure that all structures were intact. The flowchart for this study is shown in Figure 30.

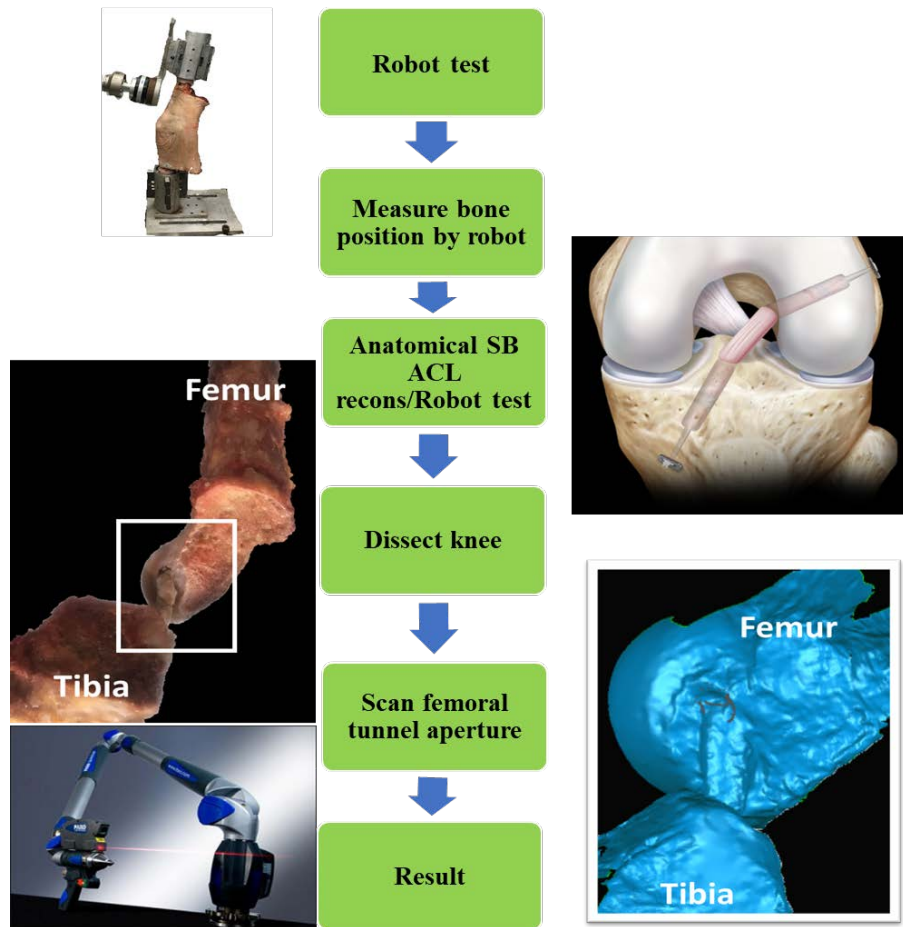


Figure 30: Flowchart of studying graft position in tunnel under various knee motions and loadings

5.2.1 Specimen Preparation

Preparation for testing followed the same protocol as described in Chapter 4.2.1. Anatomic single bundle ACL reconstruction was performed in all knee specimens via arthroscopy by the same surgeon [13, 36, 144]. The intact ACL was first excised and removed with the use of a punch, a shaver and an ablator. During removal, the ACL insertion sites on the tibia and femur were marked with an awl and ablator. Previously harvested human cadaver hamstring grafts were

used. The grafts were passed the loop of EndoButton (Smith & Nephew, UK), then folded and used a ultra-braided sutures with a tapered needle to fix the free end. The ACL graft was trimmed to be 8-mm in diameter. A guide wire (2.4 mm diameter) was inserted into the center of femoral ACL footprint and the femoral tunnel was drilled with a 7.5-mm cannulated femoral drill and dilated with an 8-mm dilator through the accessory medial portal. Another guide wire was inserted into the center of tibial ACL footprint from the anteromedial aspect of tibia using a tibial drill guide system (Smith and Nephew Endoscopy, Andover, MA). The tibial ACL aimer angle was set to 55° and the tibial tunnel was opened with a 7.5-mm drill, and then dilated with an 8-mm dilator, then the graft was passed through the tibial tunnel. EndoButton (Smith & Nephew, UK) was flipped and fixed to the outside of the femur. Following graft placement, twenty plunging movements were applied to the knees for pre-tensioning. The hamstring graft was tensioned at 30° of knee flexion under 40 N force using a tension-meter (Meira Corp., Nagoya, Aichi, Japan) from the distal end of the graft and a metal interference screw was placed in tibial tunnel on the tibia for fixing the graft [169]. Additionally, post-tie fixation was also applied to augment tibial fixation [31].

5.2.2 Robotic Testing

The knees were kept moist with physiologic saline solution during testing. A six-joint robotic system with a repeatability of motion within ± 0.02 mm at each joint, with a force-moment load cell that has an accuracy of ± 0.2 N and ± 0.1 Nm according to the manufacturer, was used for testing the knee specimens [86, 88, 154]. The potted tibia and femur were placed upside down in aluminum cylinders with tibial cylinder connected to the robotic arm and the femoral cylinder was fixed to a stationary base. The passive path of the intact knee flexion–extension was

determined from full extension of the knee to 90° of knee flexion in 0.5° increments by minimizing forces ($< 0.5 \text{ N}$) and moments ($< 0.25 \text{ Nm}$) in all remaining degrees of freedom [41].

The knee joints were subjected to the following loading conditions: (1) an 89.0-N anterior tibial (AT) load (simulated KT1000 test) to test anterior tibial translation (ATT) (mm) [147], (2) a 5.0-Nm internal tibial torque to test internal rotation (IR) (degrees), (3) a 5.0-Nm external tibial torque to test external rotation (ER) (degrees) [88], (4) a 7.0-Nm lateral bending moment to test valgus rotation (degrees) and (5) an 89.0-N posterior tibial (PT) load to test posterior tibial translation (PTT) (mm) [19, 20]. The ATT and PTT was measured at full extension, 15°, 30°, 45°, 60° and 90° of knee flexion, while internal/external and valgus rotations were measured at full extension, 15° and 30° of knee flexion [86].

5.2.3 Geometric Scanning and Analysis

During robotic testing, the three-dimensional surface geometry of specimen including lateral femoral condyle, ACL graft as well as the femoral tunnel aperture were scanned and probed using a digitizer (FARO Technologies Inc. Lake Mary, FL) (Figure 31a, b). The digitizer is a portable coordinate measuring machine (CMM) that allows combination of contact and non-contact 3D scanning for detailed measurement of surface. It was mounted on a metal plate and fixed knee base. The scanner coordinate system was defined by the anatomical position of the knee, with its x, y, z coordinates corresponding to medial-lateral, superior-proximal, anterior-posterior direction with respect to the femur. After robotic testing, the graft was removed from the tunnel so that the femoral tunnel was exposed for scanning. The femoral tunnel without graft was scanned and the tunnel aperture outline was measured using a probe (Figure 31c, d). The

scanning data was processed using graphics software (Geomagic, Research Triangle Park, North Carolina).

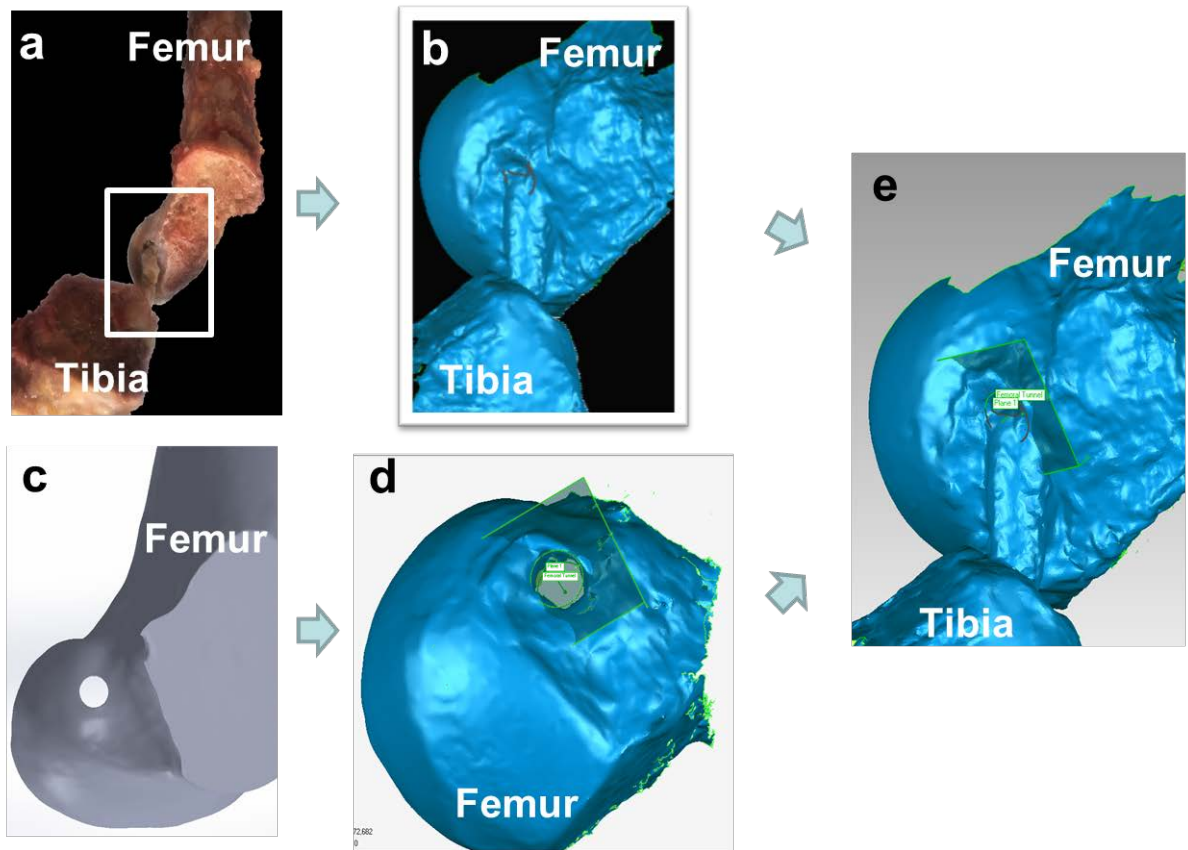


Figure 31: (a) Dissected femur with single-bundle ACL reconstruction; (b) Scan of the sample with ACL graft; (c) Femur geometry from CT scan; (d) Scan of the sample with ACL graft removed and (e) Combination of two scans

To determine the position of the ACL graft in the tunnel, the femoral tunnel was represented by a cylinder which was calculated by a best fit of an 8-mm cylinder to the scan data of the tunnel inner wall (Figure 32a). Due to individual variation of the femoral bony insertion geometry, the femoral tunnel aperture shape will be different between samples even when the drilling angle was kept constant. To standardize the graft tunnel aperture to define the graft position in the tunnel, a plane which contained the centroid of probed aperture outline points was

defined and taken to be perpendicular to the femoral tunnel longitudinal axis (Figure 32b). So, results will be based on an 8-mm diameter circle that best fits the femoral tunnel aperture.

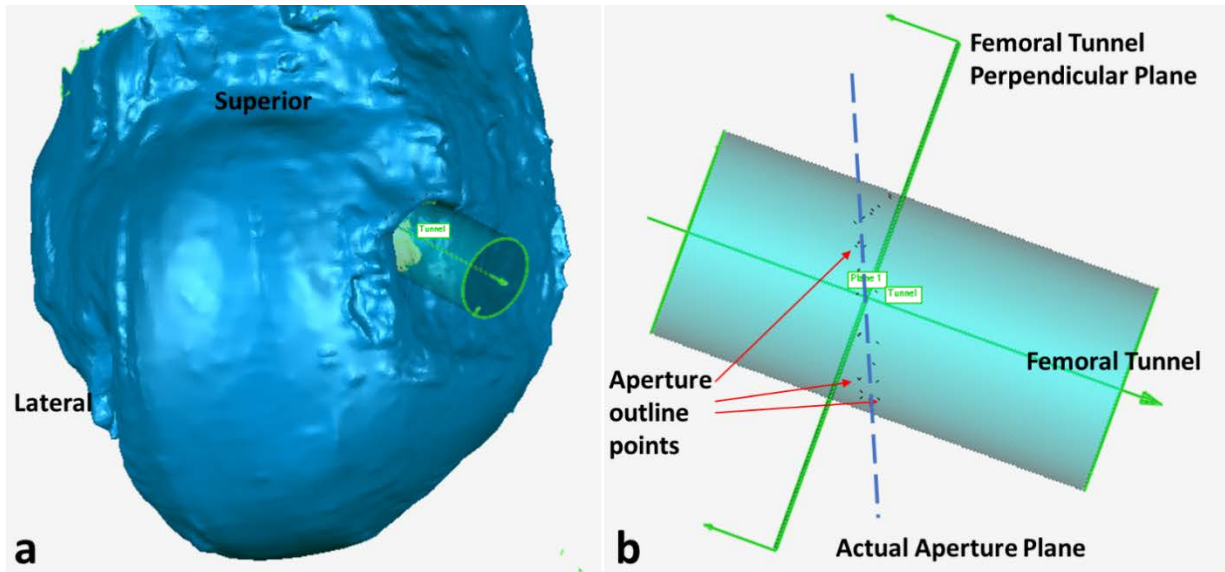


Figure 32: a) Scan of the lateral condyle and the fitted femoral tunnel; b) Standardized plane that is perpendicular to the femoral tunnel.

To determine the cross-sectional outline of the tunnel and graft at the standardized plane, both scan results, with and without the graft, were imported to the software. The two geometries were overlapped and were trimmed in software with the femoral tunnel perpendicular plane that was defined in the previous step (Figure 33). On this trimmed surface, the intercept curve between the femoral tunnel cylinder and surface would be the outline of the graft at the aperture (Figure 33).

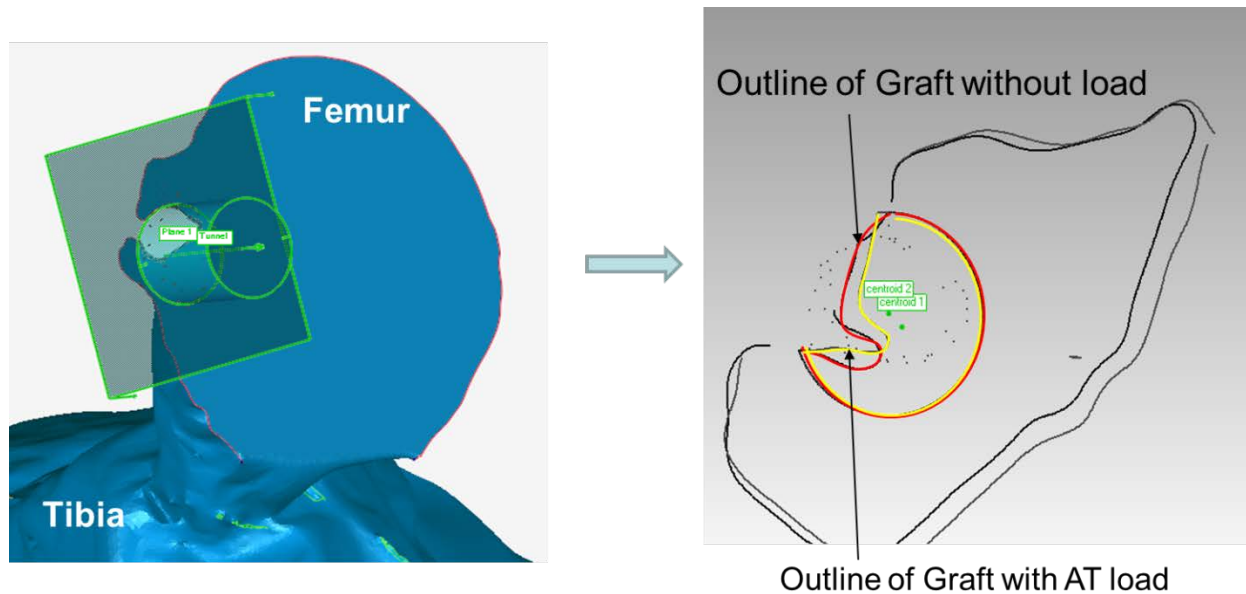


Figure 33: Left: The intercept curve between the femoral tunnel cylinder and the trimmed surface was defined as the outline of the graft at the aperture; Right: Outline of the graft at the standardized plane of the femoral tunnel with (yellow) and without (red) AT load.

Points there were created from the graft outline in software (Geomagic, Research Triangle Park, North Carolina), with a spacing of 0.01mm to assure the accuracy of calculation, were used to find the graft centroid position. The center point of the graft was determined by finding the centroid of the outline and the distance between the two centroids before and after knee motion or loading, was designated as the graft shift distance (Figure 34). Also, the center of the femoral tunnel was determined to describe the relative position of the graft center to that of the femoral tunnel. The percentage of femoral tunnel aperture that was filled by the graft was also calculated as the ratio of the cross-sectional area of graft to the area of the 4-mm radius tunnel (Figure 34).

The contact region between the graft and the tunnel was calculated by finding the portion of graft's outline that overlapping with the femoral tunnel's outline (Figure 34). The mid-point of

the contact region on the standardized plane was also calculated so that the angular of contact region could be calculated.

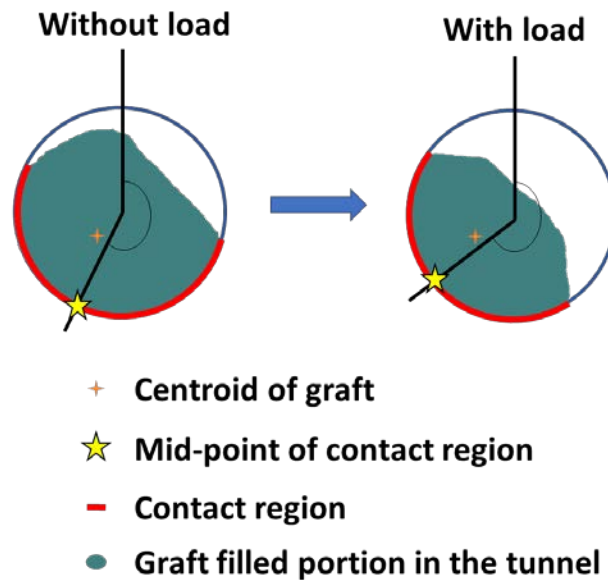


Figure 34: Graft centroid position change, percentage of the femoral tunnel been filled by the graft, percentage of contact region and the rotation of the contact region (vertical axis: superior direction based on femur).

5.3 RESULTS AND DISCUSSION

The described method was applied to six human cadaver knees (3 left, 3 right). Since the right knee has the same anterior-posterior and superior-inferior orientation but opposite medial-lateral orientation compared with left knee. All the data in this section are converted and shown based on right knee orientation.

5.3.1 Kinematics and In-Situ Force

For informational purposes, the kinematics (*Table 6*) and in-situ force (*Table 7*) for all samples was also measured during testing. For the intact knee, anterior tibial translation (ATT) in response to an 89 N anterior tibial load ranged from 5.4 ± 1.7 mm at 90° flexion to 8.1 ± 1.7 mm at 30° of flexion (*Table 6*). Posterior tibial translation in response to an 89 N posterior tibia load ranged from 3.5 ± 0.8 mm at 90° flexion to 7.3 ± 2.3 mm at 15° of flexion. In response to the 5 Nm rotational loads, internal rotation increased with increasing knee flexion and reached a maximum of $23.8^\circ \pm 3.6^\circ$ at 30° flexion. Similarly, external rotation angle was $12.6^\circ \pm 3.0^\circ$ at full extension (FE) but increased to 18.3 ± 5.3 at 30° of flexion. In response to the 7 Nm valgus moment, rotation ranged from $2.7^\circ \pm 0.5^\circ$ to $3.9^\circ \pm 1.2^\circ$ from full extension to 30° of flexion.

Removing the ACL significantly increased anterior tibial translation, it was nearly twice as large as that with the ACL intact, ranging from 9.6 ± 1.5 mm at 90° of knee flexion to 16.5 ± 1.8 mm at 30° flexion (*Figure 35*). No statistical significance was found in posterior tibial translation, internal/external rotation angle and valgus angle between ACL intact knee and ACL deficient knee. These results implied that ACL was the main constraint of the ATT and only provide a secondary constraint for posterior tibial translation, internal/external rotation and valgus rotation.

Table 6: Tibia displacement and rotation under external loads in intact, ACL deficient and ACL reconstructed knee (* indicates statistical significance compared to intact states)

		ATT (mm)	PTT (mm)	IR (degree)	ER (degree)	VAL (degree)
EF	Intact	5.5±1.7	7.0±0.4	13.3±4.7	12.6±3.0	2.7±0.5
	DEF_ACL	10.5±2.9*	7.3±1.6	14.7±4.6	13.0±3.6	2.8±0.6
	Recon.	3.3±2.0	7.1±1.0	10.5±2.6	11.6±2.4	2.6±0.5
15	Intact	7.3±1.9	7.3±2.3	21.0±4.5	16.5±4.6	3.8±1.1
	DEF_ACL	15.0±2.6*	7.5±2.2	21.7±4.6	16.7±4.9	3.8±1.0
	Recon.	5.6±3.7	7.5±1.9	19.0±3.9	16.0±4.5	3.5±1.0
30	Intact	8.1±1.7	5.7±1.9	23.8±3.6	18.3±5.3	3.9±1.2
	DEF_ACL	16.5±1.8*	5.8±1.9	23.9±3.7	18.4±5.5	4.0±1.1
	Recon.	6.9±3.4	5.9±1.6	22.4±3.8	18.3±5.4	3.7±1.3
45	Intact	7.91±0.9	4.3±0.5	N/A	N/A	N/A
	DEF_ACL	15.1±2.2*	4.4±0.9	N/A	N/A	N/A
	Recon.	7.3±2.8	4.5±0.8	N/A	N/A	N/A
60	Intact	6.8±2.0	3.7±0.5	N/A	N/A	N/A
	DEF_ACL	12.2±1.8*	3.8±0.8	N/A	N/A	N/A
	Recon.	6.5±2.6	3.8±0.8	N/A	N/A	N/A
90	Intact	5.4±1.7	3.5±0.8	N/A	N/A	N/A
	DEF_ACL	9.6±1.5*	3.6±1.0	N/A	N/A	N/A
	Recon.	5.3±1.8	3.5±1.0	N/A	N/A	N/A

Table 7: In-situ force in intact ACL and graft under external loads

		ATT (N)	PTT (N)	IR (N)	ER (N)	VAL (N)
0	ACL	71.7±23.7	20.6±17.1	34.7±13.6	21.5±14.9	9.5±3.9
	Graft	71.7±31.0	18.2±10.2	40.7±20.0	15.3±12.3	22.2±9.6
15	ACL	92.4±7.7	19.0±21.2	22.8±21.7	15.7±7.6	8.8±3.6
	Graft	77.0±42.9	11.1±6.0	31.4±19.4	17.3±17.6	14.9±10.7
30	ACL	92.2±8.0	18.6±21.0	15.1±11.1	16.2±9.9	10.4±5.0
	Graft	73.5±40.5	9.5±4.5	19.3±14.1	12.0±9.3	13.1±6.5
45	ACL	81.8±11.0	18.5±16.3	N/A	N/A	N/A
	Graft	56.9±23.4	8.6±4.8	N/A	N/A	N/A
60	ACL	67.2±11.8	16.2±15.2	N/A	N/A	N/A
	Graft	40.4±23.0	7.1±3.7	N/A	N/A	N/A
90	ACL	62.0±14.4	12.6±8.5	N/A	N/A	N/A
	Graft	39.1±27.3	7.0±6.5	N/A	N/A	N/A

After ACL reconstruction, the ATT was restored being not significantly different from that of the ACL intact knee. However, the in-situ forces of the graft in the reconstructed knee in response to the same AT load were lower than those in intact ACL (Figure 36). When compared to intact ACL, the in-situ force of the graft under the same rotational loads and valgus were all significantly lower.

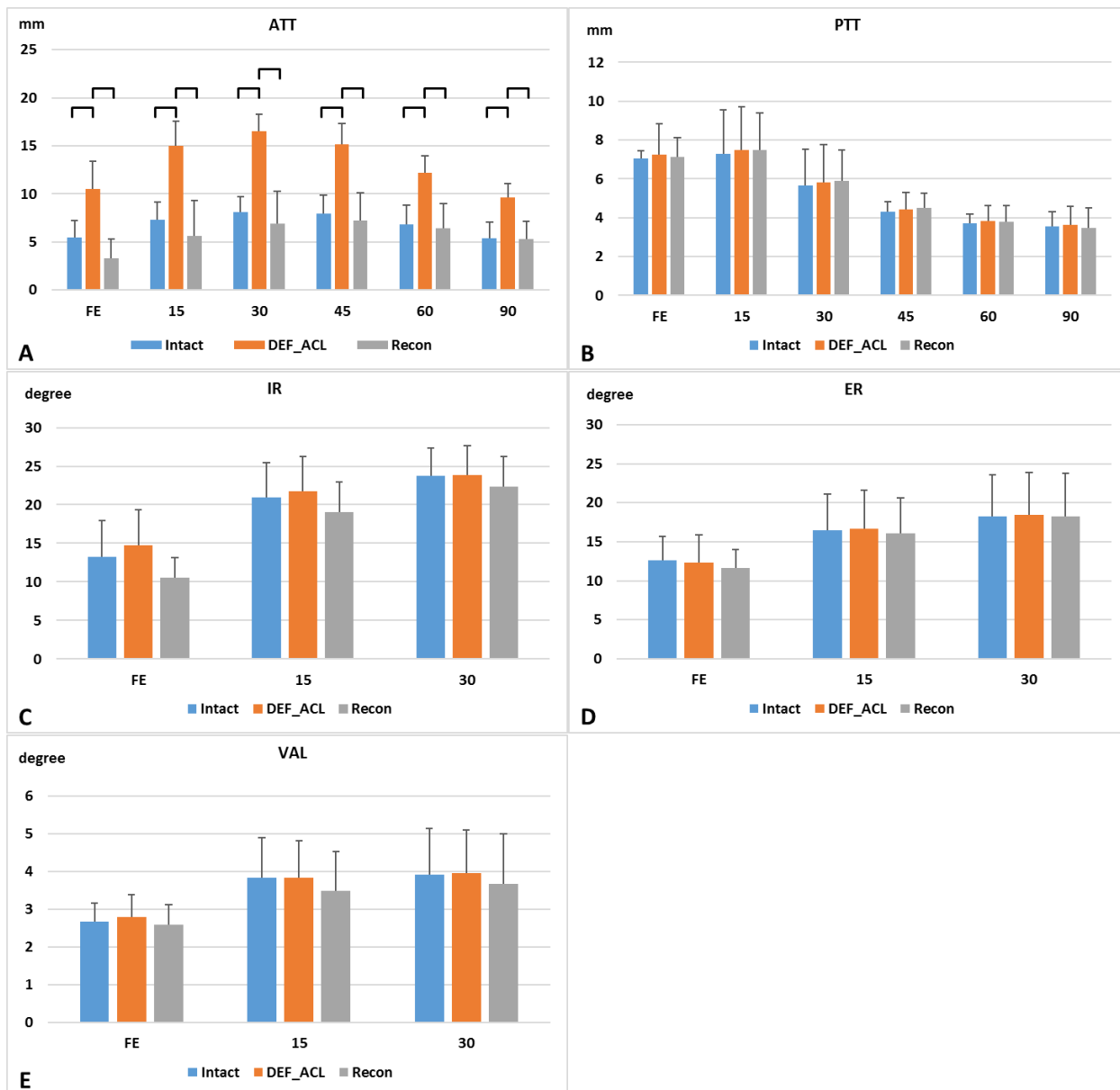


Figure 35: Tibia displacement and rotation of specimens with intact knee, ACL deficient knee and ACL reconstructed knee under: A) anterior tibial translation, B) posterior tibial translation, C) internal rotation, D) external rotation and E) valgus rotation

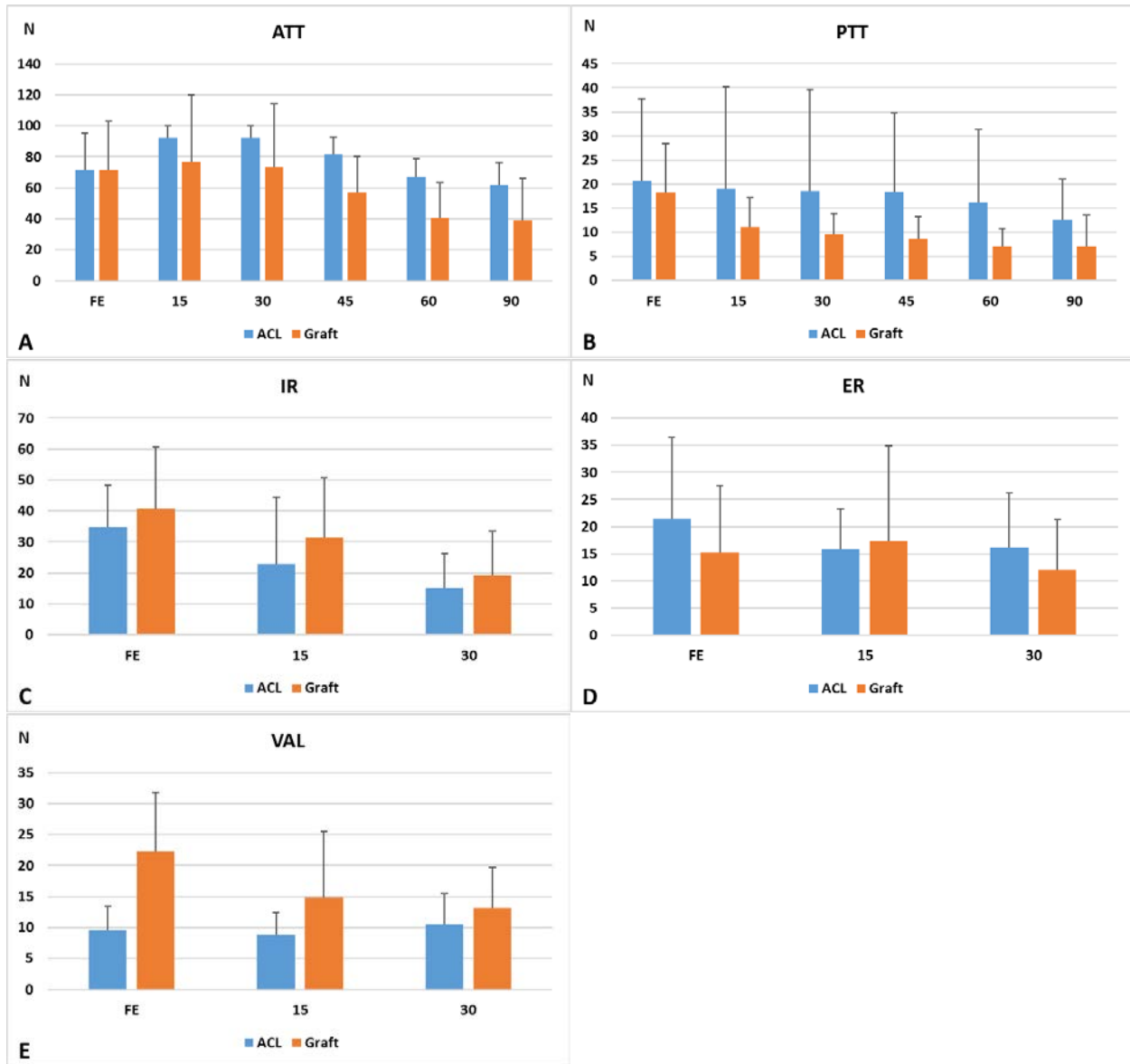


Figure 36: In-situ force in intact ACL and graft under: A) anterior tibial translation, B) posterior tibial translation, C) internal rotation, D) external rotation and E) valgus rotation.

5.3.2 Shift of the graft during flexion/extension and under external loadings

Figure 37 showed the magnitude of graft shift in femoral tunnel under passive flexion and anterior tibial (AT) translation, posterior tibial (PT) translation, internal rotation (IR), external rotation (ER), valgus rotation (VAL). During knee flexion from 0° (full extension) to 90° of knee flexion, the graft centroid was measured in full extension, 15°, 30°, 45°, 60° and 90° of knee flexion and compared to the graft position in the knee at full extension. The graft centroid shifted a magnitude of 0.21mm, 0.65mm, 0.68mm, 0.57mm, 0.67mm compared to the position in full extension knee (Table 8). The biggest shifted distance occurred at 45° knee flexion angle (0.68 ±0.45 mm), smallest shift appeared at 15° knee flexion angle (0.21±0.22 mm). The ACL graft shifted 0.67mm (8.4% of the tunnel diameter) from full extension to 90° flexion. It should be noted that the magnitude of the graft shift is being reported and may correspond to different directions of shifting.

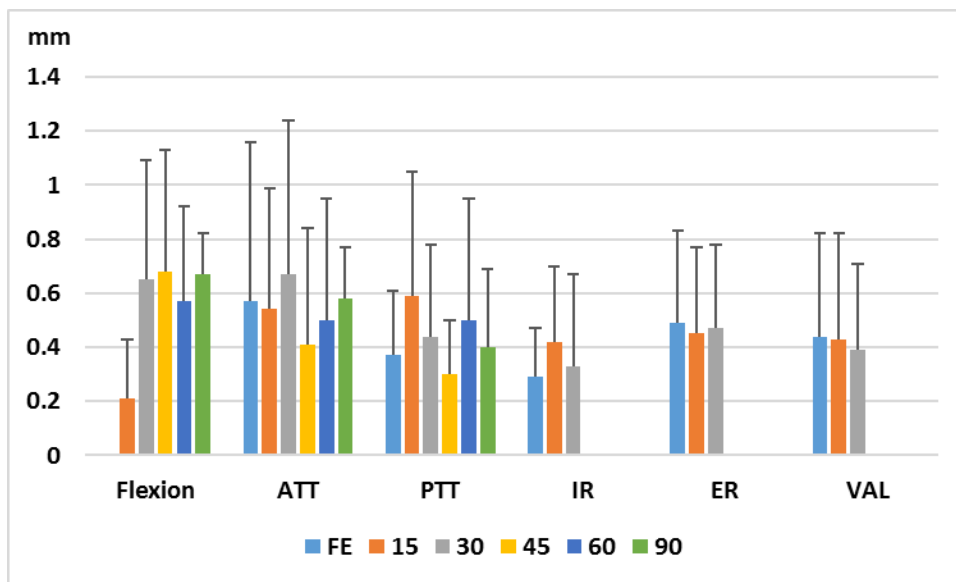


Figure 37: Magnitude of graft shift in femoral tunnel under passive flexion and external loading.

Table 8: Magnitude of graft shift with mean \pm standard deviation for each external loading condition and flexion/extension (F/E).

	F/E (mm)	ATT (mm)	PTT (mm)	IR (mm)	ER (mm)	VAL (mm)
0°	0	0.57 \pm 0.59	0.37 \pm 0.24	0.29 \pm 0.18	0.49 \pm 0.34	0.44 \pm 0.38
15°	0.21 \pm 0.22	0.54 \pm 0.45	0.59 \pm 0.46	0.42 \pm 0.28	0.45 \pm 0.32	0.43 \pm 0.39
30°	0.65 \pm 0.44	0.67 \pm 0.57	0.44 \pm 0.34	0.33 \pm 0.34	0.47 \pm 0.31	0.39 \pm 0.32
45°	0.68 \pm 0.45	0.41 \pm 0.43	0.30 \pm 0.20	n/a	n/a	n/a
60°	0.57 \pm 0.35	0.50 \pm 0.45	0.50 \pm 0.45	n/a	n/a	n/a
90°	0.67 \pm 0.15	0.58 \pm 0.19	0.40 \pm 0.29	n/a	n/a	n/a

Under AT loading, ACL graft shifted a magnitude of 0.57mm, 0.54mm, 0.67mm, 0.41mm, 0.50mm, 0.58mm at 0°, 15°, 30°, 45°, 60°, and 90° of knee flexion angle with an average shifted of 0.58mm (7.23% of the tunnel diameter) (*Table 8*). The largest shift occurred at 30° knee flexion angle (0.67 \pm 0.57 mm). Graft centroid shifts were in all three anatomical directions (medial-lateral, posterior-anterior and superior-inferior) (*Figure 38*). With AT load, the centroid of graft moved medially, anteriorly and inferiorly at all flexion angles. No significant difference was found in directional components between any two flexion angles.

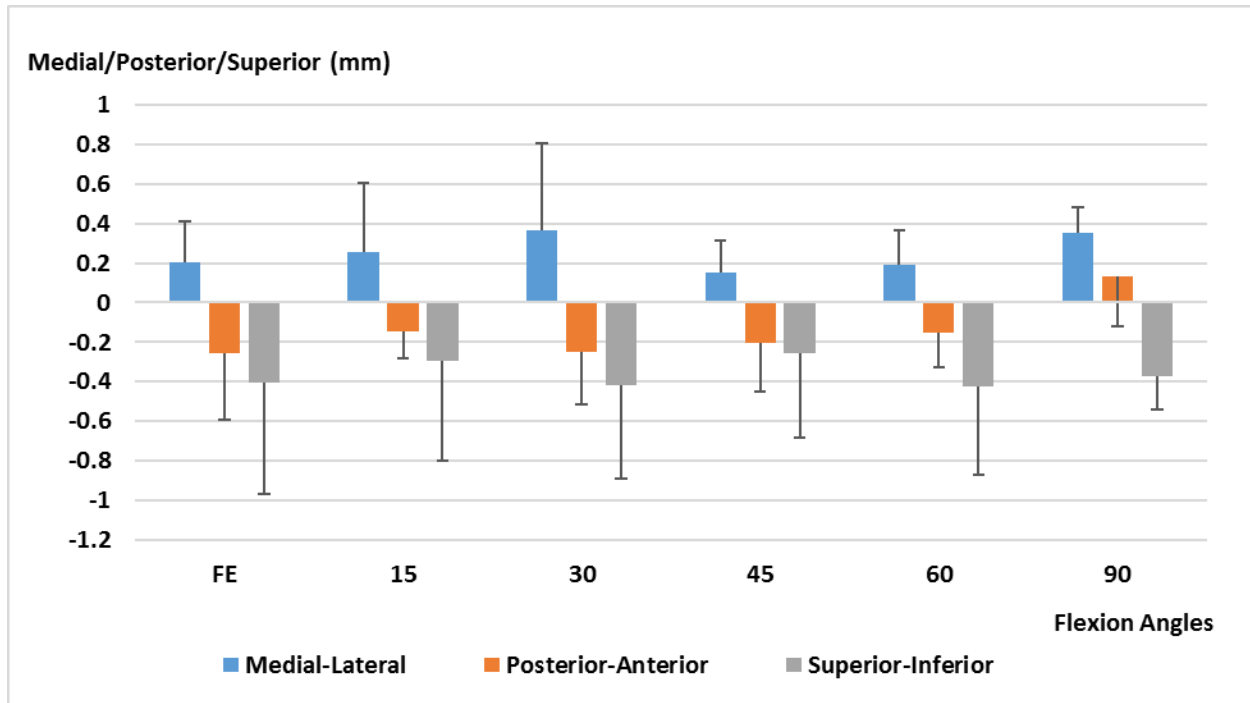


Figure 38: Change in graft centroid position under anterior tibial loading (89 N) and flexion extension.

Under external rotational torque, the ACL graft shifted a magnitude of 0.49mm, 0.45mm, 0.47mm at full extension, 15°, 30° of knee flexion, respectively, with an average shift magnitude of 0.47mm (5.9% of the tunnel diameter) under ER loading (Figure 39). With external rotational torque, the centroid of graft moved medially, anteriorly and inferiorly at full extension and 15° flexion, moved medially, posteriorly and superiorly at 30° flexion. However, no significant difference was found in directional components between any two flexion angles (Figure 39).

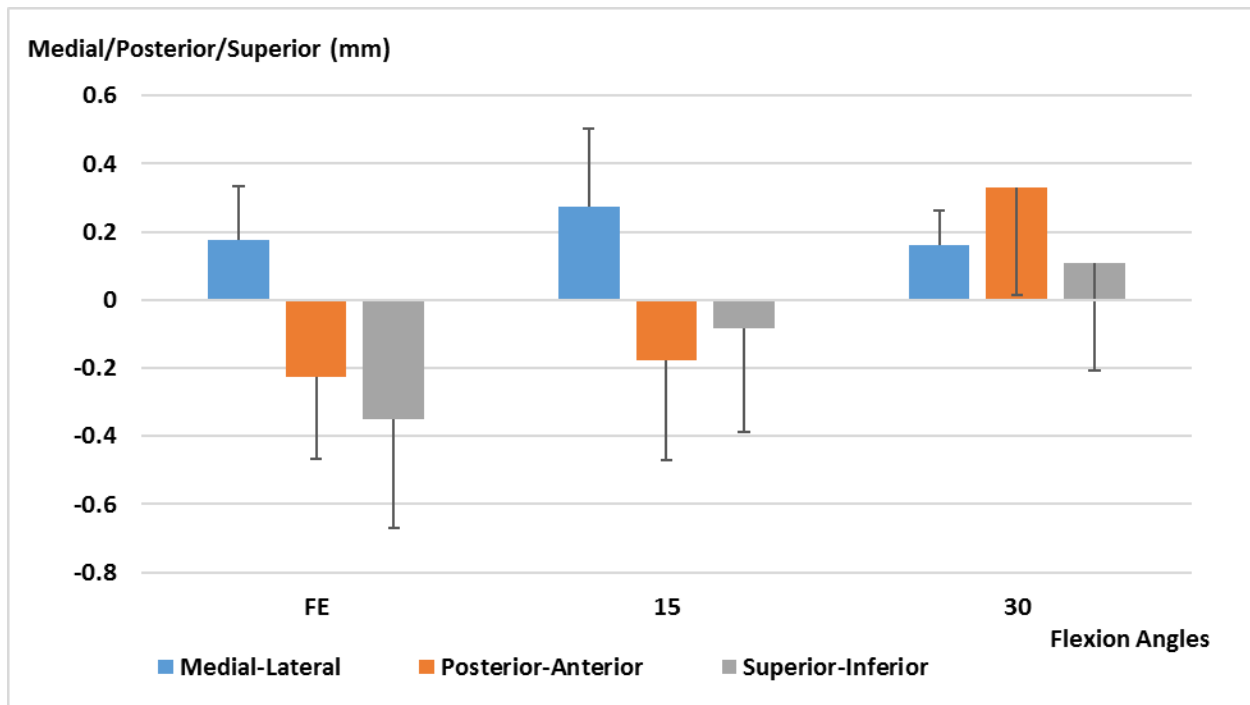


Figure 39: Graft shift under external rotational torque (5 Nm) and flexion extension

Under internal rotational torque, the graft centroid shifted a magnitude of 0.29mm, 0.42mm, 0.33mm at 0°, 15°, 30° of knee flexion angle with an average shift of 0.35mm (4.3% of the tunnel diameter) under IR loading (Figure 40). The directional components show that under IR load, the centroid of graft moved medially, posteriorly and superiorly. No significant difference was found in directional components between any two flexion angles. (Figure 40).

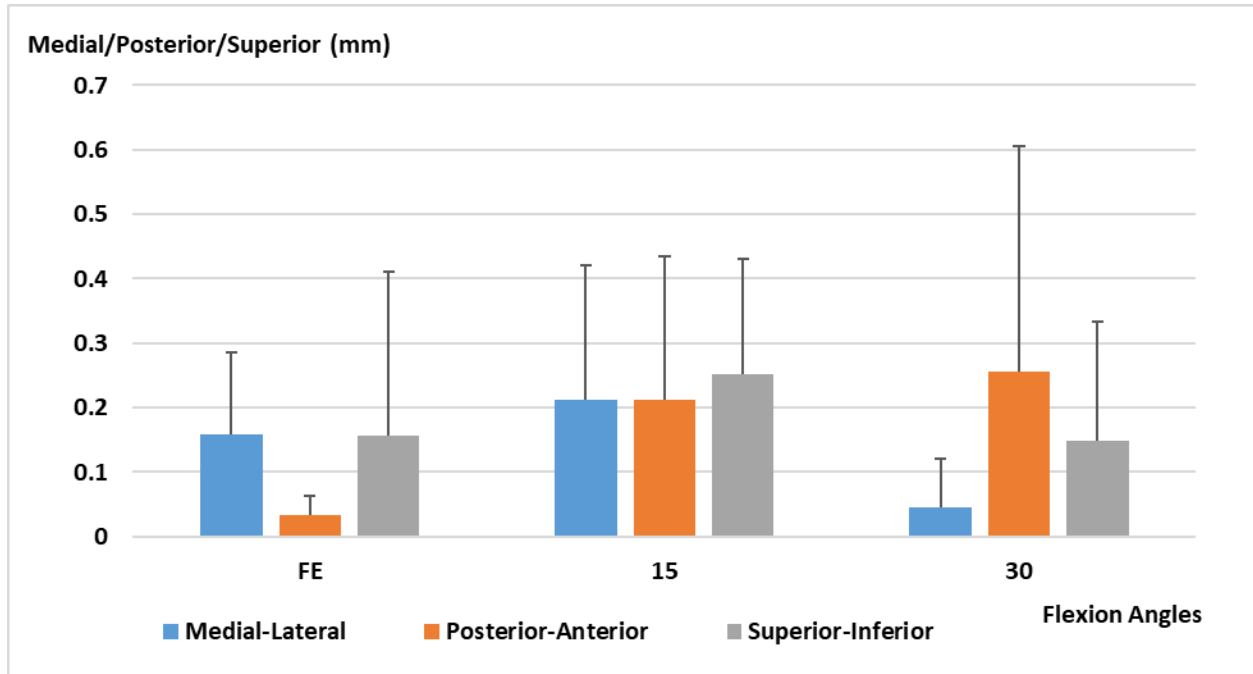


Figure 40: Graft shift under internal rotational torque (5 Nm) and flexion extension.

With 89N posterior tibial knee load, the graft centroid shifted a magnitude of 0.37mm, 0.59mm, 0.44mm, 0.30mm, 0.50mm, 0.40mm at full extension, 15°, 30°, 45°, 60°, and 90° of knee flexion, respectively, with an average shift of 0.43mm (5.4% of the tunnel diameter) (Figure 41). The largest shift occurred at 15° knee flexion angle (0.59±0.46mm). The directional components of the shift showed that under PT load, the centroid of graft moved medially at all flexion angles. Under PT load, the centroid of graft also moved posteriorly and inferiorly at low flexion angles and moved anteriorly and superiorly at high flexion angles. No significant difference was found in directional components between any two flexion angles (Figure 41).

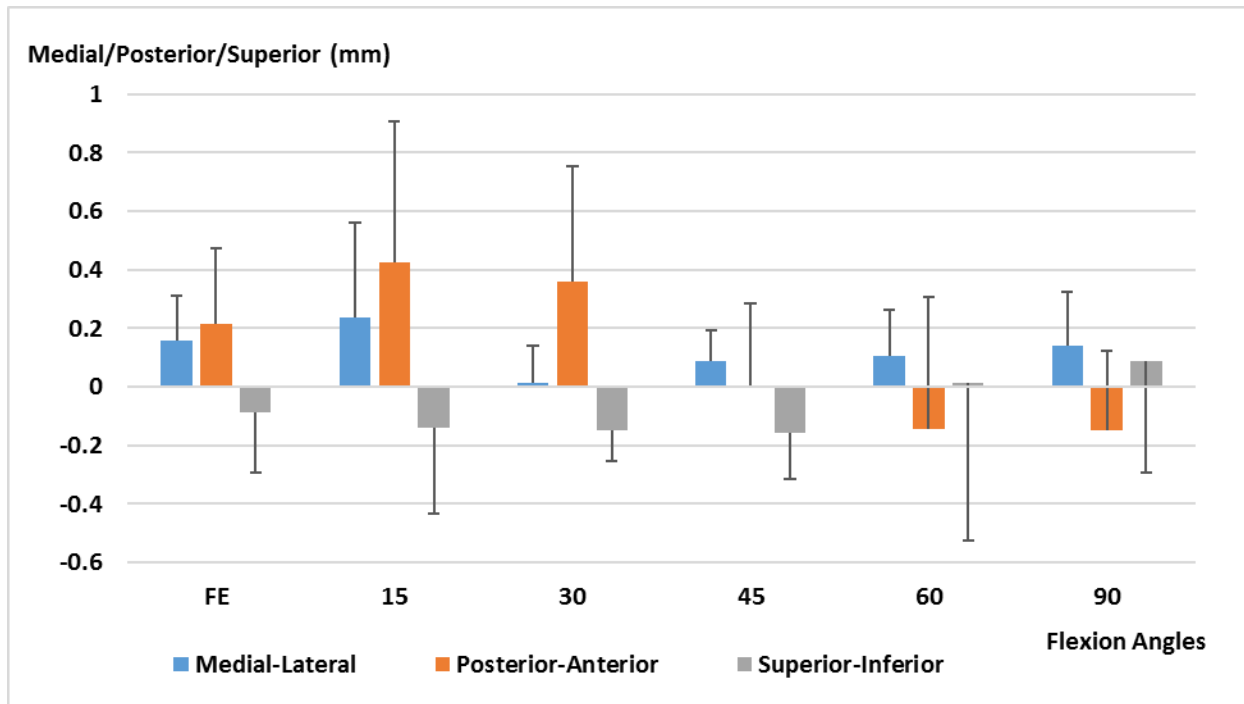


Figure 41: Graft position shift under posterior tibial load (89 N) and flexion-extension.

Under valgus loading, the graft centroid shifted a magnitude of 0.44mm, 0.43mm, 0.39mm at 0°, 15° and 30° of knee flexion, respectively, with an average shift magnitude of 0.42mm (5.3% of the tunnel diameter) (Figure 42). Directional components of the shift were also plotted in Figure 42. Results show that the graft centroid under valgus loading shifted medially and inferiorly at all flexion angles. Under valgus load, the centroid of graft also moved posteriorly at full extension and moved anteriorly at 15° and 30° flexion. No significant difference was found in directional components between any two flexion angles (Figure 42).

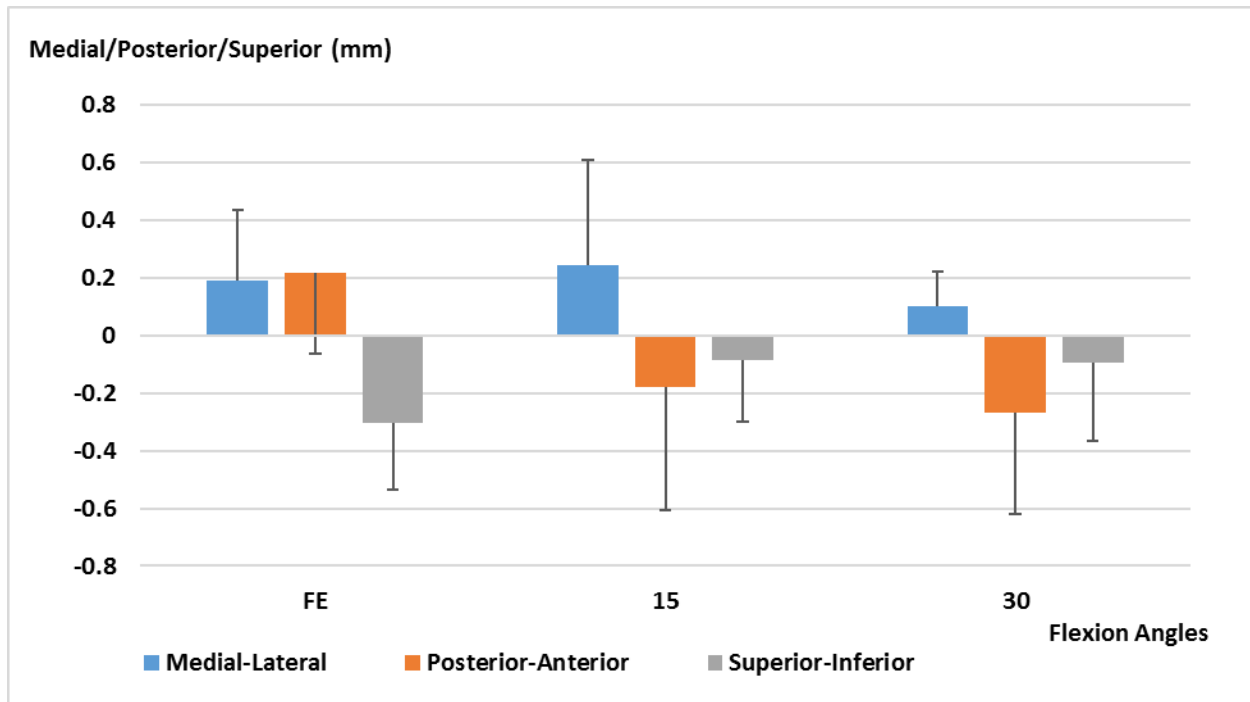


Figure 42: Graft position under valgus load (7 Nm) and flexion extension.

With hundreds of thousands ACL reconstruction being done every year, it is logical to question the importance of quantifying the ACL graft behavior that can lead to failure and tunnel enlargement. Visual inspection of the ACL tunnel and graft, a process that is often aided semi-automatically by most proprietary MR image processing software, can provide such qualitative assessment. However, visual inspection is insufficient to measure the degree to which the graft shifts and rotates or to determine the regional variations under external loadings and knee motions, with tunnel and graft outlines being scarcely assessable from MR images by the naked eye. Regarding knee stability, Kühne et al. concluded that there is no correlation between MRI findings and knee stability. A graft that appears good on MRI, with continuity and low intensity, may have more than 3-mm difference in anteroposterior translation measured by KT- 2000 [95].

We observed movement of the graft in the femoral tunnel in all specimens even all specimens restored knee laxity after anatomically reconstruction and no graft impingement. The

graft averagely shifted 0.58mm (7.2% of the tunnel diameter) under AT loading with the largest shift occurred at 30° knee flexion angle with 0.67mm (8.4% of the tunnel diameter). This means that even the ACL was reconstructed at its anatomical footprint with 40N graft initial tension, there is still a graft shift that occurs under AT load. Under PT load, the largest shift also occurred at 30° knee flexion angle with 0.59mm. Averagely it shifted 0.43mm (5.4% of the tunnel diameter), smaller than it under AT load. Though ACL is not considered to provide main constraint to knee's posterior tibial motion, there is a graft shift in reconstructed knee under PT load. During flexion-extension from full extension to 90°, the biggest shifted distance occurred at 45° knee flexion angle (0.68mm) when compared to the graft position at full extension. The results show that the centroid of the graft does move during knee's passive even without an external load. Whether this can lead to graft failure due to the exposure to cyclic bending forces due to the femoral tunnel outlet contact is unknown. However, this relative movement may have effect on the post-operation rehabilitation.

5.3.3 Percentage of tunnel area at the aperture filled by the graft

The percentage of the tunnel area filled by the graft during knee flexion/extension and external loadings is in Figure 43. During flexion-extension, the percentage of the femoral tunnel area filled increased with knee flexion angle from 66.1% (15°) to 90.4% (90°). Under AT loading, the filled area of femoral tunnel decreased when compared to the neutral position without load, ranging from 52.8% (0°) to 74.9% (90°). Under PT loading, the of tunnel area filled from 70.7% (15°) to 87.1% (90°), greater than those of neutral positions. Under IR loading,

the area ranges from 70.7% (15°) to 78.5% (30°). Under ER loading, area ranges from 67.3% (0°) to 70.6% (30°). Under valgus loading, the area coverage of femoral tunnel ranges from 66.6% (0°) to 79.0% (30°). However, no statistical significant difference was found in percentage of tunnel area filled by the graft between any flexion angles (Figure 43).

Figure 44 showed a comparison of the percentage (in Sample 14_0900L) of the tunnel filled before and after AT loading at different knee flexion angles. The percentage of the femoral tunnel filled by the graft increased with knee flexion angle and the AT load tends to reduce the percentage.

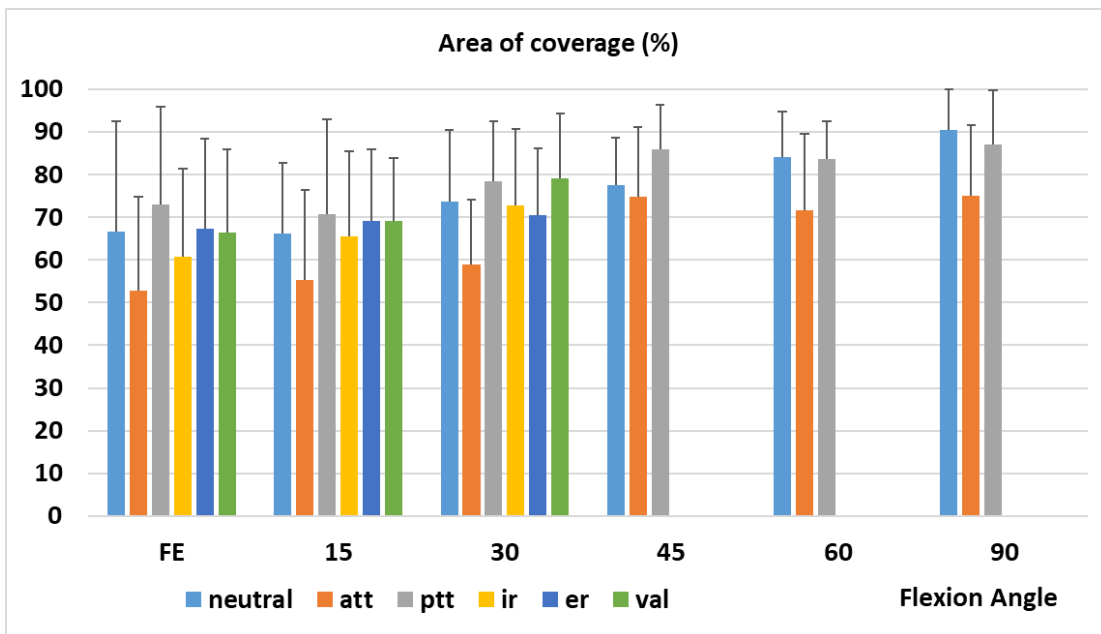


Figure 43: Percentage of femoral tunnel aperture filled by graft under external loadings and knee flexion

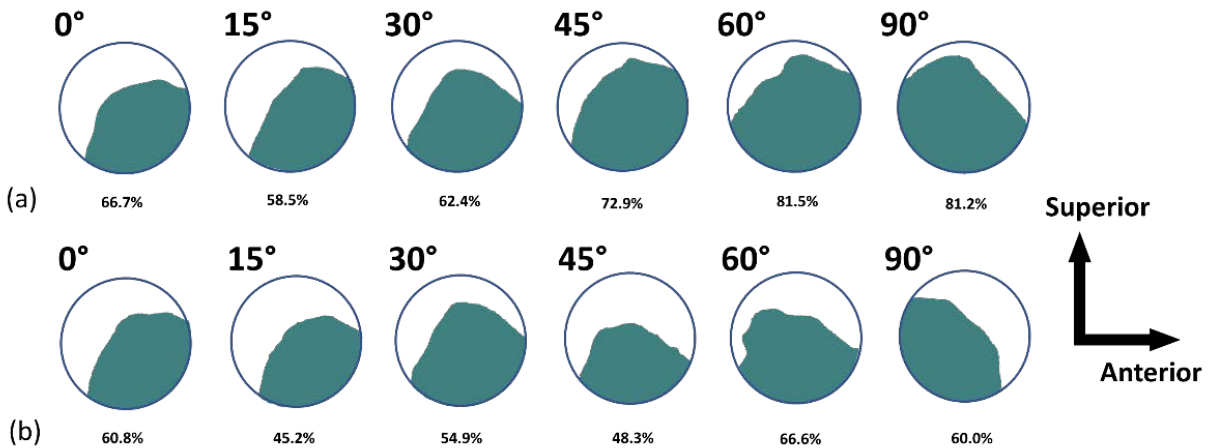


Figure 44: Femoral tunnel filled by graft under (a) knee flexion and (b) AT load (Sample 14_0900L)

The reason why graft shifts and rotates in the tunnel is that the graft does not always filled the entire tunnel due to a difference in graft size or graft contraction when loaded. A space between the graft and tunnel is frequently observed in ACL reconstructed knee. It is important to quantify the percentage that the graft in the tunnel. In this study, the result shows that when placed in a tunnel of the same diameter and tensioned, the soft tissue graft occupies approximately 70% of the tunnel area and tends to contact under anterior loading[75]. The percentage of tunnel occupied by the graft under passive flexion ranged from 67-90% and was reduced to 53-75% under anterior knee load. Under posterior knee load, the percentage increased to 71% to 87%. There is also significant motion of the graft within the tunnel. The percentage tends to increase with the flexion angle. This might be related to the distance between femoral and tibial tunnel in anatomical single bundle ACL reconstruction. The change of tunnel to tunnel distance during flexion extension leads to the graft being lengthen or shorten, thus cause the shift as well as the percentage change of the graft at the aperture. This suggests an appropriate tunnel placement as well as rehabilitation time should be considered to allow for graft healing which could reduce graft motion in the tunnel.

5.3.4 Percentage of tunnel boundary at the aperture in contact with the graft

The contact area percentage under external load and during flexion/extension is listed in *Table 9*. The contact area is defined as the percentage of tunnel circumference that is in contact with the graft. The contact area between graft and bone changes with flexion angle as well as external load (Figure 45). Under AT load, the average contact area percentage (mean: 58.4 %, range: 53.85%~63.3%) is smaller than with no knee load (mean: 61.5%, range: 54.0%~67.5%), while under PT load the percentage is bigger (mean: 65.2%, range: 57.7%~73.8%). The contact area change is relatively smaller with internal/external load. It ranges from 55.4%~59.9% for internal rotation and 57.0%~60.8% for external rotation. With valgus load, the range is 57%~66.7%. Although, all external loads tend to change the amount of tunnel-graft contact no statistically significant difference was found between graft area under any external loadings at all knee flexion angles.

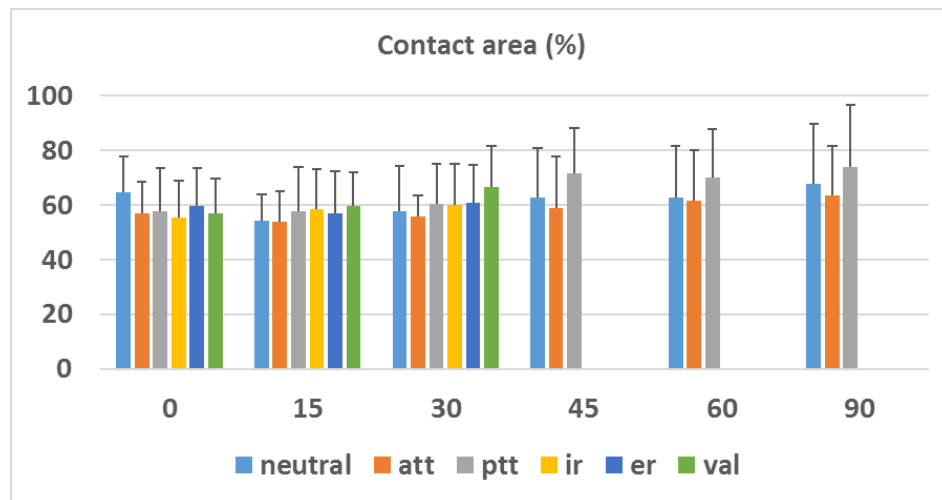


Figure 45: Percentage of graft contact area with external load and flexion/extension

Table 9: Percentage of femoral tunnel outline contact with graft for each external loading condition and flexion/extension (F/E).

	F/E	ATT	PTT	IR	ER	VAL
0°	64.5%±13.2%	57.0%±11.5%	57.7%±15.6%	55.4%±13.4%	59.8%±13.5%	57.0%±12.6%
15°	54.0% ±9.7%	53.8%±11.1%	57.7%±16.0%	58.3%±14.7%	57.0%±15.4%	59.7%±12.2%
30°	57.5%±16.7%	55.7%±7.8%	60.3%±14.9%	59.9%±15.2%	60.8%±14.0%	66.7%±15.0%
45°	62.6%±18.1%	58.9%±18.7%	71.7%±16.3%	n/a	n/a	n/a
60°	62.8%±18.9%	61.4%±18.5%	70.1%±17.8%	n/a	n/a	n/a
90°	67.5%±22.2%	63.3%±18.3%	73.8%±22.9%	n/a	n/a	n/a

The result of contact area between the graft and bone also shows that the graft shifted and changed angular position in the tunnel during knee motion and external loads. Previous studies have documented the “bungee effect” and “windshield wiper effect” of graft that moves inside the tunnel during knee motion, in either a longitudinal or a transverse direction, that may cause femoral tunnel enlargement[75, 99, 170]. The results in this study showed the that the graft tends to move around the tunnel circumference during knee flexion-extension as well as external loadings. The average bone-graft contact region percentage at neutral position is about 61.5%, ranged from 54.0% to 67.5%. Anterior loading tends to reduce the amount of graft-tunnel contact to an average value of 58.4 %, ranged from 53.85% to 63.3%. This may cause contact stress on the tunnel aperture which may contribute to tunnel enlargement after surgery. The contact area percentage before and after anterior load shows that though the centroid of graft shifted away from the tunnel center, it does not increase the contact area with the tunnel. This indicates that there might be longitudinal movement of the graft under anterior load.

5.3.5 Angular Position of contact area during flexion/extension and under external loadings

The angular position change of contact area under external load and during flexion-extension is listed in *Table 10*. Based on a right knee, a positive value means graft contact position moved counterclockwise and negative value means clockwise movement. The graft angular contact position had a larger change under PT load (mean: 11.6°, range: 1.5°~20.1°) than under AT load (mean: 10.85°, range: 3.7°~24.8°). Under AT load, the rotational position of the contact region increased with flexion angle, with an average value of 24.8° and the maximum change occurred at 90° knee flexion. Under PT load, the contact region position rotates counterclockwise based on right knee with the maximum rotation 20.1° at 60° knee flexion. The mean value for contact region rotation under IR, ER and valgus moments are 10.6° (10.4°~11.0°), 11.8° (5.8°~16.6°) and 3.8° (2.3°~5.1°), respectively (Figure 46). However, no statistically significant difference was found between rotation angles with any external loadings at all knee flexion angles.

During knee flexion-extension, the contact area rotates when the knee flexed from full extension to 90° of knee flexion. Compare to the graft position at full extension without external load, the graft rotates 5.6°, 8.3°, 7.3°, 13.8°, 32.8° at 15°, 30°, 45°, 60° and 90° knee flexion angle, respectively (Figure 47). The center of graft-tunnel contact angle tended to change from anterior distal ($158^{\circ}\pm 11.5^{\circ}$) to posterior distal ($190^{\circ}\pm 32.3^{\circ}$) during passive flexion (Figure 48). One-way repeated measures ANOVA was used to determine statistically significant ($p < 0.05$) in graft rotation at different knee flexion angles. Significant differences were found between 90° and 15°, 30°, 45° of flexions (Figure 47).

When the knee flexed from full extension to 90° flexion, the graft-bone contact region rotates as much as 32.8°. The location of graft-tunnel contact also shows there is transverse movement of graft in the tunnel. The location of graft-tunnel contact indicated that the movement of the contact region around the tunnel edge may contribute to the femoral tunnel enlargement after ACL reconstruction. Clinically, movement of the ACL graft in bone tunnel offers a potential explanation for the lack of graft-tunnel ingrowth[155]. Moreover, the graft shift in the femoral tunnel may result in tunnel enlargement, and it can be affected by tunnel position in ACL reconstruction.

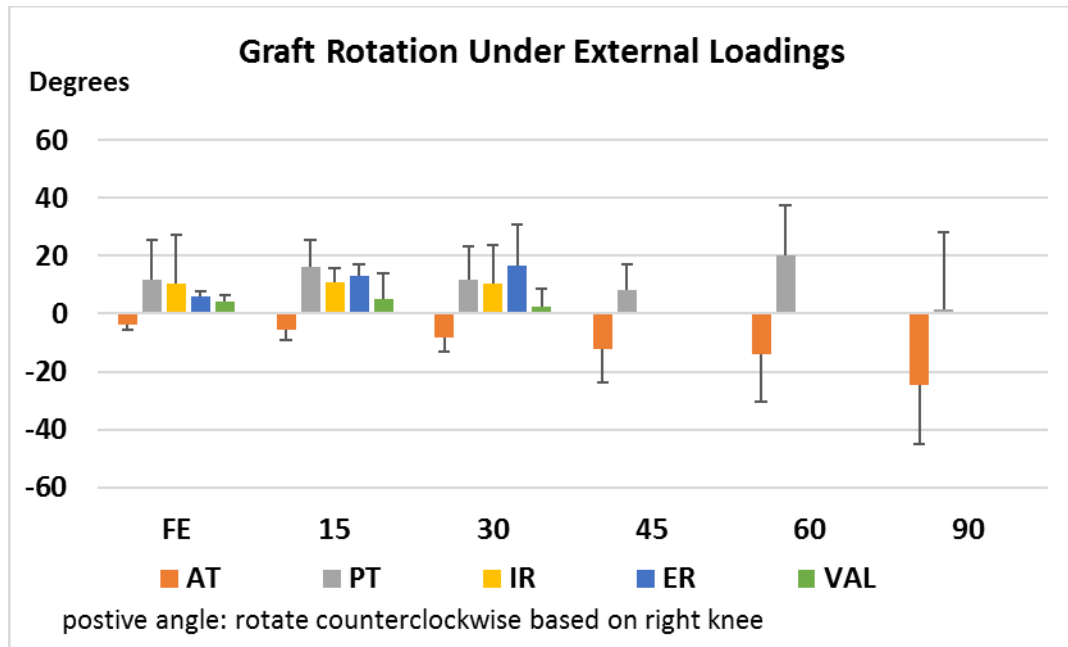


Figure 46: Contact region angular location compared to neutral position at different under external loadings.

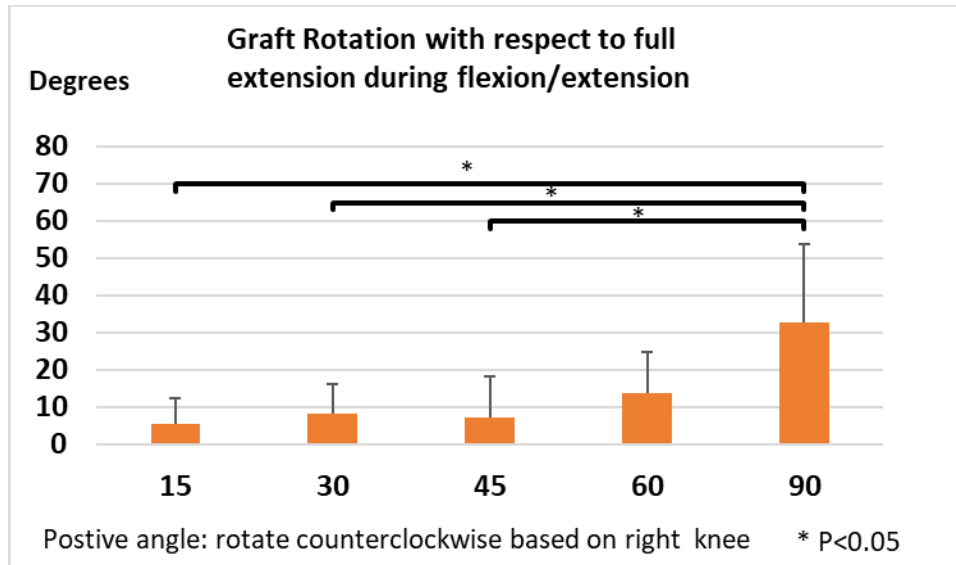


Figure 47: Contact region change in angular position as compared to the full extension position.

Table 10: Angular position change of graft in femoral tunnel for each external loading condition and flexion/extension (F/E).

	F/E	ATT	PTT	IR	ER	VAL
0°	n/a	-3.7°±1.8°	11.7°±13.9°	10.5°±16.9°	5.8°±1.8°	4.1°±2.2°
15°	5.6°±7.0°	-5.5°±3.7°	16.2°±9.2°	11.0°±4.8°	12.9°±4.3°	5.1°±9.0°
30°	8.3°±7.9°	-8.2°±5.0°	11.8°±11.5°	10.4°±13.5°	16.6°±14.3°	2.3°±6.4°
45°	7.3°±10.9°	-12.2°±11.3°	8.3°±8.9°	n/a	n/a	n/a
60°	13.8°±11.2°	-14.0°±16.5°	20.1°±17.3°	n/a	n/a	n/a
90°	32.8°±20.8°	-24.8°±20.3°	1.5°±26.9°	n/a	n/a	n/a

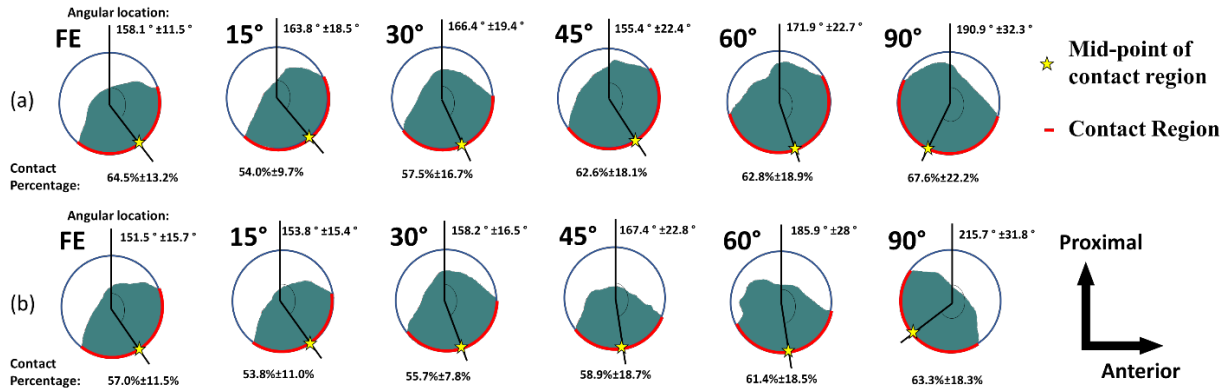


Figure 48: Percent graft-bone contact and mid-point angle during (a) passive flexion-extension and (b) under anterior tibial load.

5.4 CONCLUSION

This study investigated and quantified graft position at the different flexion angles in anatomical single bundle ACL reconstructed knees under external loads and passive flexion by using robotic system and laser scanning. To that end, the percentage of tunnel filled by graft, percentage of tunnel circumference in contact with graft, graft rotate under load or passive flexion and graft centroid shift were measured and described. Data was analyzed using one-way repeated measures ANOVA with statistical significance at $p < 0.05$. Statistical analyses were performed to compare the graft position at different flexion angle and external loading. The results showed that the ACL graft shifts and changes contact position in the femoral tunnel as the knee joint under external loads and passive motion, as described by previous studies [83, 121, 177]. The data also found that when placed in a tunnel of the same diameter and tensioned, the soft tissue graft occupies approximately 70% of the tunnel area and changed location in the tunnel with

knee motion and external load. Laser scanning offers a precise measuring method for determining the graft position in the bone tunnels.

The data obtained in this study may have important implications in biomechanical studies of ACL reconstruction. Femoral tunnel widening has been observed and reported in various studies[15, 28, 35, 79]. By distinguishing the graft behavior as well as the interaction between graft and bone during knee loading, it may provide insights into the biomechanical factors that might be related to femoral tunnel enlargement and may be useful for determining appropriate rehabilitation time. Clinically, numerous ACL reconstruction techniques have been proposed[10, 41, 72]. Our methodology might provide guidance in evaluating the graft behavior in the reconstructed ACL at time zero, and in determining the optimal femoral tunnel location. This experimental method may provide useful information on the design of ex-vivo biomechanical experiments of other soft tissue reconstructions, such as in PCL or MCL reconstructions. Finally, having knowledge of the contact area and centroid position of the graft can be necessary to compare to three-dimension finite element models that are developed to simulate and predict biomechanical behavior of ACL graft in reconstructed knees. Certain limitations of this study should be noted. First, this study uses laser scanning as tool to measure the change of the graft on the femoral tunnel aperture of cadaver knee which only provide information on surface, and the quality of scanning depends on the knee dissection. Second, since this study was performed on cadaver specimen, other biological factors such as healing and muscle forces were not included in this study.

6.0 FINITE ELEMENT MODEL OF THE GRAFT AND TUNNEL FOR SINGLE BUNDLE ACL RECONSTRUCTION

This research applied knee kinematic data from robotic testing in a computational approach to study ACL graft behavior with different knee loading conditions. The objectives of this research were to determine the ACL graft deformation on anatomically reconstructed knee model, graft force and contact pressure between graft and bone during flexion/extension and external loadings using a combined experimental-finite element (FE) model. The hypothesis was that ACL graft moves in the tunnel and may increase contact pressure between the ACL graft and tunnel. To conduct this study, finite element analysis will be developed with consideration of material properties, mesh, boundary conditions and loads. The geometry of the model was rebuilt from CT scanning and kinematic data of knee will be obtained through robotic testing, which are described in Chapter 5.2.3. Three-dimensional joint kinematics were recorded during knee testing as described in Chapter 4.3.1. An FE model of the femur-graft-tibia complex was constructed for to simulate flexion extension, anterior/posterior translation at 0°, 15°, 30°, 45°, 60°, 90° and internal/external rotation, valgus at 0°, 15° and 30°, using bone model generated from CT images. An isotropic hyperelastic material model with material coefficients taken from the literature was used to represent the ACL graft. Tunnel position were registered after ACL reconstruction. FE predictions were validated by comparing ACL graft position to experimental measurements.

6.1 BACKGROUND AND SIGNIFICANCE

The ACL plays a critical role act as joint stabilizers and movement restrainers in the physiological kinematics of the knee joint, being the primary restraint against anterior tibial translation and also limiting knee hyperextension [40, 96]. ACL rupture is a serious and the most common ligament injury, with an increasing number of 100 000 to 200 000 incidences per year in the United States alone, among which half of patients choose to have ACL reconstruction[161]. Knowledge of biomechanics of the knee and the behavior of ACL graft are indispensable to evaluate the graft strain, its positions in tunnel and to improve surgical procedures. While experimental studies have limitations such as their high cost, computational models are a good alternative to study several biomechanical quantities with reduced costs and time. In particular, the finite element (FE) method can provide accurate and medically relevant results [12, 74, 91, 105, 131, 141, 175]. The FE simulation technique permits a precise calculation of both spatial and temporal variations of stresses, strains and contact areas/forces in different situations that are reproduceable[93, 132, 165]. Therefore, FE analysis is a powerful tool in providing biomechanical information that can be extremely useful in a clinical context.

The existing FE models of the ACL and ACL graft, vary in parameters, such as the degree of complexity, material model and loading conditions. Due to the complex anatomy and various structures of the knee joint, many of the FE studies simplify the analysis by not including parts such as the menisci and the articular cartilage or other ligaments [47, 62, 70, 116, 131, 133, 165]. Some studies chose to represent the knee ligaments with one-dimensional truss/beam [2, 17] or spring [70, 104, 116] elements with simplified material properties. Despite the increased ease in obtaining kinematic and force data, this approach does not allow to determine the stress distribution in the ligaments [139, 182]. When using three-dimensional representations of the

ligaments, the challenge is to develop a material model that can characterize the behavior of ligaments. To this matter, isotropic [139, 145, 146, 165, 182], transversely isotropic [43, 48, 62, 105, 132, 133] and anisotropic hyperelastic material models [90, 176] have been used. Although a widely studied topic on the FE modeling context, the development of a trustworthy model of such a complex structure as the knee joint is still a very challenging process. The difficulties are increased when a good description of the ligaments behavior is required.

The overall goal of this work is to develop a 3D FE model that enables a biomechanical analysis of the graft behavior after an ACL reconstruction. This work aims to provide clinical relevant information regarding the forces, strain and displacement changes that occur in an ACL graft during flexion extension and under external loads.

6.2 METHODS

Computed tomography (CT) images were taken of a knee specimen and used to obtain the geometry of the femur and tibia. Polygonal surfaces were extracted from the CT data to generate the subject-specific finite element model of the knee. The ACL graft was modeled as cylinder with diameter equal to that of the femoral and tibial tunnels. The femoral and tibial tunnel positioning were from an experimental ACL reconstruction which was performed by an experienced surgeon. The knee sample was tested robotically after ACL reconstruction, and was subjected to anterior/posterior loads, internal/external and valgus moments at different flexion angles. The FE model was analyzed using the experimentally measured kinematics to determine graft positions, contact forces, and graft forces. The predicted results were compared to experimental values as validation.

6.2.1 Constitutive model of the ACL graft

Different mathematical models have been developed to capture the mechanical behavior of soft tissues. For ligaments, this is most often described by the stress-strain behavior under uniaxial tension. An elastic strain energy function W_e , proposed by Veronda and Westmann for describing incompressible isotropic hyperelastic material behavior was given as[171]:

$$W_e = \alpha \exp[\beta(\bar{I}_1 - 3)] + C_1(\bar{I}_2 - 3) \quad (6-1)$$

The material constants (α, β, C_1) , which had been determined according to the experimentally obtained stress-deformation gradient data of the human ACL as, $\alpha = 0.26$, $\beta = 11.35$, $C_1 = -1.49$ [141, 165].

In order to implement this strain energy function into the finite element software (ANSYS), the form had to be manipulated. In the software, default form of the strain energy potential for the polynomial option is given by:

$$W = \sum_{i,j=1}^N c_{ij}(\bar{I}_1 - 3)^i(\bar{I}_2 - 3)^j + \sum_{k=1}^N \frac{1}{d_k} (J - 1)^{2k} \quad (6-2)$$

where:

W = strain energy potential

\bar{I}_1 =first deviatoric strain invariant, $\bar{I}_1 = \lambda_1^2 + \lambda_2^2 + \lambda_3^2$, with λ_i are stretch ratios for the unit fibers that are initially oriented along the directions of three axis in the coordinate systems and

\bar{I}_2 =second deviatoric strain invariant, $\bar{I}_2 = \lambda_1^2 \lambda_2^2 + \lambda_2^2 \lambda_3^2 + \lambda_3^2 \lambda_1^2$

J = determinant of the elastic deformation gradient \mathbf{F}

N, c_{ij}, d = material constants

The ligament was assumed to be incompressible, so the value of J was set equal to 1. In general, there is no limitation on the value of N. A higher value of N can provide a better fit to the exact solution. It may however cause a numerical difficulty in fitting the material constants, and it also requires more computational calculations. For these reasons, the Taylor series expansion of $\alpha \exp[\beta(I_1 - 3)]$ was taken up to the third order.

Given $x = I_1 - 3$, the Taylor series expansion of $\alpha \exp[\beta(I_1 - 3)]$ is:

$$\alpha e^{\beta x} = \alpha \left(1 + \beta x + \frac{\beta^2 x^2}{2!} + \frac{\beta^3 x^3}{3!} + \frac{\beta^4 x^4}{4!} + \dots \right) \quad (6-3)$$

Then, with experimentally obtained parameters of **equation** (6-1) ($\alpha = 0.26$, $\beta = 11.35$, $C_1 = -1.49$) [141, 165], in **equation** (6-3), $\alpha = 0.26$, $\alpha\beta = 2.95$, $\alpha \frac{\beta^2}{2!} = 16.7493$, $\alpha \frac{\beta^3}{3!} = 63.3592$. Therefore, in this polynomial form of the strain energy function the coefficients of the first, second and third orders are 2.95, 16.7463, and 63.3592, respectively. This polynomial strain energy function was then implemented into the software as a third order polynomial equation with the coefficients $C10 = 2.95$, $C20 = 16.7463$, $C30 = 63.3592$ and $C01 = -1.49$. The femur and tibia were assumed to be linear elastic, with Young's Modulus = 19.4 GPa and Poisson's ratio = 0.33[85]

6.2.2 Transformations between the local coordinate system and global coordinate system

As shown in Figure 49, three registration screws were placed in the femur and three in the tibia prior to CT scan and robotic test. The global coordinate system was defined by the digitizer on the experiment base with its three axes aligned with specimen's anatomical directions (anterior-posterior, medial-lateral, superior-inferior). A local coordinate system was defined on tibia from three tibial registration screws. The origin of the local coordinates system was taken as one of the

registration screws. The three orthogonal axes of local coordinates system were defined as follow: the first orthogonal axis (\mathbf{i}') was the unit vector from the origin to one of other two registration screws; the second orthogonal axis (\mathbf{j}') is found by taking the cross product of the first axis (\mathbf{i}') and the unit vector connecting the two other registration screws; and the cross product of the first and second orthogonal axis yielded the third axis (\mathbf{k}').

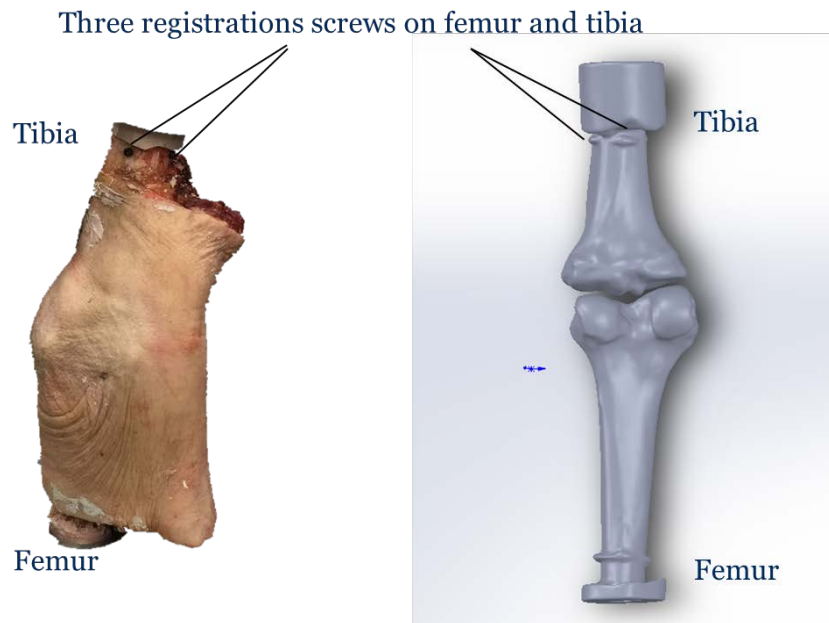


Figure 49: Placement of registration screws and geometry of femur and tibia from CT scan

The local coordinate system that was fixed in the body of interest was used to describe objects' changing position and orientation with respect to the global reference frame (**Equation 6-5**). By doing this, registration screws position measured with the digitizer during the robotic test could be related to the local coordinates of the sample, and the measured rigid body displacement of the tibia from the test could be applied in the finite element model.

The position and orientation in the local coordinate system (FE model) (\mathbf{i}' , \mathbf{j}' , \mathbf{k}') can be transformed to a global reference frame (digitizer/scanner) (\mathbf{i} , \mathbf{j} , \mathbf{k}) by the global position of the

local coordinate system origin and global description of the three orthogonal unit vectors (i, j, k) that represent the axes of the local coordinate system as follow [54] (Figure 50):

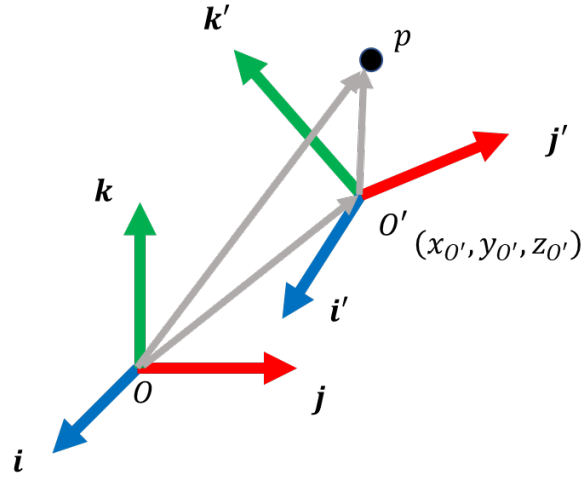


Figure 50: Local coordinate system (i', j', k') defined with respect to the global reference frame (i, j, k)

$$\overrightarrow{Op} = \overrightarrow{OO'} + \overrightarrow{O'p} \quad (6-4)$$

$$\begin{pmatrix} x \\ y \\ z \\ 1 \end{pmatrix} = \begin{pmatrix} i^T i' & i^T j' & i^T k' & x_{O'} \\ j^T i' & j^T j' & j^T k' & y_{O'} \\ k^T i' & k^T j' & k^T k' & z_{O'} \\ 0 & 0 & 0 & 1 \end{pmatrix} \begin{pmatrix} x' \\ y' \\ z' \\ 1 \end{pmatrix} \quad (6-5)$$

Thus, there is a transformation from the global coordinate system to local coordinate system as,

$$T_{G2L} = \begin{pmatrix} i^T i' & i^T j' & i^T k' & x_{O'} \\ j^T i' & j^T j' & j^T k' & y_{O'} \\ k^T i' & k^T j' & k^T k' & z_{O'} \\ 0 & 0 & 0 & 1 \end{pmatrix} \quad (6-6)$$

where the values of $x_{O'}$, $y_{O'}$, $z_{O'}$ correspond to the location of the origin of the local coordinate system. The result is three orthogonal unit vectors local to the body, but defined in a global reference frame (i, j, k). The transformation from local to global coordinate system can be found by taking the inverse:

$$\mathbf{T}_{L2G} = \mathit{inv}(\mathbf{T}_{G2L}) \quad (6-7)$$

Thereby, the position and orientation of the bones that is measured during the robotic test in scanner's global coordinate system can be converted and applied to the FE model analysis as a displacement in its local coordinate system.

6.2.3 Geometry

Three-dimensional solid models of the tibia and femur were generated from a computer tomography (CT) scan of the same cadaver knee (46 yrs old, female, right knee) used in Chapter 5.0 (Figure 49). The Standard Digital Imaging and Communications in Medicine (DICOM) images were acquired from the CT imaging (LightSpeed VCT, GE) with the following parameters: (i) scan matrix size = 512 x 512; (ii) pixel size = 0.2734 mm; (iii) slice thickness = 0.6224 mm. The CT scans the femur and tibia in slices and captures a digital grey scale image of each slice. Each slice was taken axially along the femur and tibia. The raw imaging data was then post-processed and used to generate 3-D solid models using digital imaging software packages (MIMICS, Materialise NV). Bones were distinguished and separated from soft tissue by defining radiographic density threshold that corresponds to bone by the software, and generate a 3-D surface model of the femur and tibia. To further process the surface geometry of the bones, the 3-D surface model was exported and imported in to modeling software (Geomagics Studio, Morrisville, NC) which was used to patch any holes and smooth sharp edges and surface irregularities due to inherent thresholding and slice spacing of the CT imaging. Once surface irregularities were removed, a solid model of the femur and tibia were imported into software (Dassault Systemes SolidWorks Corp., Waltham, MA) for further manipulation. In order to measure the rigid body motion of the femur and tibia, three aluminum screws were

implanted in the femur and three in the tibia (Figure 49). The three registration points were measured in specimen by digital measurement (Faro arm, Faro Inc.) and also determined in CT scanning by including the registration screws in the software.

The edges of femoral and tibial tunnel entrances and exits were probed in the specimen and their corresponding positions in FE model was determined by applying transformation from their position in global coordinate system to local coordinate system. The tunnels were placed in the model by subtracting cylinders with same diameter as tunnel and passing through the outlines of the femoral and tibia tunnel (Figure 51).

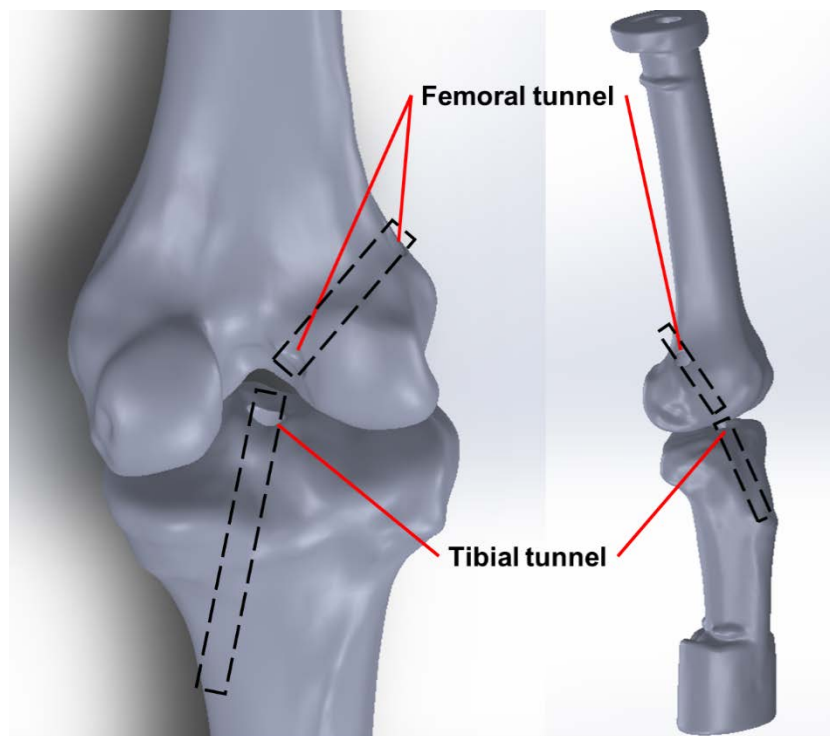


Figure 51: femoral and tibia tunnel in the FE model

The portion of graft in the tibia tunnel was assumed to have a cylindrical of the same diameter as the tunnel. The end face of the graft on the tibia side was attached to the end surface of the tunnel. On the femur side, the graft was assumed to be 5mm longer than the femoral tunnel in

order to apply an initial tension. The middle portion was assumed to have cylinder shape which connected femoral portion and tibial portion graft (Figure 52). And the graft was modelled with an isotropic hyper-elastic material model as describe previously

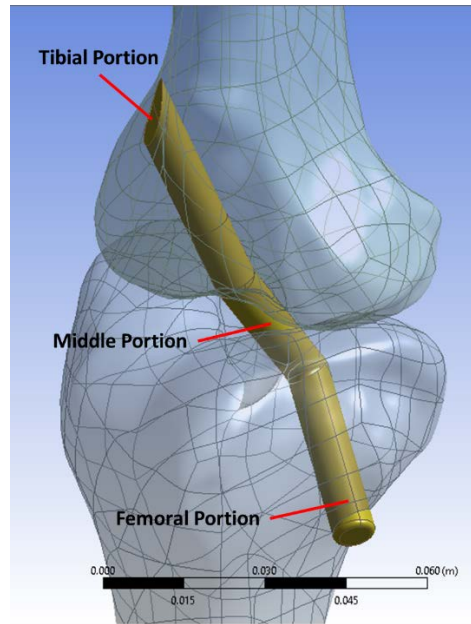


Figure 52: Geometry of graft represented by two portions determined by tibial and femoral tunnel and a third portion treated as a cylinder connecting the two portions

6.2.4 Boundary and initial conditions

The analysis of the FE model was divided into two stages: the analysis due to initial tensioning of the graft and the application of the known bone displacement measured during the robotic test. Deformation of the graft was calculated in analysis 1 and then applied in analysis 2 together with the kinematics of the bones (Figure 53).

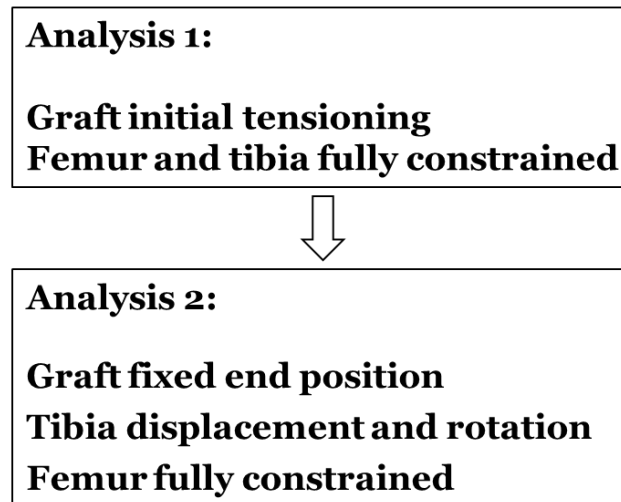


Figure 53: Two steps of analysis used in the finite element model.

6.2.4.1 Analysis 1: Application of initial graft tension

In ACL reconstruction an initial tension is applied to the graft. In this study, a force of 40N along the graft axis was applied at full extension of the knee. This initial tension is same as surgeons applied to the experimental study in Chapter 4.3.1.

In analysis 1, the femur and tibia were held fixed at full extension, displacement and rotation in all directions were set to be zero. The end surface of the tibial graft on the tibia side was rigidly fixed to the tunnel surface and a 40 N load was applied along the direction of the long axis of femoral tunnel on femoral side. The contact interface between the graft and the tunnel was set to be frictional, and two frictional coefficient of 0.2 and 0.8 were modelled and the results were compared (Figure 54)[12]. Analysis 1 simulates the graft fixation procedure and result with a graft tension. The result of this analysis will be used as the initial conditions for the second analysis.

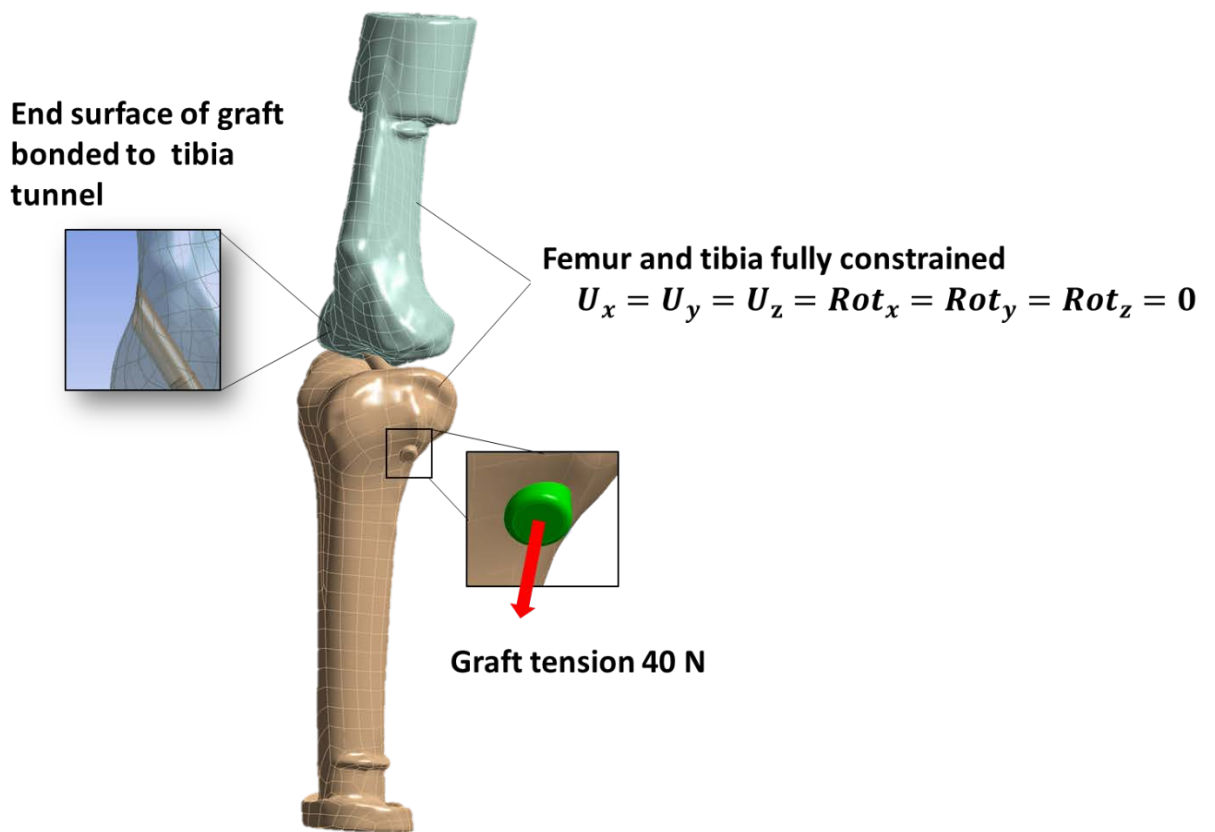


Figure 54: Boundary conditions used in analysis 1 for the calculation graft deformation due to initial tensioning.

6.2.4.2 Analysis 2: Application of Tibial Displacement

In the second analysis, the input of kinematic data of the tibia displacement, that was obtained from the robotic testing will, be applied to the model. In the experimental study described in Chapter 4.3.1, specimen was manipulated by the robotic system and rigid-body motion of bones in three-dimensions was measured by a spatial digitizer ((Faro arm, Faro Inc.)) with positional accuracies of 0.03mm. The passive flexion-extension path of the joint was determined by

methods previously described in Chapter 4.0 and the location of the three tibial registration screws were digitized at 3° increments from 0° to 90° of flexion, while the femur remained fixed. Also, when the specimen was tested under external loads (ATT, PTT at 0°, 15°, 30°, 45°, 60° and 90° degrees of flexion, IR, ER, VAL at 0°, 15° and 30° degrees of flexion), the three tibia registration screws were digitized at 0.5 mm increments of displacement through the range of motion of the tibia. The kinematic data measured by the digitizer in its global coordinate system was transformed to local coordinates and applied as displacement boundary conditions of the tibia in the FE model (Figure 55).

In this model, the results of the first analysis corresponding to the 40N initial fixation tension, was used as the initial state with the end surface of graft on the femur side will be fixed at its extended position. Experimental data for the knee under flexion-extension, AT, PT, IR, ER and VAL will be applied to the tibia.

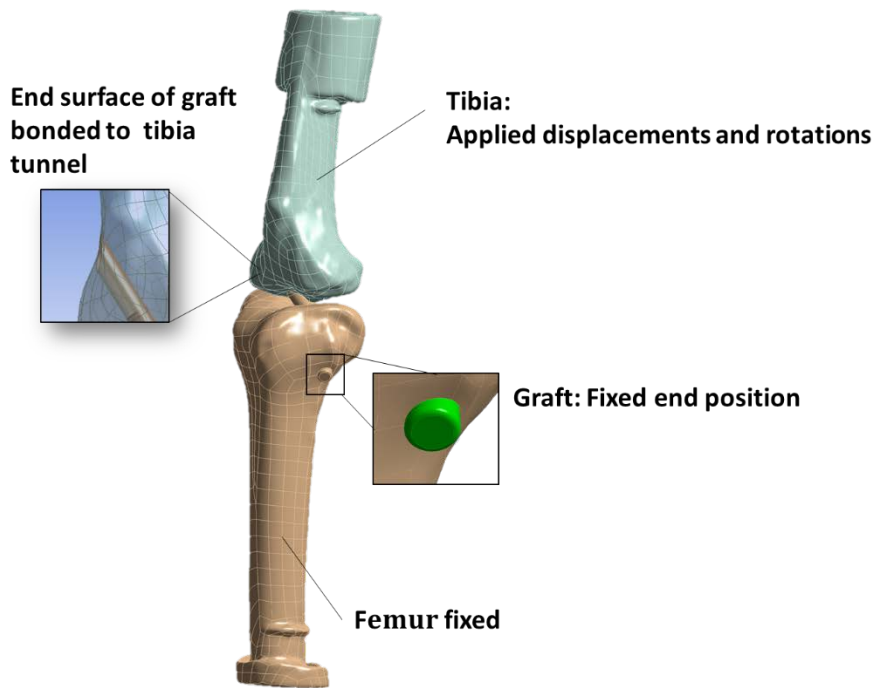


Figure 55: Boundary conditions used in analysis 2 for modeling the knee motion and external loads.

6.2.5 Model and experimental comparison of results

The experimental measurement of graft position in the tunnel using a scanner/digitizer measurement device (Faro arm, Faro Inc.) and the graft force measured in the same study by robotic system as described in Chapter 5 are compared with the results of FE model. The model's validity was assessed by comparing graft force and position under external load of the FE models with those of the experimental test under the same loading conditions. Relative error caused by using polynomial approximation with third order Taylor series expansion in material constitutive equation will be analyzed. Some differences were expected in graft force because of the assumptions of isotropy and cylindrical shape and that the hamstring graft used for the experiment had variations in geometry and material properties.

The graft force and the center of the graft at femoral tunnel aperture under external loads (AT, PT, IR, ER, VAL) at full extension will be calculated and compared with experiment results. The interpretation of the validation test is based on the assumption that if graft force and graft position change match those of the FE model under approximately identical conditions, then the model validation test is successful, building confidence in the assumption that graft force and position values at other flexion angles would have accurate matches between actual and FE model results.

6.3 RESULTS AND DISCUSSION

To check to error associated with truncating the Taylor series at 3rd order, equations 6-1 and 6-2 were evaluated at all nodes in the model at the end of a full flexion cycle. The average relative error between the model and the Taylor series approximation for the model during flexion was 0.70% and the maximum relative error was 5.2%, which was sufficiently small to consider Taylor series at 3rd order a valid approximation.

6.3.1 Graft Position

The center of the graft at the femoral tunnel aperture was evaluated under external load and flexion extension. Graft shift under external load was calculated as the difference of the center position between loaded and unloaded graft at a flexion angle. While the graft shift during passive flexion was calculated as the difference of the center position between full extension and a given flexion angle. The results were compared to experiment measurements.

Under AT loading, ACL graft shifted a magnitude of 0.063mm, 0.30mm, 0.51mm, 0.48mm, 0.22mm, 0.24mm at full extension, 15°, 30°, 45°, 60°, and 90° of knee flexion angle with an averagely shifted magnitude of 0.30mm (3.8% of the tunnel diameter). The largest shift occurred at 30° knee flexion angle with 0.51 mm. Graft centroid shifts in all three anatomical directions (medial-lateral, posterior-anterior and superior-inferior) were all smaller in magnitude than those measured experimentally (Figure 56). However, they were all within the range of 95% confidence intervals of average experimental measurements.

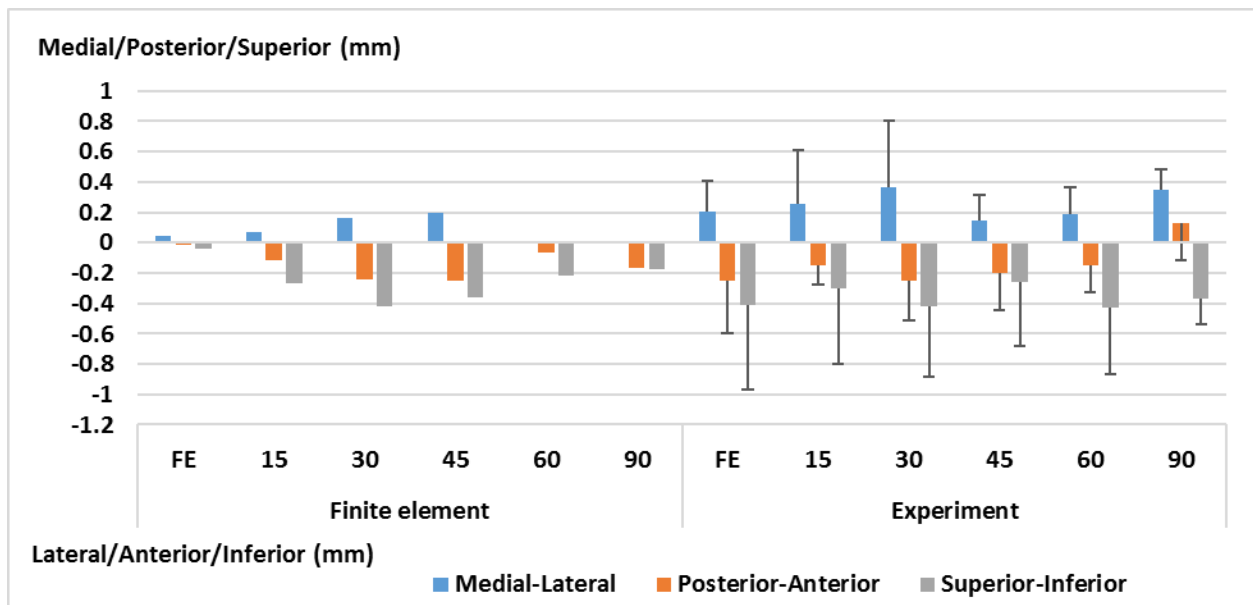


Figure 56: Graft shift under anterior tibial (AT) load with respect to the position without external load at different knee flexion angles

With 89N posterior tibial load, the graft shift more at low flexion angles. Graft centroid shifted a magnitude of 0.23mm, 0.25mm, 0.22mm, 0.23mm, 0.083mm, 0.062mm at full extension, 15°, 30°, 45°, 60°, and 90° of knee flexion angle with an averagely shifted magnitude of 0.18mm (2.2% of the tunnel diameter). The largest shift occurred at 45° knee flexion angle with 0.23mm.

The directional components show that under PT loads, the centroid of graft moved mainly in posterior and superior direction (Figure 57).

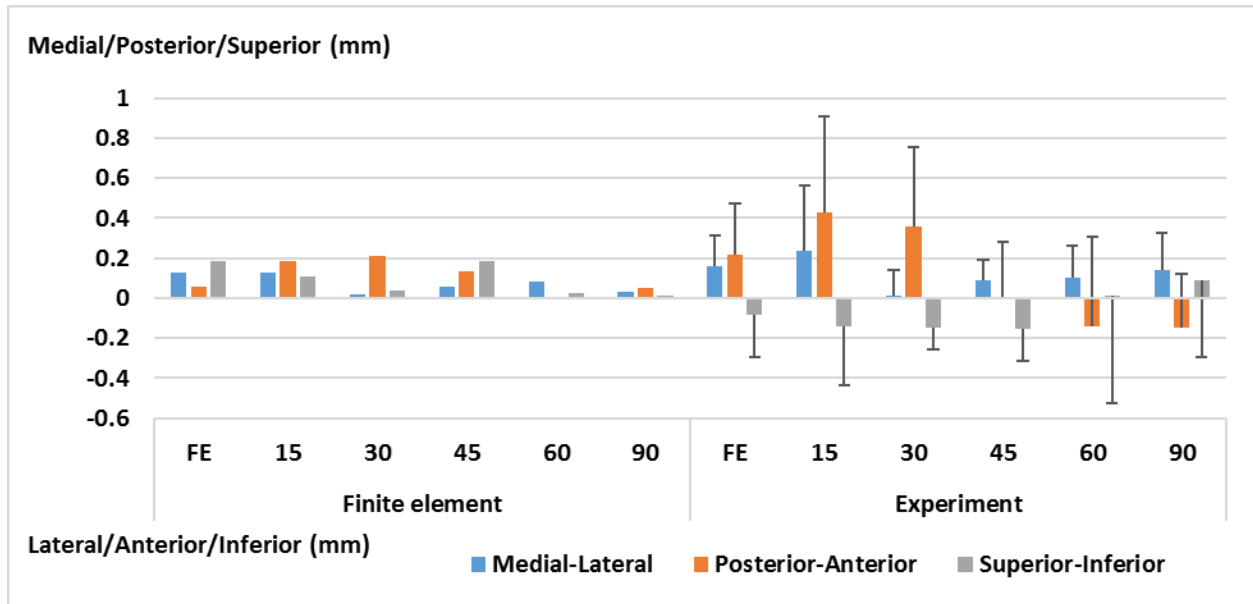


Figure 57: Shift of graft center under posterior tibial (PT) load with respect to the position without external load at different knee flexion angles

Under internal rotation, graft centroid shifted a magnitude of 0.076mm, 0.058mm, 0.26mm at full extension, 15°, 30° of knee flexion angle with an averaged shifted magnitude of 0.13mm (1.6% of the tunnel diameter). The maximum shift occurred at 30° knee flexion angle with 0.26mm. The directional components show that under ER loads, the centroid of graft moved medially, posteriorly and superiorly, matching the result of experimental measurement (Figure 58).

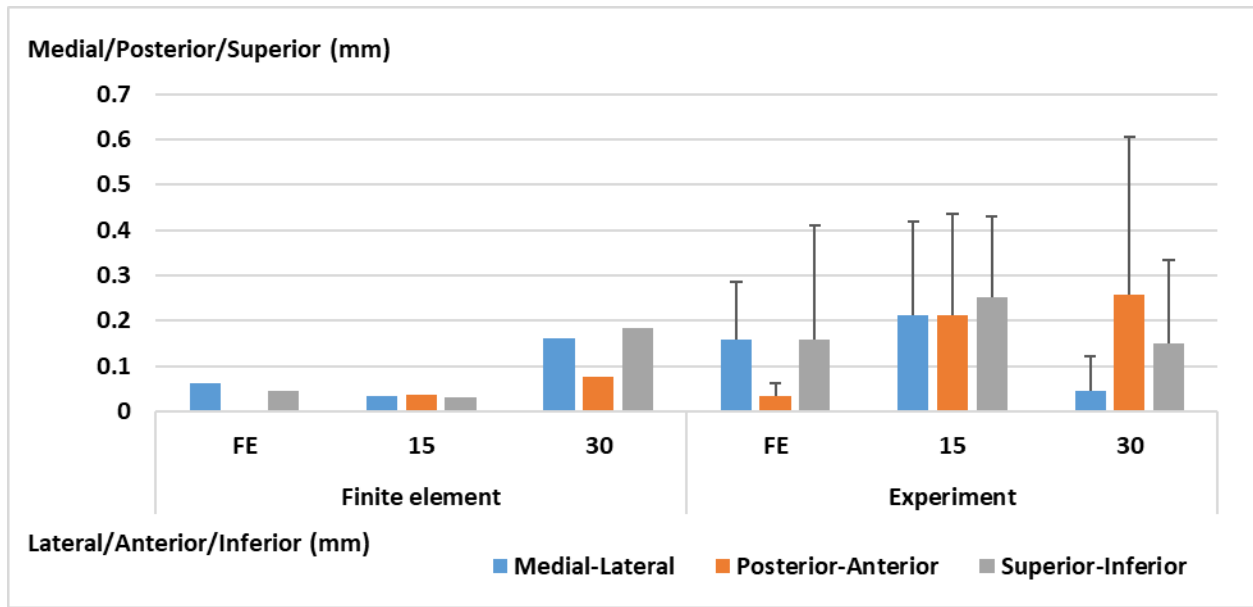


Figure 58: Shift of graft center under internal rotation (IR) load with respect to the position without external load at different knee flexion angles

Under external rotation, ACL graft shifted a magnitude of 0.17mm, 0.15mm, 0.30mm at full extension, 15°, 30° of knee flexion angle with an averaged shifted magnitude of 0.21mm (2.6% of the tunnel diameter). The maximum shift occurred at 30° knee flexion angle with 0.30mm. With external rotation, the centroid of graft mainly moved medially, anteriorly and inferiorly at full extension and 15° flexion, moved medially, posteriorly and superiorly at 30° flexion (Figure 59).

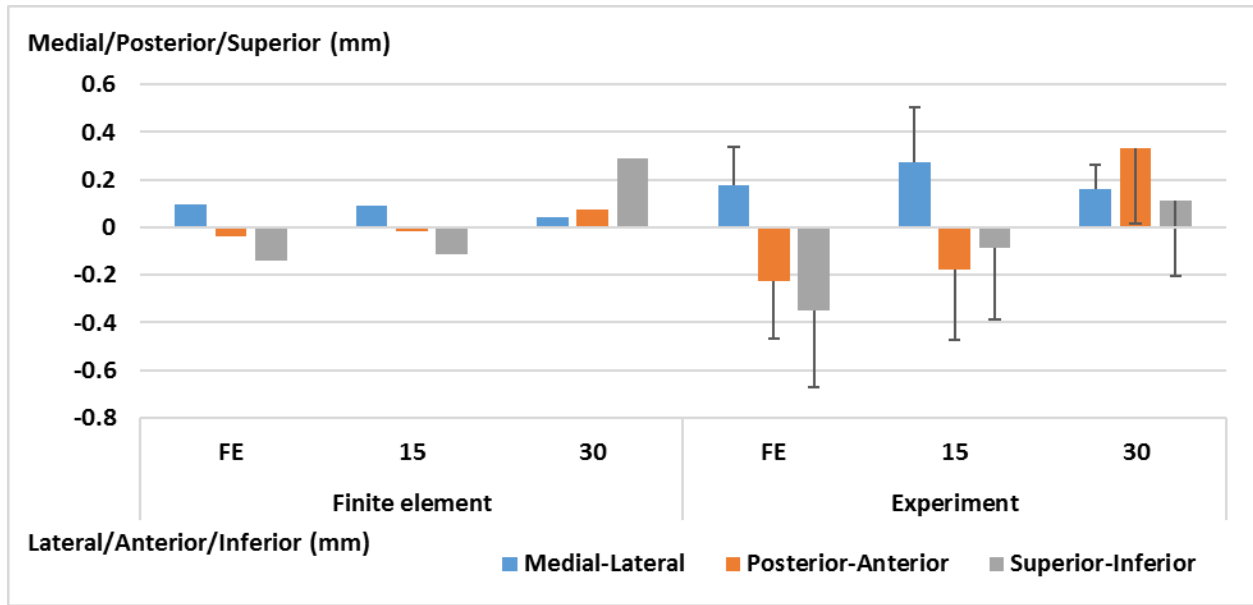


Figure 59: Shift of graft center under external rotation (ER) load with respect to the position without external load at different knee flexion angles

Under valgus loading, graft centroid shifted a magnitude of 0.19mm, 0.24mm, 0.13mm at full extension, 15° and 30° of knee flexion angle with an averagely shifted magnitude of 0.19mm (2.3% of the tunnel diameter), smaller than experiment results. Directional components of the shift were also calculated. Results shows that the graft centroid under valgus loading shifted medially and inferiorly at all flexion angles. Under valgus loads, the centroid of graft also moved posteriorly at full extension and moved anteriorly at 15° and 30° flexion (Figure 60).

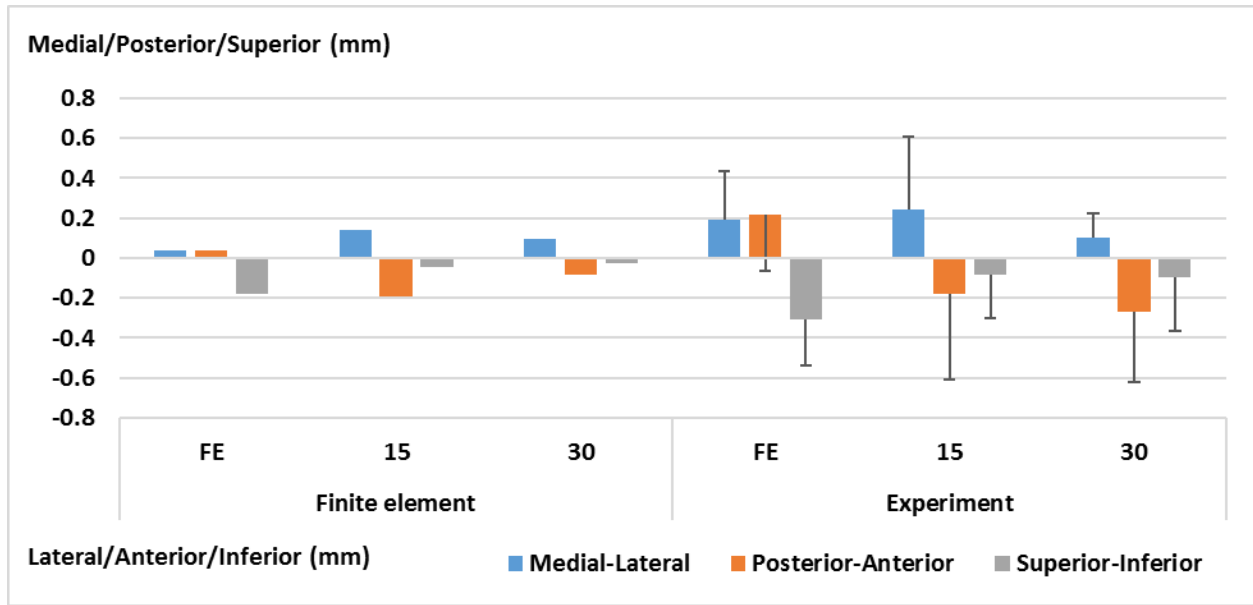


Figure 60: Shift of graft center under valgus rotation (VAL) load with respect to the position without external load at different knee flexion angles

During knee passive flexion from full extension to 90° flexion without external loads, graft centroid shifted a magnitude of 0.085mm, 0.10mm, 0.057mm, 0.073mm, 0.14mm at 15° and 30° 45°, 60° and 90° flexion compared to the graft position at knee full extension. Directional components of the shift matched the experimental test results. However, the magnitudes of the shift were averagely 15% of the value from experiment measurement (Figure 61). This could due to the idealized graft geometry, no space existed between the graft and tunnel. While in experiment test, a gap between the graft and the bone was usually observed in reconstructed knee.

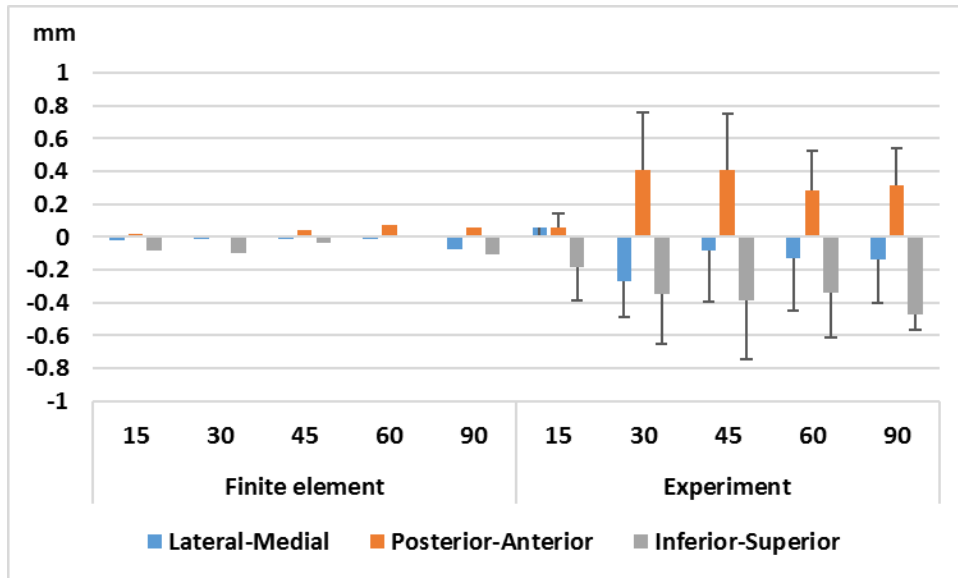


Figure 61: Graft shift in flexion with respect to the position without external load at full extension

The reason to the difference between FE model and experiment results could be: (1) graft geometry. In experiment test, a gap was usually observed in reconstructed knee. The gap allows graft to move within femoral aperture without contacting the bone. While in FE model, the graft was treated as cylinder connecting femoral and tibial tunnel with same diameter as the tunnel. Any shift or rotation caused by external load or flexion would give rise to contact between graft and bone. The resultant frictional force or graft end constraint force could contribute to smaller shift of the graft or rotation; (2) material model. The graft was harvest from hamstring which was also soft tissue with anisotropic hyperelastic properties. The graft in FE model bears contact force and also frictional force between graft and bone, which were in the transverse direction. With an isotropic hyperelastic material model used in modelling the graft, FE model result could be affected.

6.3.2 Graft-Tunnel Contact Position

The graft-tunnel contact positions during flexion and under external loads are plotted in Figure 62, along with experiment results as a comparison. It is noted that both the experiment and FE model results were converted to a left knee representation, and the positive position indicate a clockwise rotation of the graft on a left knee. The graft angular contact position increased as the knee flexed from full extension to 90° flexion, showing the same trend as found in experiment test. It moves a greater amount from 45° to 90° flexion when compared to experiment result. Under external loads, however, the FE model shows smaller positional change when compared to experiment results. The maximum change in angular position under AT load occurred at 30° of flexion with -3.6°. The maximum change under PT load occurred at 15° of flexion with 7.2°. Angular change was larger at higher flexion angles when the knee was under internal rotation. External rotational loading of the tibia caused graft angle change, but angle did not change much between different knee flexion angles, with average value of 6.8°. Valgus rotational loading caused maximum angle change at full extension, with a value of 12.6°.

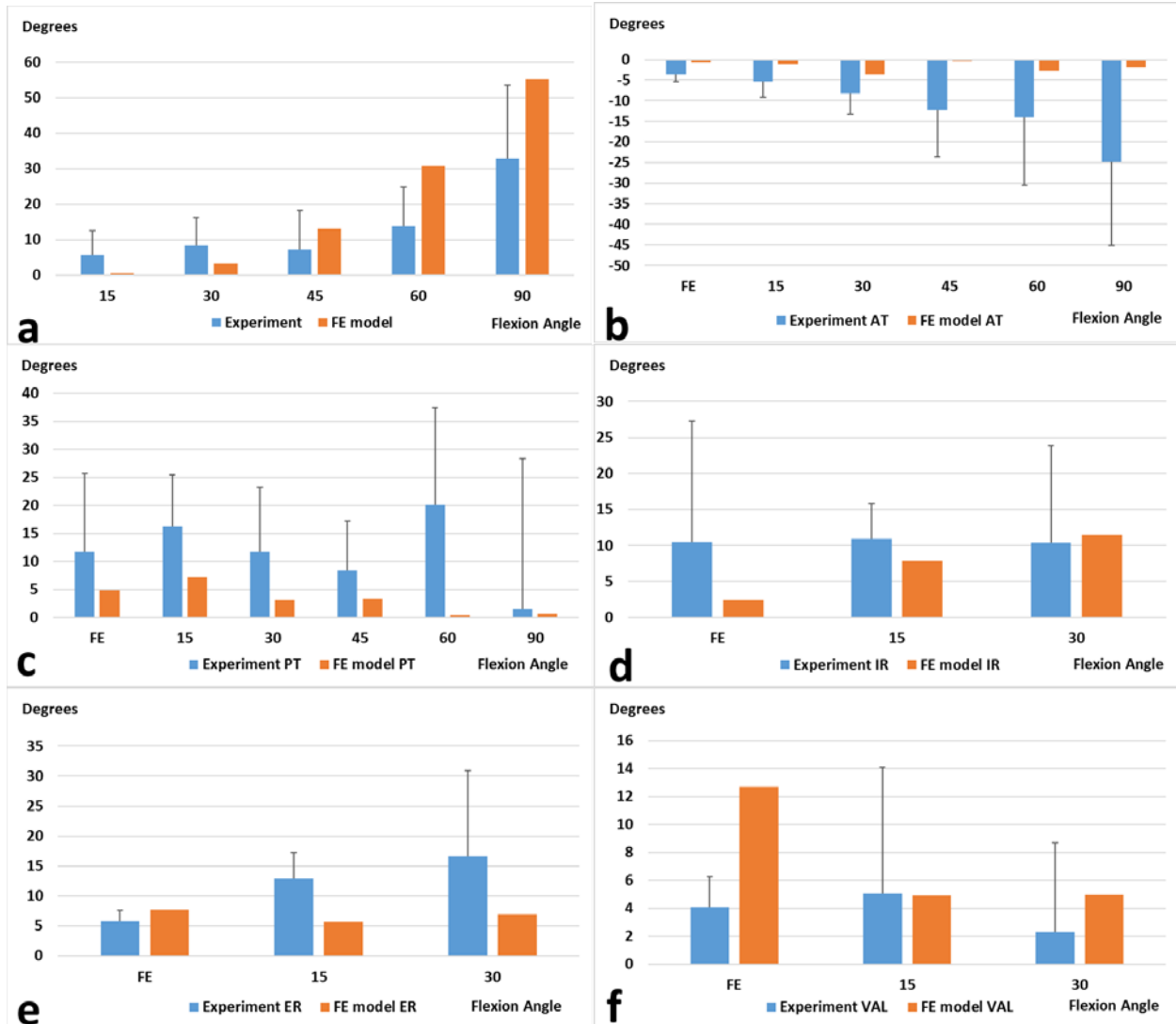


Figure 62: Graft-tunnel contact angular position change in the femoral tunnel based on left knee model during: (a) flexion; (b) anterior tibia (AT) load; (c) posterior tibia (AT) load; (d) internal rotational (IR) load; (e) external rotational (ER) load; (f) valgus rotational (VAL) load.

The FE model showed that the graft-tunnel contact position changes in the femoral tunnel during flexion and under external loads. The position changes by up to 55° during flexion from full extension to 90° of extension implying that the so-called “wiper effect” occurs during most of flexion angles. This could be an important mechanical contribution to the femoral tunnel enlargement after ACL reconstruction[50, 75, 174, 177]. The data also suggests that different

regions of femoral tunnel aperture, particularly the anterior region, may be under significantly more contact force from the graft than other areas of the aperture during the anterior translation test, potentially cause femoral tunnel enlargement further to the anterior side of the aperture.

6.3.3 Graft force

In this study the graft force was evaluated during flexion and under external loads at six flexion angles using a subject-specific finite element model of the knee joint. The graft force was evaluated at the mid-section of the graft as the force in the direction of the graft's long axis (Figure 63). The graft force during knee flexion at full extension 15°, 30°, 45°, 60° and 90° degrees was calculated (Figure 64). Average graft force through flexion was 60.1N with the maximum force occurred at 30° flexion (99.4N). In experiment test, the graft force during knee flexion was minimized by robotic system, the graft force measured by robot was the force cause by external forces. Differences in FE model was that the initial force applied on the graft was carried over to the result of graft force. To evaluate the increased graft force by external loads in FE model and compared with experiment test result, the value of graft forces at each flexion angles after tensioning but without extra external loads were set as baseline. And the increased graft force by external loads was calculated by subtracted the baseline forces from the resultant graft force external loads.

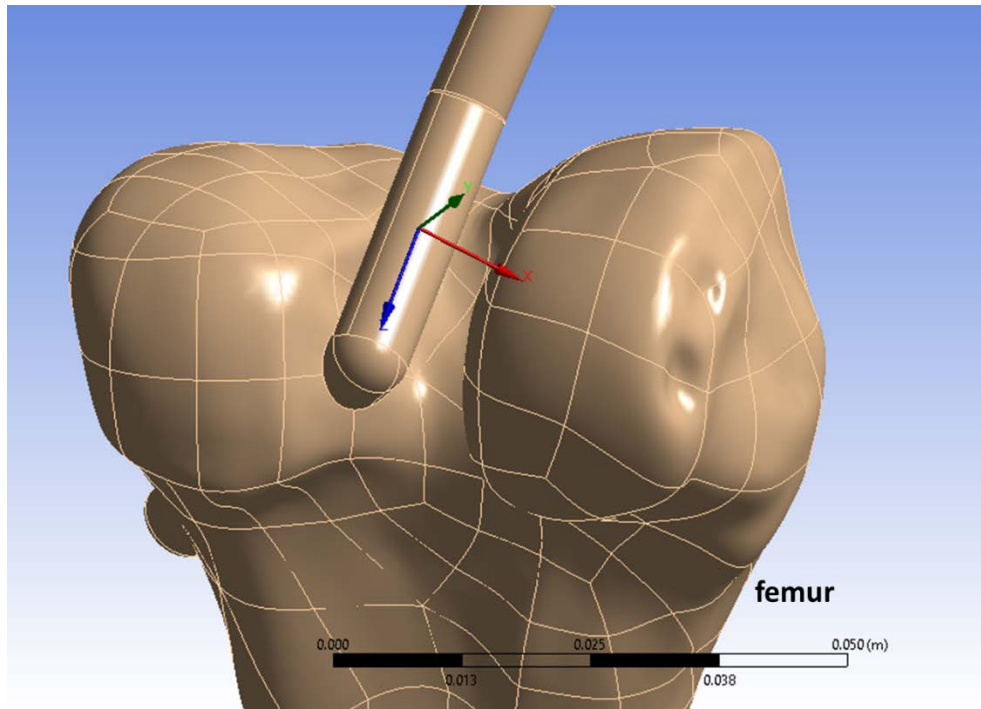


Figure 63: Coordinate at the mid-section of the graft with z axis in the direction of the graft's long axis

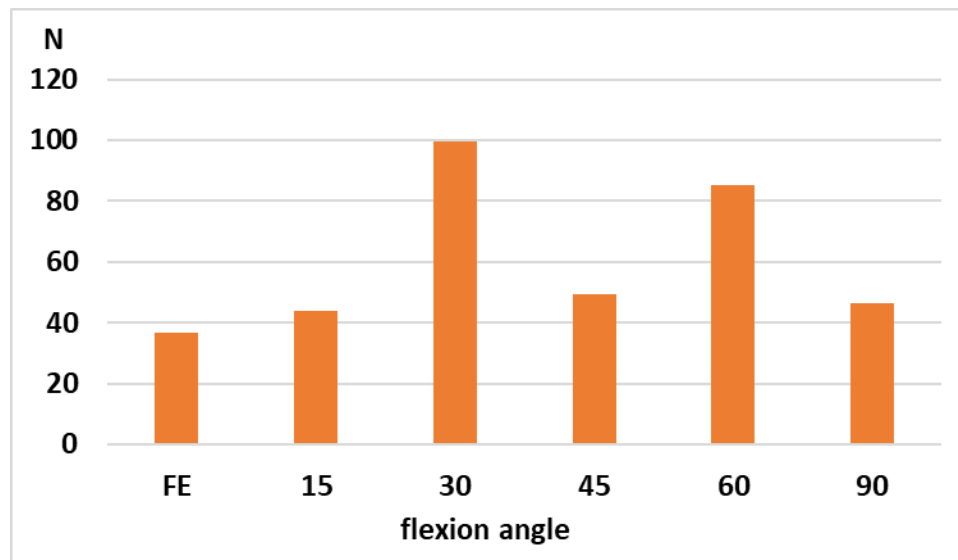


Figure 64: Graft force during passive knee flexion from full extension (FE) to 90° knee flexion.

After ACL reconstruction, the relative position of femur and tibia in response to external loads at full extension 15°, 30°, 45°, 60° and 90° degrees of flexion were recorded, including tibial translation and tibial rotation. With the experimentally obtained knee kinematics input as boundary conditions in the FEM of the ACL, the calculated forces in the graft model were 61.27N, 61.17N, 51.86N, 48.87N, 42.21N and 4.54N in response to the AT loads at full extension, 15°, 30°, 45°, 60° and 90° degrees of flexion (Figure 65). The corresponding experimental in-situ forces in the graft under the same loading conditions were 71.7N, 77.0N, 73.5N, 56.9N, 40.4N, 39.1N at full extension, 15°, 30°, 45°, 60° and 90° degrees of flexion (Figure 65). The calculated force in the graft model varied from the experimental results by $-14.8\text{N} \pm 11.4\text{ N}$.

The graft forces under PT loads, were higher than the average of experiment measurement. The graft forces were 38.9N, 43.2N, 39.1N, 35.2N, 19.0N and 12.1N at full extension, 15°, 30°, 45°, 60° and 90° degrees of flexion, while experimental measurement results were 18.2N, 11.1N, 9.5N, 8.6N, 7.1N and 7.0N at corresponding flexion angles.

With the knee model, the graft forces were calculated with 5 Nm internal/external rotational load and 7 Nm valgus at full extension, 15° and 30° degrees of flexion. The calculated force of the graft was 31.7N, 35.8N, 8.8N under internal rotation, 25.1N, 12.5N, 8.6N under external rotation and 31.5N, 31.2N, 31.6N under valgus load at full extension, 15° and 30° degrees of flexion respectively (Figure 65). The calculated graft force in FE model was 83.5%, 103.9%, 194.0% of average graft forces that measured in experimental test in response to internal rotation, external rotation and valgus load. The simulated ACL reconstructed knee in the FE model yielded a close match with the experimental result regarding to the graft force under

external loads, within the range of 95% confidence intervals of average experimental measurements, in support of the validity of the proposed FE model.

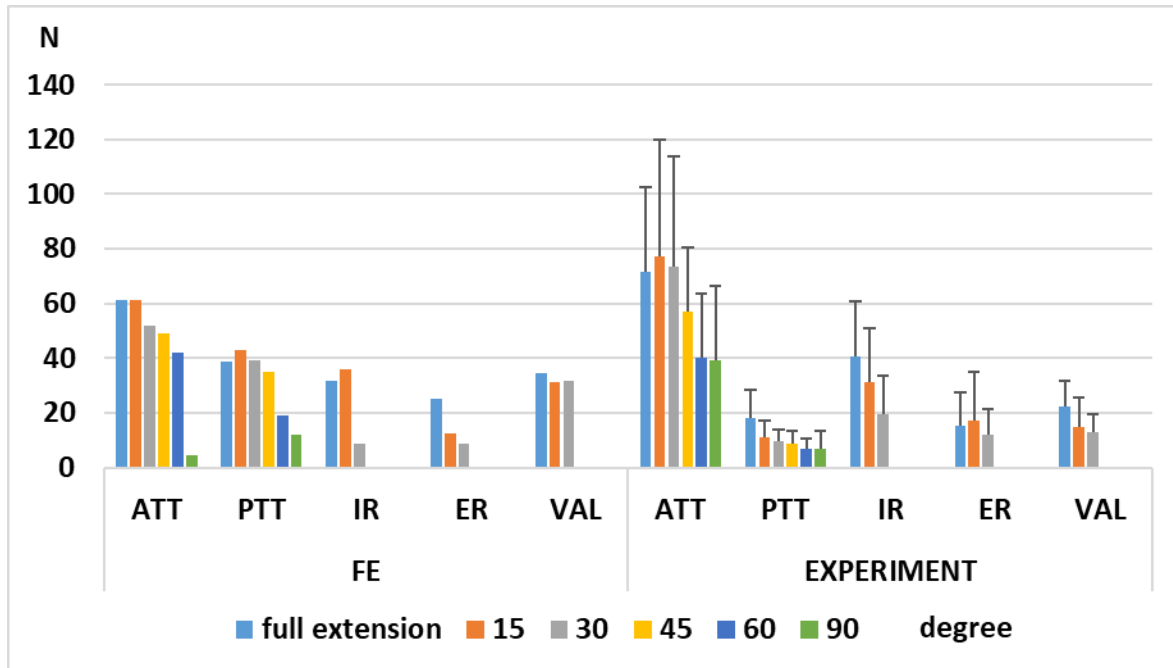


Figure 65: Graft force under external loads under different flexion angles

6.3.4 Frictional Coefficient

Different values of frictional coefficient between the bone tunnel and graft were evaluated in previous studies [12, 30]. Chizari et al. assumed that the interaction between the bone (cortical and cancellous) and graft had a friction coefficient of 0.25 [30], while Bae et al. used the value of 0.1 when using finite element modeling to analyze two techniques of ACL reconstruction [12]. Considering the roughness of the bone tunnel and the interaction between soft tissue and bone,

two different friction coefficients (0.2 and 0.8) were considered to the model. The constrained force at the end surface of graft on the femoral side and maximum von-Mises stress were compared to see the effect of frictional coefficient to the results.

The graft end constraint force result shows that with a high friction coefficient, the graft end constraint force was lower at low flexion angle and higher at high flexion angle when compared to the result of model with the lower friction coefficient (Figure 66). However, the mean graft end constraint force at the end surface of graft on the femoral side does not vary with different frictional coefficients. The maximum von Mises stress in the graft, however, increased with increasing coefficient of friction (Figure 67). The increasing von Mises stress suggests that with higher coefficient of friction, the interaction of the graft and bone tunnel could cause the tunnel enlargement or the graft to fail.

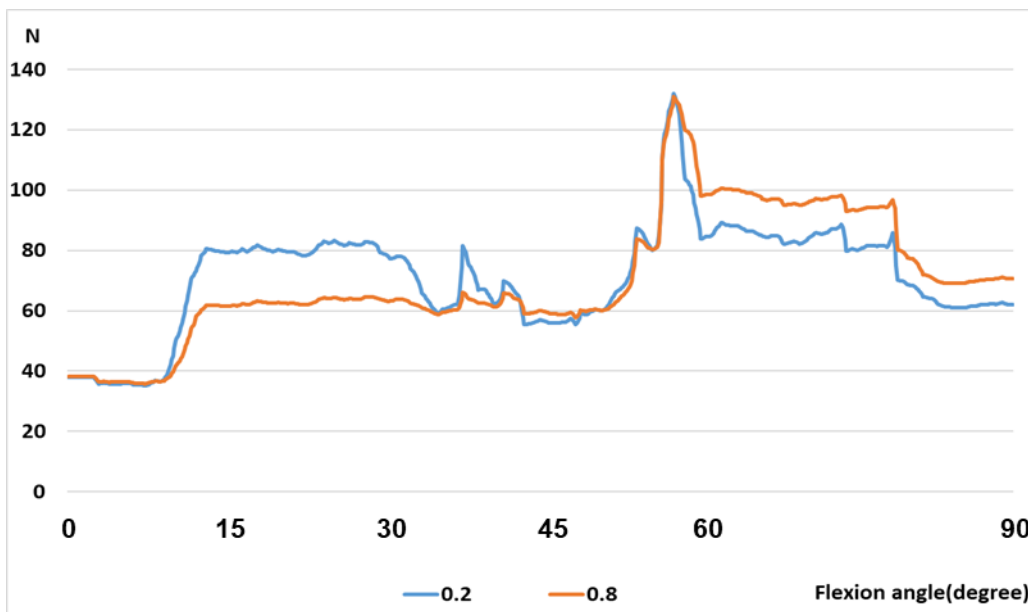


Figure 66: Graft force with two frictional coefficients (0.2 and 0.8) between graft and femoral tunnel

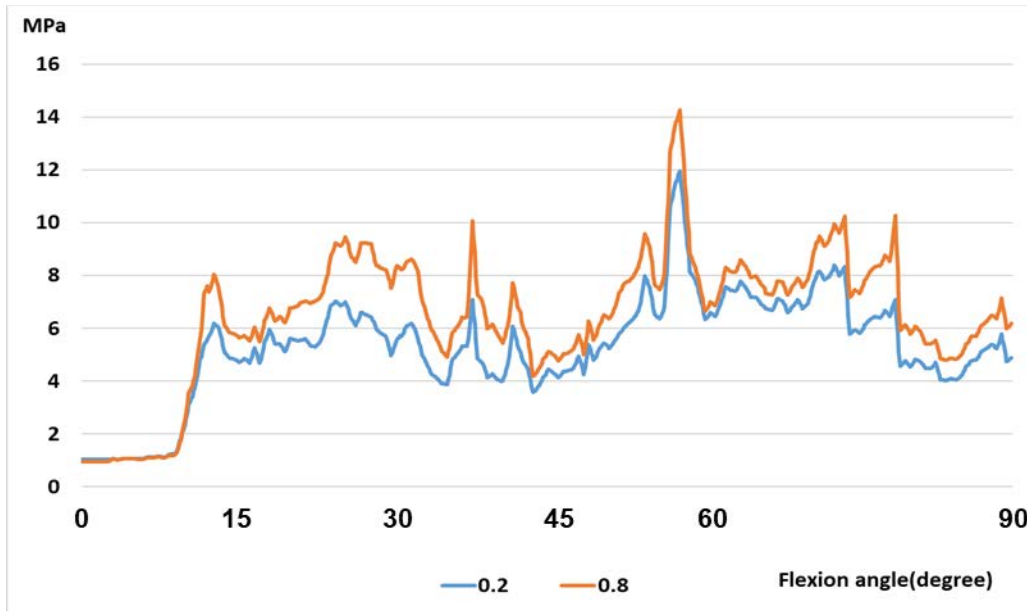


Figure 67: Maximum von-Mises stress in graft during knee flexion in the FE model with frictional coefficient 0.2 and 0.8

Figure 68 showed the maximum von-Mises stress in the ACL graft when the at 90° knee flexion. The location of maximum von-Mises stress occurred at the contact interface between graft and tunnel aperture. In the figure, we could also notice the high stress concentration at the place where graft bend to accommodate to knee flexion. The bending of the graft could also contribute to the high stress of the graft.

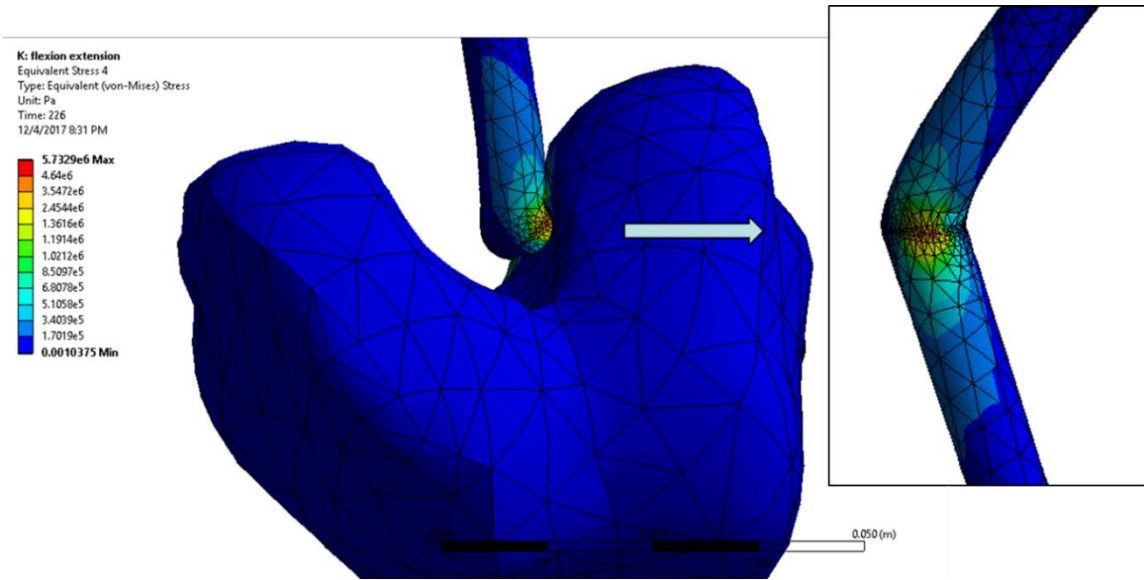


Figure 68: Location of maximum von-Mises stress in the ACL graft at 90° knee flexion

6.3.5 Mesh Sensitivity Analysis

To evaluate the effect of mesh refinement effect on the model result, the number of elements in the ACL graft was varied by changing element edge lengths. Two different sizes of elements were tested in this study, one with maximum edge lengths $2.7e-3m$ and the other one with 15% smaller edge lengths (Figure 69). The constrained force at the end surface of graft on the femoral side and the maximum von-Mises stress were compared between two models' results.

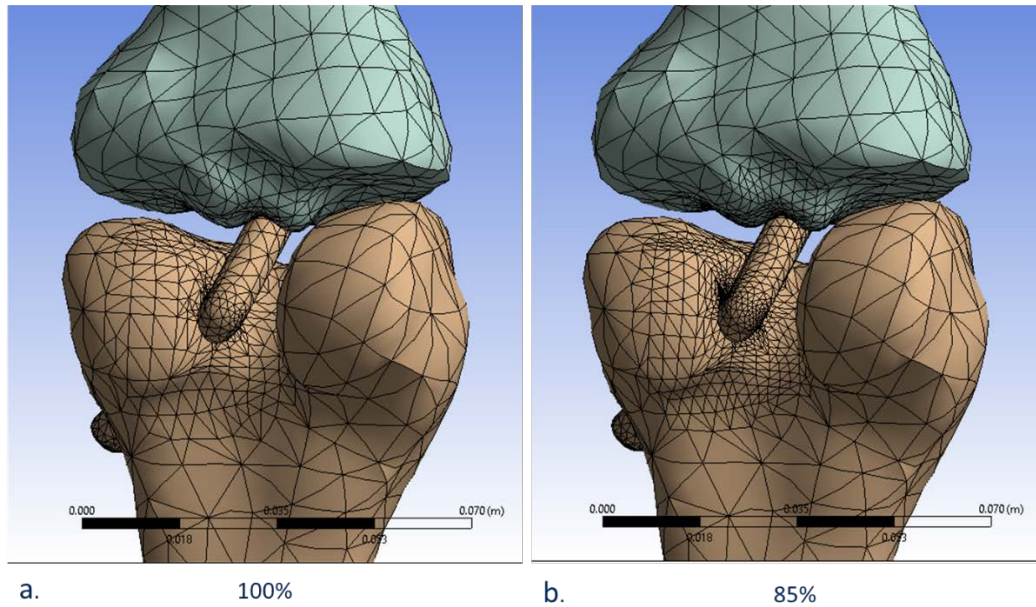


Figure 69: Two different sizes of elements were tested in this study: a) 100% (maximum edge lengths 2.7e-3m) and b) 85% edge lengths.

The mesh sensitivity analysis reveals that the magnitude of graft end constraint force has only a very minor change with finer mesh (Figure 70). The maximum relative difference is about 8% at 57° knee flexion. The difference of maximum von-Mises stress with two models are greater than those of graft end constraint force, with an average value of 4.9 MPa for refined model and 5.3 MPa for unrefined model (Figure 71). However, the average error in graft end constraint force between the two model is 0.6% and 7.3% relative difference in maximum von-Mises stress, indicating that the model result of graft force is almost unchanged by applying extra mesh refinement to the original mesh.

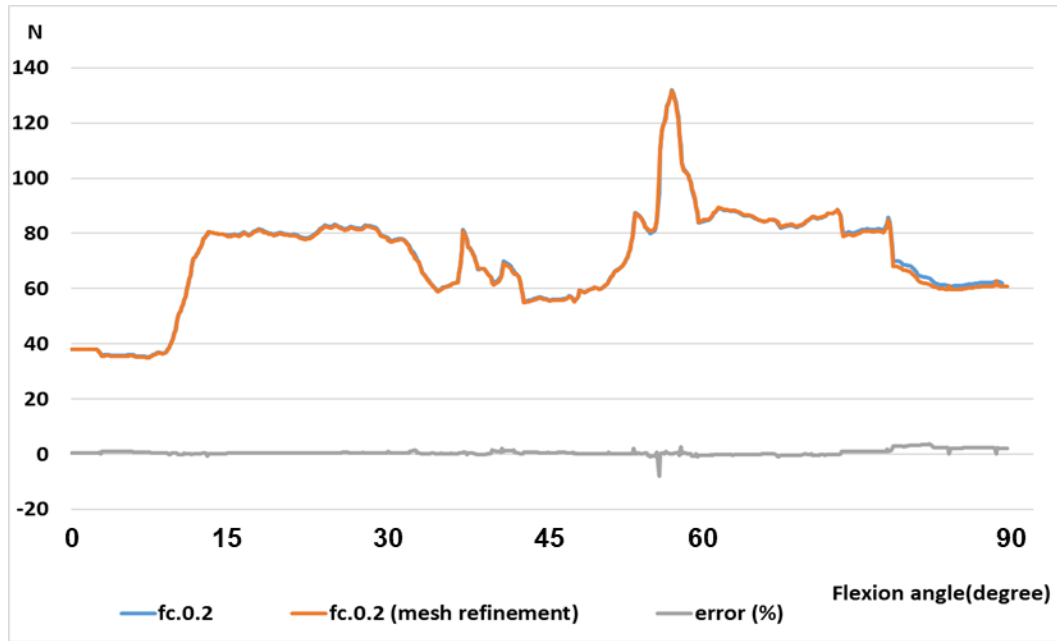


Figure 70: Graft end constraint force during knee flexion for the model and with 85% element size

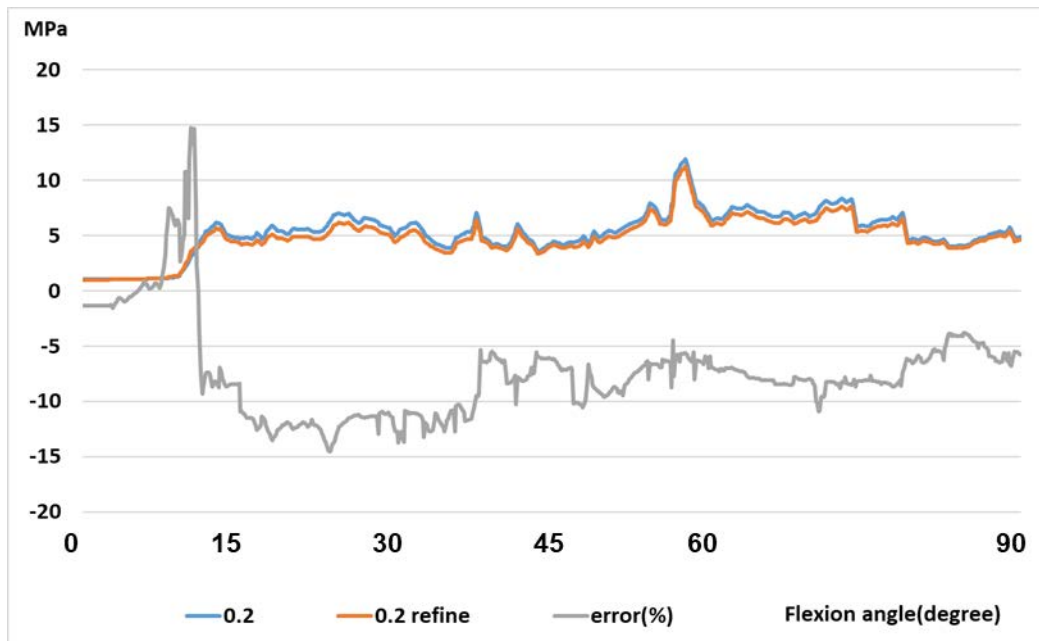


Figure 71: Maximum von-Mises stress in graft during knee flexion for the model and with 85% element size

6.3.6 Graft Initial Tension

In this study, two different initial graft tensions (40 N and 60 N) were assessed. The maximum von-Mises stress and graft end constraint force corresponding to initial graft tensions of 40 and 60 N during flexion are reported (Figure 72). The average graft end constraint force at the end surface of graft for 40 N pretension is 71.1N during flexion, and 94.8N for 60N fixation tension. With a 40N pretension, the maximum von-Mises stress was 1.0MPa at full extension without other external knee loads. While a pretension of 60 N produced high stresses in the graft, with maximum von-Mises stress 1.8MPa at full extension without other external knee loads (Figure 73). In both cases, the maximum von-Mises stress appeared in the posterior region of the femoral insertion of the graft. As flexion progressed, the maximum von-Mises stress of the graft increased up to 14.8 MPa with an initial graft tension of 60 N and 12.0 MPa with 40 N of pretension. Possibly, a small part of this high stress value is due to numerical problems associated to the excessive mesh distortion in the femoral tunnel aperture area or due to the graft under bending.

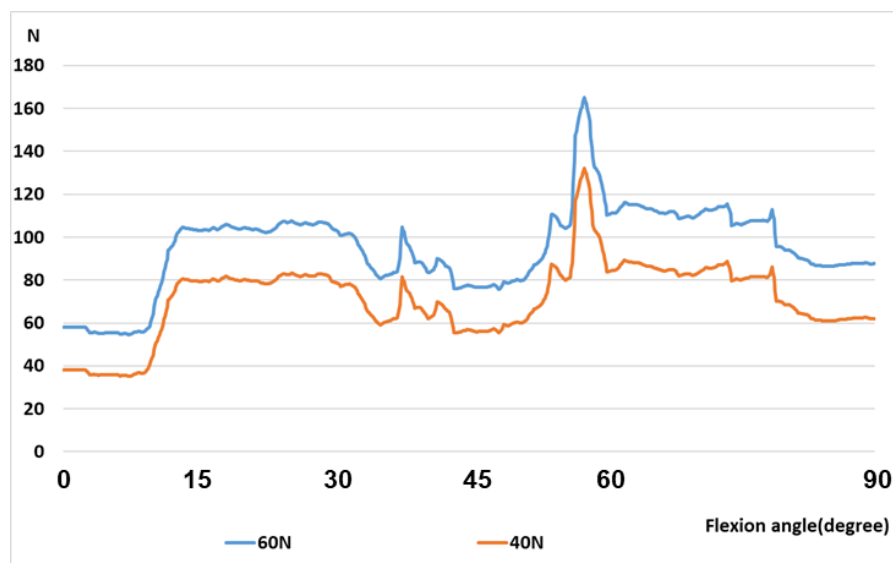


Figure 72: Graft force during flexion with 40 and 60 N initial tension

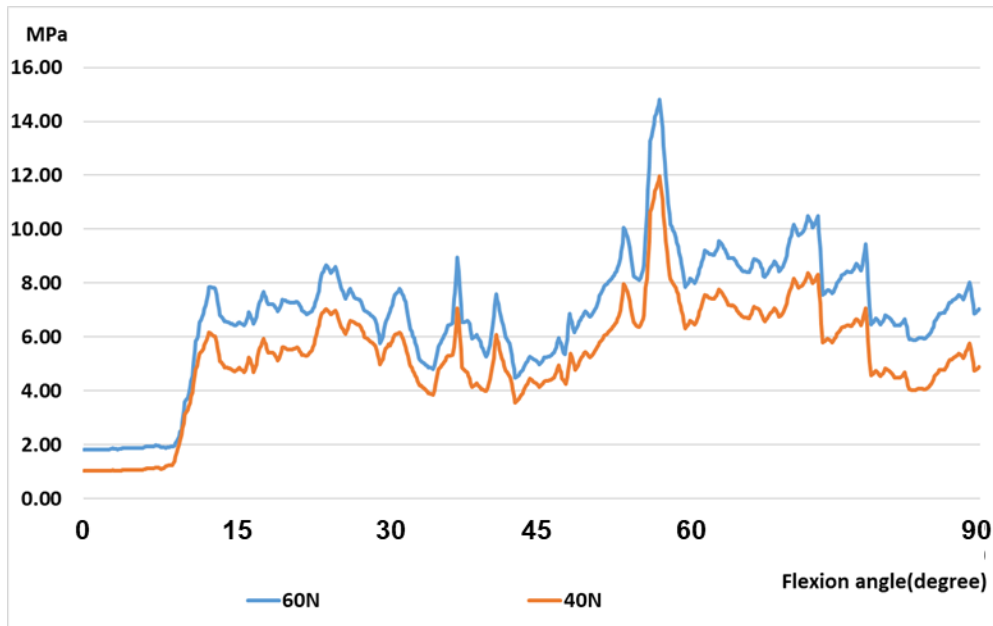


Figure 73: Maximum von-Mises stress in the graft during flexion with 40 and 60 N initial tension

In ACL reconstruction, graft is tensioned when it is fixed. In recent years, a great emphasis has been put on tension of the grafts to improve the results of the ACL[19, 56, 84, 102]. However, these are still debates about the amount of initial tension should be applied to the graft during fixation. While many clinical investigators have suggested an initial tension about 40N[19, 56], Kampen et al. performed a clinical study to analyze the influence of the graft tensioning on the knee stability of 38 ACL reconstructed patients. In their work, They compared 20 and 40 N tensioned grafts and found a graft tension of 20 N was sufficient to restore the knee kinematics and they proposed a low tension to minimize the risk of graft degradation[84].. In a finite element study, Pena et al. used 0, 20, 40 or 60N to investigate the effect of graft tensioning on the knee joint biomechanics [133]. The femur was fixed, and a 134 N anterior load was applied to the tibia, specifically at the midpoint of the transepicondylar line, allowing the tibia to move in every degree of freedom. Their results show that the ATT after reconstruction was significantly closer to that of the intact knee with 60 N of pretension. However, 60N pretension produces a

high tension in the graft during knee movement. Suggs et al. developed a 3D computational knee model to simulate ACL reconstruction to study the effect of graft initial tensioning in the knee joint kinematics [167]. They assumed the graft to be rigidly fixed to the bone at the midpoint of the length of each tunnel. Contact between the graft and the tunnel was assumed to be frictionless. A simulated 134 N anterior tibia load was applied to the midpoint of the transepicondylar line while the knee was fixed at 0°, 30°, 60° and 90° of flexion. They compared the knee kinematics after ACL reconstruction under an anterior tibial load of 134 N with 0 and 40 N of initial tension. They found over-constrained displacements under 40 N of pretension. One the contrary, in our study, the obtained graft tension results showed that a model with low graft initial tension (40N) better matches the experimental results in the aspect of graft force than model with 60N graft initial tension. Both models (40N and 60N) had a high stress between the graft and bone. This may indicate that graft damage may occur at the contact region.

6.3.7 Tunnel to Tunnel Distance

The tunnel to tunnel distance was calculated during knee flexion-extension (Figure 74). The average distance is 31.1 mm. Results show there is not a linear relationship between the distance and the flexion angle. Tunnel to tunnel distance has its minimum length at full extension (27.6 mm) and maximum length at 57° flexion (33.2 mm). Correlation coefficients between tunnel to tunnel distance and graft end constraint force at the end surface of graft as well as the maximum von-Mises stress during flexion with different sets of graft initial tension and friction coefficient were calculated (Table 11). Tunnel to tunnel distance has a strong correlation to the graft end constraint force during flexion when friction coefficient was 0.2 regardless how much initial tension applied to the graft. However, the correlation coefficient between tunnel to tunnel distance and maximum von-Mises stress was high as long as the initial tension applied to the graft was 40N. Increasing friction coefficient would decrease the correlation between the tunnel to tunnel distance and graft end constraint force. Changing initial tension has minor effect on the correlation coefficient. This suggests that the maximum von-Mises stress during knee flexion was mostly determined by the tunnel to tunnel distance, but the graft end constraint force can be affected by the friction coefficient. When the distance between femoral and tibial tunnels increases, the graft is being stretched which change the contact with the bone tunnel, thus increasing the graft force and affect the stress in the graft.

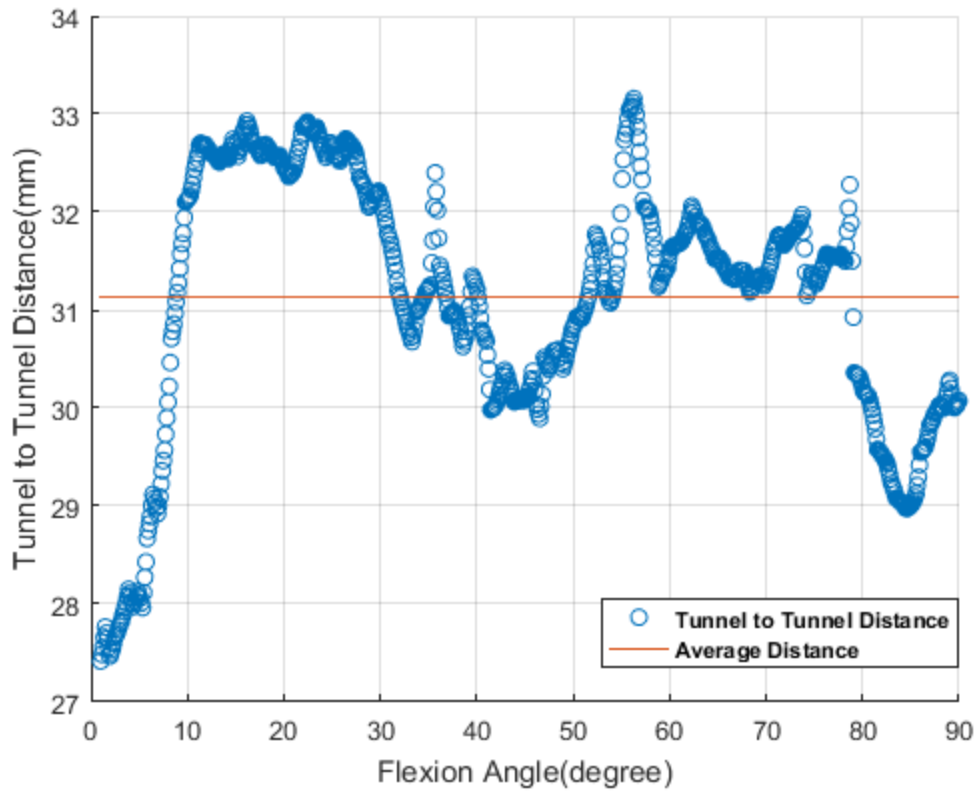


Figure 74: Calculated distance between femoral and tibial tunnel during flexion extension

Table 11: Correlation coefficient between tunnel to tunnel distance and graft end constraint force as well as the maximum von-Mises stress with different initial tension and frictional coefficient

	Tunnel to Tunnel distance
40N, $\mu=0.2$ (force)	0.64
40N, $\mu=0.2$ (Stress)	0.73
40N, $\mu=0.8$ (force)	0.33
40N, $\mu=0.8$ (Stress)	0.71
60N, $\mu=0.2$ (force)	0.60
60N, $\mu=0.2$ (Stress)	0.54

From the results of the analysis, the correlation coefficient between graft end constraint force and tunnel to tunnel distance, the graft force mainly depends on the distance between femoral and tibial tunnels. The oscillations in the graft force such as shown in Figure 72 might be explained as the result of the changing tunnel to tunnel distance. But the interaction between graft and bone, the friction of contact between graft and bone also affects the result. Previous finite element study used small values (0.1 or 0.25) for the frictional coefficient between the graft and bone[12, 30]. However, considering the roughness of the bone tunnel after drilling, a higher frictional coefficient may be more reasonable. In this study, when friction coefficient changed from 0.2 to 0.8 in the model, the average graft end constraint force during flexion decrease slightly (71.1N vs. 70.1N), and maximum graft end constraint force also had a mild change (132.1N vs. 130.9N). With 0.8 friction coefficient, the average stress of the graft increased. Changing the initial tension applied on the graft affected the maximum force in the graft but did not change the trend of increased tension during flexion. This FE model included frictional effect between the ACL graft and the bone, and also an initial tension applied to the graft. Thus, the FEM of the ACL reconstruction and the data obtained have added important new information to those reported previously in literature [74, 139].

6.4 CONCLUSION

The motivation for this study was to develop a computational knee model that could be used to examine the graft behavior and contact between graft and bone in the ACL reconstructed knee. The specific objectives of this study were to: 1) create a solid model of the human knee joint from three-dimensional CT scan, 2) determine graft position within femoral tunnel and graft force under external loads, and 3) determine the effects of graft initial tension and friction coefficient. The femur and tibia were considered to be linear elastic material and graft was modelled as hyperelastic isotropic material. Initial tension in fixing the graft was considered. This model was validated by comparing to experimental results obtained in chapter 5.

A 3-D finite element model of a human ACL was constructed based on the geometry of a 43-year-old female cadaveric knee. Kinematics data was determined experimentally from the same cadaveric knee and was applied as the boundary conditions of the model. The graft was modeled as cylinder connecting femoral and tibial tunnel. The graft was assumed to be fixed at full extension and a 40 N load was applied along the direction of the long axis of the graft model on femoral side. The graft force in the ACL was calculated when the knee was subjected to external load and flexion extension. The calculated forces of the graft under external load from full extension to 90° degrees of flexion were compared to those in situ forces in the graft obtained experimentally.

This computational analysis had three primary weaknesses: sample size (n=1); idealized graft geometry; and the use of an isotropic hyperelastic constitutive equation in the finite element model. Previous study in Chapter 5 of the graft position in the femoral tunnel shown that there are variations in the position and rotation patterns between specimens. Also in this study, a

correlation between the tunnel to tunnel distance and graft end constraint force was found in the FE model. Therefore, the graft force and position under external loads depends on the tunnel position, but location of the femoral and tibial tunnel might vary between different specimen. Also knee kinematics may change with different tunnel positions. This study used only a single validated FE model based on a single specimen. In the future, a population of finite element models could be constructed and validated to predict the variation in the population on a subject-specific basis and assess the results of this study. Furthermore, the graft geometry was assumed to have same shape as femoral and tibial tunnel and a cylinder connecting two portions. The assumption will decrease the shift of the graft at the femoral tunnel, and increase the contact force between graft and bone. In addition, the effects of fixation types were neglected to simplify the simulation model. In future work, a model with realistic geometry of the ACL graft could achieve with more accurate simulation results. Finally, the material properties of the hamstring graft were assumed to be isotropic and hyperelastic, and the viscoelastic characteristics of the graft were not considered. Soft tissues like ligament and hamstring are known to show viscoelastic behavior under tensile conditions [141]. In the context of the current study, use of an isotropic hyperelastic material might have very little effect on the change of the magnitudes of the graft force and shift. Even though a few weaknesses exist, our results are similar to previous experimental data that examined six cadaveric knees.

This study established a methodology to assess the ACL graft behavior under clinical exams using a computational model.

7.0 SUMMARY

The understanding of intact ACL and ACL graft behavior during knee motion is important to improving ACL reconstruction. The three objectives to this study were designed to develop a characterization of strains of AM and PL bundles, determine the role AM and PL bundles during knee flexion and under external loads, and identify graft position in reconstructed knee.

Chapter 4 gives the experiment setup that was developed to quantify longitudinal, transverse and shear strain behavior of intact AM and PL bundle of ACL. The DIC measurement results show that AM and PL bundles were not isometric in flexion/extension and possess different strains, the main changes being lengthening of the AM bundle and shortening of the PL bundle during flexion. The changes in strain correlated with their length changing participation in total ACL action as the knee flexed. These data could also provide insight into tunnel placement as well as fixation angle of the ACL reconstruction.

In addition to the DIC measurement, another strain measurement technique with markers and scanner was used and the results were compared to those of DIC. Features such as the strain distribution and surface geometry may not be accurate as those are measured by DIC. These markers may not capture the true AM or PL strain during knee flexion and under external loads since limited number of markers can be placed on the ACL

Chapter 5 investigated the ACL graft behavior in cadaver knee under external loads and passive flexion. The percentage of tunnel filled by graft, percentage of tunnel circumference in

contact with graft, graft-tunnel contact under load or passive flexion and graft centroid location were measured. Such an approach has not been attempted before in the analysis of ACL grafts and the results show that the graft shifts and changes contact location in the femoral tunnel under loading and flexion. When placed in a tunnel of the same diameter and tensioned, the graft initially occupies approximately 70% of the tunnel area. With AT load, the percentage of tunnel area by graft decreased, while under PT load the percentage of graft area increased slightly. These data could provide insight into normal in-vivo ACL graft behavior and function and may be useful for determining appropriate rehabilitation time. Further, having knowledge of regional graft behavior data can be useful for validation of 3D computational models which are used to predict biomechanical stresses in a finite element analysis.

Chapter 6 utilizes the bone features and tunnel position from the experiment study described in Chapter 5 to build finite element model of the experiment. A 3-D finite element model of a human ACL was constructed based on the geometry of a 43-year-old female cadaveric knee. Kinematics data was determined experimentally from the same cadaveric knee and was applied as the boundary conditions of the model. The graft was modeled as cylinder connecting femoral and tibial tunnel. It was fixed at full extension and a 40 N load was applied along the direction of the long axis of the graft model. The graft force in the ACL was calculated when the knee was subjected to external load and flexion extension. The calculated forces of the graft under external load from full extension to 90° degrees of flexion were compared to experimentally measured graft forces.

APPENDIX A

LAGRAGIAN STRAIN CALCULATION FROM LASER SCANNER WITH MATLAB

```
clear
close all

S=importdata('beadsimport.xlsx');
data1=S.data.neutral0(:,2:4);
data2=S.data.val0(:,2:4);

%% Group points

for i=1:size(data1,1)
    newdata1(i,:)=data1(size(data1,1)+1-i,:);
    newdata2(i,:)=data2(size(data2,1)+1-i,:);
end

figure(1)
scatter3(newdata1(:,1),newdata1(:,2),newdata1(:,3))
a = [1:size(data1,1)]'; b = num2str(a); c = cellstr(b);
dx = 0.01; dy = 0.01; dz=0.01; % displacement so the text does not overlay
the data points
text(newdata1(:,1)+dx, newdata1(:,2)+dy,newdata1(:,3)+dz, c(1:size(data1,1)));

figure(2)
scatter3(newdata2(:,1),newdata2(:,2),newdata2(:,3))
a = [1:size(data2,1)]'; b = num2str(a); c = cellstr(b);
dx = 0.01; dy = 0.01; dz=0.01; % displacement so the text does not overlay
the data points
text(newdata2(:,1)+dx, newdata2(:,2)+dy,newdata2(:,3)+dz, c(1:size(data1,1)));

% clear

prompt = {'Enter neutral position:node 1 label:','Enter node 2 label:','Enter
node 3 label:','Enter loaded position:node 1 label:','Enter node 2
label:','Enter node 3 label:'};
dlg_title = 'Input';
```

```

num_lines = 1;
defaultans = {'1','2','3','1','2','3'};

answer = inputdlg(prompt,dlg_title,num_lines,defaultans);

answer=str2double(answer);
neut1=newdata1(answer(1),:);
neut2=newdata1(answer(2),:);
neut3=newdata1(answer(3),:);

load1=newdata2(answer(4),:);
load2=newdata2(answer(5),:);
load3=newdata2(answer(6),:);

% Setting up local coord on neutral position
vz=cross(neut2-neut1,neut3-neut1);
cz=norm(vz);
vz=vz/cz;

vx=neut2-neut1; % longitudinal
cx=norm(vx);
vx=vx/cx;

vy=-cross(vx,vz); % transverse

V=[vx;vy;vz];

p3_local=(neut3-neut1)*V^(-1);
p2_local=(neut2-neut1)*V^(-1);
p1_local=(neut1-neut1)*V^(-1);

% Setting up local coord on deformed position
uz=cross(load2-load1,load3-load1);
cuz=norm(uz);
uz=uz/cuz;

ux=load2-load1; % longitudinal
cux=norm(ux);
ux=ux/cux;

uy=-cross(ux,uz); % transverse

U=[ux;uy;uz];
% Trans_v2u=V\U;

p3load_local=(load3-load1)*U^(-1);
p2load_local=(load2-load1)*U^(-1);
p1load_local=(load1-load1)*U^(-1);

% calculate translation

```

```

translation = p1load_local-p1_local;
p1b=p1_local;
p2b=p2load_local-translation;
p3b=p3load_local-translation;

exx=(p3load_local(1)-p3_local(1))/p3load_local(1)+...
  (((p3load_local(1)-p3_local(1))/p3load_local(1))^2+...
  ((p3load_local(2)-p3_local(2))/p3load_local(1))^2+...
  ((p3load_local(3)-p3_local(3))/p3load_local(1))^2)/2

eyy=(p3load_local(2)-p3_local(2))/p3load_local(2)+...
  (((p3load_local(1)-p3_local(1))/p3load_local(2))^2+...
  ((p3load_local(2)-p3_local(2))/p3load_local(2))^2+...
  ((p3load_local(3)-p3_local(3))/p3load_local(2))^2)/2

ezz=(p3load_local(3)-p3_local(3))/p3load_local(3)+...
  (((p3load_local(1)-p3_local(1))/p3load_local(3))^2+...
  ((p3load_local(2)-p3_local(2))/p3load_local(3))^2+...
  ((p3load_local(3)-p3_local(3))/p3load_local(3))^2)/2

exy=(p3load_local(1)-p3_local(1))/p3load_local(2)/2+...
  (p3load_local(2)-p3_local(2))/p3load_local(1)/2+...
  (((p3load_local(1)-p3_local(1))/p3load_local(1))*((p3load_local(1)-
p3_local(1))/p3load_local(2))+...
  ((p3load_local(2)-p3_local(2))/p3load_local(1))*((p3load_local(2)-
p3_local(2))/p3load_local(2))+...
  ((p3load_local(3)-p3_local(3))/p3load_local(1))*((p3load_local(3)-
p3_local(3))/p3load_local(2)))/2

exz=(p3load_local(1)-p3_local(1))/p3load_local(3)/2+...
  (p3load_local(3)-p3_local(3))/p3load_local(1)/2+...
  (((p3load_local(1)-p3_local(1))/p3load_local(1))*((p3load_local(1)-
p3_local(1))/p3load_local(3))+...
  ((p3load_local(2)-p3_local(2))/p3load_local(1))*((p3load_local(2)-
p3_local(2))/p3load_local(3))+...
  ((p3load_local(3)-p3_local(3))/p3load_local(1))*((p3load_local(3)-
p3_local(3))/p3load_local(3)))/2

eyz=(p3load_local(3)-p3_local(3))/p3load_local(2)/2+...
  (p3load_local(2)-p3_local(2))/p3load_local(3)/2+...
  (((p3load_local(1)-p3_local(1))/p3load_local(2))*((p3load_local(1)-
p3_local(1))/p3load_local(3))+...
  ((p3load_local(2)-p3_local(2))/p3load_local(2))*((p3load_local(2)-
p3_local(2))/p3load_local(3))+...
  ((p3load_local(3)-p3_local(3))/p3load_local(2))*((p3load_local(3)-
p3_local(3))/p3load_local(3)))/2

```

APPENDIX B

MATLAB CALCULATION OF DISPLACEMENT AND ROTATION OF LOCAL COORDINATE SYSTEM

```
clear
clc

Fem_sph_CT = [78.721588 98.990831 132.299244;
90.161314 70.063818 134.687513;
57.899217 86.963401 130.979839];
Tib_sph_CT = [64.1438, 89.1681, -144.5768;
85.9950, 100.6534, -142.4999;
90.9795, 76.5965, -145.5774];
Tib_sph_Faro = [64.2070 442.3012 -174.0728;
86.5045 443.1486 -156.3166;
97.4442 445.9812 -183.4876];
Fem_sph_Faro = [84.5240 170.8101 -199.5927;
100.5654 168.7417 -181.2746;
119.6874 171.8031 -205.7351];

%
% Fem_sph_CT = [58.05, 111.925, 106.702;80.556,124.261,102.329;105.845,
105.864,103.397]
% Tib_sph_CT = [65.513,108.553,-112.698;99.632,123.525, -113.727;118.178,
90.982, -113.203]
% Tib_sph_Faro = [169.527,187.026,407.587;178.407,151.062,409.772; 214.358,
155.055, 400.665]
% Fem_sph_Faro = [157.016,213.651,188.955; 161.467, 187.953, 188.505; 191.772,
179.80, 189.207]

CT_origin = Tib_sph_CT(1,1:3);
Faro_origin = Tib_sph_Faro(1,1:3);

%%----- CT DATA -----
% vector from ct origin to sphere two and three
one_two_ct = [Tib_sph_CT(2,1:3) - CT_origin];

one_three_ct = [Tib_sph_CT(3,1:3) - CT_origin];

% cross to make orthogonal vector
z_ct = cross(one_two_ct, one_three_ct);
```

```

y_ct = cross(one_three_ct, z_ct);

%%% Normalizing to make unit vectors
x_ct = one_three_ct/(norm(one_three_ct));
y_ct = y_ct/(norm(y_ct));
z_ct = z_ct/(norm(z_ct));

%%----- FARO DATA -----

one_two_d =(Tib_sph_Faro(2,1:3) - Faro_origin);
one_three_d = (Tib_sph_Faro(3,1:3) - Faro_origin);

%%% cross to make orthogonal vectors

z_faro = cross(one_two_d, one_three_d);
y_faro = cross(one_three_d, z_faro);

%%% normalizing

x_faro = one_three_d/(norm(one_three_d));
y_faro = y_faro/(norm(y_faro));
z_faro = z_faro/(norm(z_faro));

T_ltog_ct = [1,0,0,0;
             CT_origin', x_ct', y_ct', z_ct'];
T_gtol_ct = inv(T_ltog_ct);

T_ltog_faro = [1,0,0,0;
              Faro_origin', x_faro', y_faro', z_faro'];
T_gtol_faro = inv(T_ltog_faro);

data = xlsread('15VAL_data.xlsx');
% FE_data = data;
for i=1:size(data,1)
FE_data(3*i-2,:) = data(i,1:3)/1000;
FE_data(3*i-1,:) = data(i,6:8)/1000;
FE_data(3*i,:) = data(i,11:13)/1000;

data_backward(i,:)=data(size(data,1)+1-i,:);

FE_data_backward(3*i-2,:) = data_backward(i,1:3)/1000;
FE_data_backward(3*i-1,:) = data_backward(i,6:8)/1000;
FE_data_backward(3*i,:) = data_backward(i,11:13)/1000;

end

vect_fe_data = [ones(1,size(FE_data,1));FE_data.'];
vect_fe_data_ct = T_ltog_ct*T_gtol_faro*vect_fe_data;

vect_fe_data_backward = [ones(1,size(FE_data_backward,1));FE_data_backward.'];
vect_fe_data_ct_backward = T_ltog_ct*T_gtol_faro*vect_fe_data_backward;

```

```

%%%% Finding Starting Positions

vect_fem_faro = [ones(1,size(Fem_sph_Faro,1));Fem_sph_Faro.'];
vect_fem_ct = T_ltog_ct*T_gtol_faro*vect_fem_faro;

for i = 1:length(vect_fe_data_ct)
    fe_data_ct(:,i) = vect_fe_data_ct(:,length(vect_fe_data_ct)+1-i);
    fe_data_ct_backward(:,i) =
vect_fe_data_ct_backward(:,length(vect_fe_data_ct_backward)+1-i);
end

fe_data_ct_1 = fe_data_ct(:,1:3);
fe_data_ct_2 = fe_data_ct(:,7:end);

fe_data_ct_1_backward = fe_data_ct_backward(:,1:3);
fe_data_ct_2_backward = fe_data_ct_backward(:,7:end);

final_fe_data_ct = horzcat(fe_data_ct_1(2:4,:), fe_data_ct_2(2:4,:));
final_fe_data_ct_backward = horzcat(fe_data_ct_1_backward(2:4,:),
fe_data_ct_2_backward(2:4,:));

tib_COM_ct = [84.2181, 85.7059, -22.6089];
%tib_COM_ct = [88.96180,90.52223, -73.36820];
vect_tib_com_ct = [ones(1,size(tib_COM_ct,1)); tib_COM_ct.'];
tib_COM_faro = T_ltog_faro*T_gtol_ct*vect_tib_com_ct;

%%%% Calculating Center or Mass of Tibia rotation and translation %%%

fect = final_fe_data_ct;
fect_backward = final_fe_data_ct_backward;

for j = 1:length(fect);
    for i = 1:length(fect)/3
        tib_1(:,i) = fect(:,3*i - 2);
        tib_2(:,i) = fect(:,3*i -1);
        tib_3(:,i)= fect(:,3*i);

        tib_1_backward(:,i) = fect_backward(:,3*i - 2);
        tib_2_backward(:,i) = fect_backward(:,3*i -1);
        tib_3_backward(:,i)= fect_backward(:,3*i);

    end
end
COM(:,1) = [1;84.2181; 85.7059; -22.6089];

% COM(:,1) = [1;88.96180; 90.52223; -73.36820]
for i = 1:size(data,1)-2;
    origin1(:,i) = tib_1(:,i);

```

```

origin2(:,i) = tib_1(:,i+1);

one_two_1(:,i) =(tib_2(:,i) - tib_1(:,i));
one_two_2(:,i) = (tib_2(:,i+1) - tib_1(:,i+1));

one_three_1(:,i) = (tib_3(:,i) - tib_1(:,i));
one_three_2(:,i) = (tib_3(:,i+1) - tib_1(:, i+1));

z_1(:,i) = cross(one_two_1(:,i), one_three_1(:,i));
y_1(:,i) = cross(one_three_1(:,i), z_1(:,i));
x_1(:,i) = one_three_1(:,i);

z_1(:,i) = z_1(:,i)/(norm(z_1(:,i)));
y_1(:,i) = y_1(:,i)/norm(y_1(:,i));
x_1(:,i) = x_1(:,i)/norm(x_1(:,i));

z_2(:,i) = cross(one_two_2(:,i), one_three_2(:,i));
y_2(:,i) = cross(one_three_2(:,i), z_2(:,i));
x_2(:,i) = one_three_2(:,i);

z_2(:,i) = z_2(:,i)/norm(z_2(:,i));
y_2(:,i) = y_2(:,i)/norm(y_2(:,i));
x_2(:,i) = x_2(:,i)/norm(x_2(:,i));

R(:, :) = [dot(x_1(:,i),x_2(:,i)) dot(y_1(:,i),x_2(:,i))
dot(z_1(:,i),x_2(:,i));...
dot(x_1(:,i),y_2(:,i)),dot(y_1(:,i),y_2(:,i)),
dot(z_1(:,i),y_2(:,i));...
dot(x_1(:,i),z_2(:,i)),dot(y_1(:,i),z_2(:,i)),dot(z_1(:,i),z_2(:,i))];
T(:, :) = origin2(:,i) - origin1(:,i);
A(:, :) = [R(:, :), T(:, :); 0,0,0,1];
% T1(:, :)= [1,0,0,0;
% origin1(:,i), x_1(:,i), y_1(:,i), z_1(:,i)]
% T2(:, :)= [1,0,0,0;
% origin2(:,i), x_2(:,i), y_2(:,i), z_2(:,i)]
% A(:, :) = inv(T1(:, :))*(T2(:, :))
% B(:, :) = [A(2:4,2:4),A(2:4,1);0,0,0,1]
rot_data(i, :) = rxyzsolv(A);
% for j = 2:31
% COM(:,j) = T2(:, :)*inv(T1(:, :))*[COM(:,j-1)]
% end
% end

origin1_backward(:,i) = tib_1_backward(:,i);
origin2_backward(:,i) = tib_1_backward(:,i+1);

one_two_1_backward(:,i) =(tib_2_backward(:,i) - tib_1_backward(:,i));
one_two_2_backward(:,i) = (tib_2_backward(:,i+1) - tib_1_backward(:,i+1));

one_three_1_backward(:,i) = (tib_3_backward(:,i) - tib_1_backward(:,i));
one_three_2_backward(:,i) = (tib_3_backward(:,i+1) - tib_1_backward(:,
i+1));

```

```

    z_1_backward(:,i) = cross(one_two_1_backward(:,i),
one_three_1_backward(:,i));
    y_1_backward(:,i) = cross(one_three_1_backward(:,i), z_1_backward(:,i));
    x_1_backward(:,i) = one_three_1_backward(:,i);

    z_1_backward(:,i) = z_1_backward(:,i)/(norm(z_1_backward(:,i)));
    y_1_backward(:,i) = y_1_backward(:,i)/norm(y_1_backward(:,i));
    x_1_backward(:,i) = x_1_backward(:,i)/norm(x_1_backward(:,i));

    z_2_backward(:,i) = cross(one_two_2_backward(:,i),
one_three_2_backward(:,i));
    y_2_backward(:,i) = cross(one_three_2_backward(:,i), z_2_backward(:,i));
    x_2_backward(:,i) = one_three_2_backward(:,i);

    z_2_backward(:,i) = z_2_backward(:,i)/norm(z_2_backward(:,i));
    y_2_backward(:,i) = y_2_backward(:,i)/norm(y_2_backward(:,i));
    x_2_backward(:,i) = x_2_backward(:,i)/norm(x_2_backward(:,i));

    R_backward(:, :) = [dot(x_1_backward(:,i),x_2_backward(:,i))
dot(y_1_backward(:,i),x_2_backward(:,i))
dot(z_1_backward(:,i),x_2_backward(:,i));...

dot(x_1_backward(:,i),y_2_backward(:,i)),dot(y_1_backward(:,i),y_2_backward(
,i)), dot(z_1_backward(:,i),y_2_backward(:,i));...

dot(x_1_backward(:,i),z_2_backward(:,i)),dot(y_1_backward(:,i),z_2_backward(
,i)),dot(z_1_backward(:,i),z_2_backward(:,i))];
    T_backward(:, :) = origin2_backward(:,i) - origin1_backward(:,i);
    A_backward(:, :) = [R_backward(:, :), T_backward(:, :); 0,0,0,1];
%     T1(:, :) = [1,0,0,0;
%         origin1(:,i), x_1(:,i), y_1(:,i), z_1(:,i)]
%     T2(:, :) = [1,0,0,0;
%         origin2(:,i), x_2(:,i), y_2(:,i), z_2(:,i)]
%     A(:, :) = inv(T1(:, :))*((T2(:, :)))
%     B(:, :) = [A(2:4,2:4),A(2:4,1);0,0,0,1]
    rot_data_backward(i, :) = rxyzsolv(A_backward);
%     for j = 2:31
%         COM(:,j) = T2(:, :)*inv(T1(:, :))*[COM(:,j-1)]
%     end
% end

end

for i = 2:size(data,1)-2;
    Ansys_input(1, :)=rot_data(1, :);
    Ansys_input(i, :)=rot_data(i, :)+Ansys_input(i-1, :);

    Ansys_input_backward(1, :)=rot_data_backward(1, :);
    Ansys_input_backward(i, :)=rot_data_backward(i, :)+Ansys_input_backward(i-
1, :);

end

%% Final input data to Ansys remote displacement

```

```
NewInput(:,1:3)=Ansys_input(:,4:6);  
NewInput(:,4:6)=Ansys_input_backward(:,1:3);  
  
disp('Finished!')
```

BIBLIOGRAPHY

1. Adachi N, Ochi M, Uchio Y, Iwasa J, Kuriwaka M, Ito Y (2004) Reconstruction of the anterior cruciate ligament. *Bone Joint J* 86–B
2. Adouni M, Shirazi-Adl A, Shirazi R (2012) Computational biodynamics of human knee joint in gait: From muscle forces to cartilage stresses. *J Biomech* 45:2149–2156
3. Aglietti P, Zaccherotti G, Simeone AJ V., Buzzi R (1998) Anatomic versus non-anatomic tibial fixation in anterior cruciate ligament reconstruction with bone-patellar tendon-bone graft. *Knee Surgery, Sport Traumatol Arthrosc Springer-Verlag* 6:S43–S48
4. Amis AA, Dawkins GP (1991) Functional anatomy of the anterior cruciate ligament. Fibre bundle actions related to ligament replacements and injuries. *J Bone Joint Surg Br Bone and Joint Journal* 73:260–7
5. Amis AA, Jakob RP (1998) Anterior cruciate ligament graft positioning, tensioning and twisting. *Knee Surgery, Sport Traumatol Arthrosc Springer-Verlag* 6:S2–S12
6. Amis A, Dawkins G (1991) Functional anatomy of the anterior cruciate ligament. Fibre bundle actions related to ligament replacements and injuries. *J Bone Joint Surg Br* 73:260–267
7. Araujo PH, Asai S, Pinto M, Protta T, Middleton K, Linde-Rosen M, Irrgang J, Smolinski P, Fu FH (2015) ACL Graft Position Affects in Situ Graft Force Following ACL Reconstruction. *J Bone Jt Surg* 97:1767–1773
8. Arendt EA, Agel J, Dick R (1999) Anterior Cruciate Ligament Injury Patterns Among Collegiate Men and Women. *J Athl Train* 34:86–92
9. Arendt E, Dick R (1995) Knee Injury Patterns Among Men and Women in Collegiate Basketball and Soccer NCAA Data and Review of Literature. *Am J Sports Med SAGE Publications* 23:694–701
10. Au AG, Raso VJ, Liggins AB, Otto DD, Amirfazli a. (2005) A three-dimensional finite element stress analysis for tunnel placement and buttons in anterior cruciate ligament reconstructions. *J Biomech* 38:827–832

11. Bach BR, Boonos CL (2001) Anterior Cruciate Ligament Reconstruction. *AORN J* 74:151–164
12. Bach BR, Tradonsky S, Bojchuk J, Levy ME, Bush-Joseph CA, Khan NH (1998) Arthroscopically assisted anterior cruciate ligament reconstruction using patellar tendon autograft. *Am J Sports Med* 26:20
13. Bae JY, Kim G-H, Seon JK, Jeon I (2015) Finite element study on the anatomic transtibial technique for single-bundle anterior cruciate ligament reconstruction. *Med Biol Eng Comput Springer Berlin Heidelberg*
14. Ballmer PM, Jakob RP (1988) The non operative treatment of isolated complete tears of the medial collateral ligament of the knee. A prospective study. *Arch Orthop Trauma Surg* 107:273–276
15. Barber FA, McGuire DA, Johnson DH (2003) Should allografts be used for routine anterior cruciate ligament reconstructions? *Arthrosc J Arthrosc Relat Surg* 19:421–425
16. Barber FA, Spruill B, Sheluga M (2003) The effect of outlet fixation on tunnel widening. *Arthrosc J Arthrosc Relat Surg* 19:485–492
17. Barranger Y, Doumalin P, Dupré JC, Germaneau A Digital Image Correlation accuracy: influence of kind of speckle and recording setup.
18. Bendjaballah M, Shirazi-Adl A, Zukor D (1997) Finite element analysis of human knee joint in varus-valgus. *Clin Biomech Elsevier* 12:139–148
19. Beynnon BD, Fleming BC (1998) Anterior cruciate ligament strain in-vivo: A review of previous work. *J Biomech* 31:519–525
20. Beynnon BD, Johnson RJ, Fleming BC, Kannus P, Kaplan M, Samani J, Renström P (2002) Anterior cruciate ligament replacement: comparison of bone-patellar tendon-bone grafts with two-strand hamstring grafts. A prospective, randomized study. *J Bone Joint Surg Am* 84–A:1503–13
21. Beynnon BD, Uh BS, Johnson RJ, Fleming BC, Renström PA, Nichols CE (2001) The elongation behavior of the anterior cruciate ligament graft in vivo. A long-term follow-up study. *Am J Sports Med American Orthopaedic Society for Sports Medicine* 29:161–6
22. Biau DJ, Tournoux C, Katsahian S, Schranz P, Nizard R (2007) ACL Reconstruction. *Clin Orthop Relat Res PAP*
23. Boden BP, Dean GS, Feagin JA, Garrett WE (2000) Mechanisms of anterior cruciate ligament injury. *Orthopedics* 23:573–8
24. Brown TD, Ferguson AB (1980) Mechanical Property Distributions in the Cancellous Bone of the Human Proximal Femur. *Acta Orthop Scand Taylor & Francis* 51:429–437

25. Buoncristiani AM, Tjoumakaris FP, Starman JS, Ferretti M, Fu FH (2006) Anatomic Double-Bundle Anterior Cruciate Ligament Reconstruction. *Arthrosc J Arthrosc Relat Surg* 22:1000–1006
26. Butler DL (1990) Surface Stain Variation in Human Patellar tendon and Knee Cruciate Ligaments. *J Biomed Eng*
27. Butler DL, Kay MD, Stouffer DC (1986) Comparison of material properties in fascicle-bone units from human patellar tendon and knee ligaments. *J Biomech Elsevier* 19:425–432
28. Cerulli G, Benoit DL, Lamontagne M, Caraffa A, Liti A (2003) In vivo anterior cruciate ligament strain behaviour during a rapid deceleration movement: case report. *Knee Surgery, Sport Traumatol Arthrosc* 11:307–311
29. Cheung P, Chan W, Yen C, Cheng S, Woo S, Wong T, Wong W (2010) Femoral tunnel widening after quadrupled hamstring anterior cruciate ligament reconstruction. *J Orthop Surg (Hong Kong)* 18:198–202
30. Chhabra A, Starman JS, Ferretti M, Vidal AF, Zantop T, Fu FH (2006) Anatomic, Radiographic, Biomechanical, and Kinematic Evaluation of the Anterior Cruciate Ligament and Its Two Functional Bundles. *J Bone Jt Surg* 88
31. Chizari M, Wang B, Snow M, Barrett M (2008) Experimental and numerical analysis of screw fixation in anterior cruciate ligament reconstruction. *AIP Conf Proc* 1045:61–70
32. Choi SH, Ha JK, Jun DJ, Seo JG, Park JH (2017) Additional post-tie for unstable femoral suspensory fixation during anterior cruciate ligament reconstruction using TightRope® RT : clinical reports on 3 cases. *Arthrosc Orthop Sport Med* 4:34–38
33. Ciarelli MJ, Goldstein SA, Kuhn JL, Cody DD, Brown MB (1991) Evaluation of orthogonal mechanical properties and density of human trabecular bone from the major metaphyseal regions with materials testing and computed tomography. *J Orthop Res Wiley Subscription Services, Inc., A Wiley Company* 9:674–682
34. Claes S, Vereecke E, Maes M, Victor J, Verdonk P, Bellemans J (2013) Anatomy of the anterolateral ligament of the knee. *J Anat* 223:321–328
35. Clancy WG, Nelson DA, Reider B, Narechania RG (1982) Anterior cruciate ligament reconstruction using one-third of the patellar ligament, augmented by extra-articular tendon transfers. *J Bone Jt Surg* 64
36. Clatworthy MG, Annear P, Bulow J-U, Bartlett RJ (1999) Tunnel widening in anterior cruciate ligament reconstruction: a prospective evaluation of hamstring and patella tendon grafts. *Knee Surgery, Sport Traumatol Arthrosc Springer-Verlag* 7:138–145
37. Cohen SB, Fu FH (2007) Three-portal technique for anterior cruciate ligament reconstruction: use of a central medial portal. *Arthroscopy* 23:325.e1-5

38. Comninou M, Yannas IV (1976) Dependence of stress-strain nonlinearity of connective tissues on the geometry of collagen fibres. *J Biomech* 9:427–433
39. Crammond G, Boyd SW, Dulieu-Barton JM (2013) Speckle pattern quality assessment for digital image correlation. *Opt Lasers Eng* 51:1368–1378
40. Crawford C, Kainer M, Jernigan D, Banerjee S, Friedman C, Ahmed F, Archibald LK (2005) Investigation of postoperative allograft-associated infections in patients who underwent musculoskeletal allograft implantation. *Clin Infect Dis* 41:195–200
41. Dargel J, Gotter M, Mader K, Pennig D, Koebke J, Schmidt-Wiethoff R (2007) Biomechanics of the anterior cruciate ligament and implications for surgical reconstruction. *Strategies Trauma Limb Reconstr* 2:1–12
42. Debandi A, Maeyama A, Lu S, Hume C, Asai S, Goto B, Hoshino Y, Smolinski P, Fu FH (2011) Biomechanical comparison of three anatomic ACL reconstructions in a porcine model. *Knee Surgery, Sport Traumatol Arthrosc* 19:728–735
43. Delfico AJ, Garrett WE, Warren R, al. et (1998) Mechanisms of injury of the anterior cruciate ligament in soccer players. *Clin Sports Med Mosby, St. Louis* 17:779–85, vii
44. Dhaher YY, Kwon T-H, Barry M (2010) The effect of connective tissue material uncertainties on knee joint mechanics under isolated loading conditions. *J Biomech* 43:3118–3125
45. Duthon VB, Barea C, Abrassart S, Fasel JH, Fritschy D, Ménétrey J (2006) Anatomy of the anterior cruciate ligament. *Knee Surgery, Sport Traumatol Arthrosc Springer-Verlag* 14:204–213
46. Edwards A, Bull AMJ, Amis AA (2007) The attachments of the anteromedial and posterolateral fibre bundles of the anterior cruciate ligament. *Knee Surgery, Sport Traumatol Arthrosc Springer-Verlag* 15:1414–1421
47. Edwards A, Bull AMJ, Amis AA (2008) The attachments of the anteromedial and posterolateral fibre bundles of the anterior cruciate ligament. *Knee Surgery, Sport Traumatol Arthrosc Springer-Verlag* 16:29–36
48. Ellis BJ (2012) FINITE ELEMENT MODELING OF KNEE AND SHOULDER LIGAMENTS by The University of Utah May 2012 Copyright © Benjamin James Ellis 2012 All Rights Reserved.
49. Ellis BJ, Lujan TJ, Dalton MS, Weiss JA (2006) Medial collateral ligament insertion site and contact forces in the ACL-deficient knee. *J Orthop Res* 24:800–810
50. Fahey M, Indelicato PA (1994) Bone Tunnel Enlargement After Anterior Cruciate Ligament Replacement. *Am J Sports Med* 22:410–414

51. Fahey M, Indelicato PA (1994) Bone Tunnel Enlargement After Anterior Cruciate Ligament Replacement. *Am J Sports Med* SAGE Publications 22:410–414
52. Feagin JAJ, Curl WW (1996) Isolated tear of the anterior cruciate ligament: 5-year followup study. *Clin Orthop Relat Res* 4–9
53. Feller JA, Cooper R, Webster KE (2002) Current Australian trends in rehabilitation following anterior cruciate ligament reconstruction. *Knee* 9:121–126
54. Ferretti A, Papandrea P, Conteduca F, Mariani PP Knee ligament injuries in volleyball players.
55. Fischer KJ, Manson TT, Pfaeffle HJ, Tomaino MM, Woo .-Y (2001) A method for measuring joint kinematics designed for accurate registration of kinematic data to models constructed from CT data. *J Biomech* 34:377–383
56. Fithian DC, Paxton EW, Stone M Lou, Luetzow WF, Csintalan RP, Phelan D, Daniel DM (2005) Prospective Trial of a Treatment Algorithm for the Management of the Anterior Cruciate Ligament-Injured Knee. *Am J Sports Med* 33:335–346
57. Fleming B, Beynnon B, Howe J, McLeod W, Pope M (1992) Effect of tension and placement of a prosthetic anterior cruciate ligament on the anteroposterior laxity of the knee. *J Orthop Res* 10:177–186
58. Franck C, Hong S, Maskarinec SA, Tirrell DA, Ravichandran G (2007) Three-dimensional Full-field Measurements of Large Deformations in Soft Materials Using Confocal Microscopy and Digital Volume Correlation. *Exp Mech* Kluwer Academic Publishers-Plenum Publishers 47:427–438
59. Freedman KB, D’Amato MJ, Nedeff DD, Kaz A, Bach BR (2016) Arthroscopic Anterior Cruciate Ligament Reconstruction: A Metaanalysis Comparing Patellar Tendon and Hamstring Tendon Autografts. <http://dx.doi.org/101177/03635465030310011501> SAGE PublicationsSage CA: Los Angeles, CA
60. Fu FH, Bennett CH, Lattermann C, Ma CB (1999) Current trends in anterior cruciate ligament reconstruction. Part 1: Biology and biomechanics of reconstruction. *Am J Sports Med* American Orthopaedic Society for Sports Medicine 27:821–30
61. Fu FH, Bennett CH, Ma CB, Menetrey J, Lattermann C (2000) Current trends in anterior cruciate ligament reconstruction. Part II. Operative procedures and clinical correlations. *Am J Sports Med* American Orthopaedic Society for Sports Medicine 28:124–30
62. Fujii M, Sasaki Y, Araki D, Furumatsu T, Miyazawa S, Ozaki T, Linde-Rosen M, Smolinski P, Fu FH (2016) Evaluation of the semitendinosus tendon graft shift in the bone tunnel: an experimental study. *Knee Surgery, Sport Traumatol Arthrosc* 24:2773–2777
63. Gardiner JC, Weiss JA (2003) Subject-specific finite element analysis of the human medial collateral ligament during valgus knee loading. *J Orthop Res* 21:1098–1106

64. Gasser TC, Ogden RW, Holzapfel GA (2006) Hyperelastic modelling of arterial layers with distributed collagen fibre orientations. *J R Soc Interface The Royal Society* 3:15–35
65. Gifstad T, Drogset JO, Grøntvedt T, Hortemo GS (2014) Femoral fixation of hamstring tendon grafts in ACL reconstructions: the 2-year follow-up results of a prospective randomized controlled study. *Knee Surgery, Sport Traumatol Arthrosc Springer Berlin Heidelberg* 22:2153–2162
66. Girgis, Fakhry G. M.D., PhD.; Marshall, John L. D.V.M., M.D.; MONA JEM ARSAMD (1975) *The Cruciate Ligaments of the Knee Joint: Anatomical. Functi... : Clinical Orthopaedics and Related Research. Clin Orthop Relat Res* 106:216–231
67. Gundiah N, Ratcliffe MB, Pruitt LA (2007) Determination of strain energy function for arterial elastin: Experiments using histology and mechanical tests. *J Biomech* 40:586–594
68. Hamada M, Shino K, Horibe S, Mitsuoka T, Miyama T, Shiozaki Y, Mae T (2001) Single- versus bi-socket anterior cruciate ligament reconstruction using autogenous multiple-stranded hamstring tendons with EndoButton femoral fixation: A prospective study. *Arthroscopy* 17:801–807
69. HAMNER DL, BROWN CH, STEINER ME, HECKER AT, HAYES WC (1999) Hamstring Tendon Grafts for Reconstruction of the Anterior Cruciate Ligament: Biomechanical Evaluation of the Use of Multiple Strands and Tensioning Techniques*. *J Bone Jt Surg* 81
70. Harner CD, Hyun Baek G, Vogrin TM, Carlin GJ, Kashiwaguchi S, L-Y Woo S Quantitative Analysis of Human Cruciate Ligament Insertions.
71. Haut Donahue TL, Hull ML, Rashid MM, Jacobs CR, Donahue TLH, Hull ML, Rashid MM, Jacobs CR (2002) A Finite Element Model of the Human Knee Joint for the Study of Tibio-Femoral Contact. *J Biomech Eng* 124:273
72. Hefzy MS, Grood ES, Noyes FR (1989) Factors affecting the region of most isometric femoral attachments. Part II: The anterior cruciate ligament. *Am J Sports Med* 17:208–216
73. Herbort M, Tecklenburg K, Zantop T, Raschke MJ, Hoser C, Schulze M, Petersen W, Fink C (2013) Single-bundle anterior cruciate ligament reconstruction: a biomechanical cadaveric study of a rectangular quadriceps and bone--patellar tendon--bone graft configuration versus a round hamstring graft. *Arthroscopy* 29:1981–90
74. Hess T, Duchow J, Roland S, Kohn D (2002) Single-versus two-incision technique in anterior cruciate ligament replacement: influence on postoperative muscle function. *Am J Sports Med American Orthopaedic Society for Sports Medicine* 30:27–31
75. Hirokawa S, Tsuruno R (2000) Three-dimensional deformation and stress distribution in an analytical/computational model of the anterior cruciate ligament. *J Biomech* 33:1069–1077

76. Höher J, Möller HD, Fu FH (1998) Bone tunnel enlargement after anterior cruciate ligament reconstruction: fact or fiction? *Knee Surgery, Sport Traumatol Arthrosc* 6:231–240
77. Hollis J, Takai S, Adams D, Horibe S, Woo S (1991) The effects of knee motion and external loading on the length of the anterior cruciate ligament (ACL): a kinematic study. *J Biomech Eng* 113:208–14
78. Holzapfel GA, Gasser TC, Ogden RW (2000) A New Constitutive Framework for Arterial Wall Mechanics and a Comparative Study of Material Models. *J Elast Kluwer Academic Publishers* 61:1–48
79. Hootman JM, Dick R, Agel J (2007) Epidemiology of collegiate injuries for 15 sports: summary and recommendations for injury prevention initiatives. *J Athl Train* 42:311–9
80. Iorio R, Di Sanzo V, Vadalà A, Conteduca J, Mazza D, Redler A, Bolle G, Conteduca F, Ferretti A (2013) ACL reconstruction with hamstrings: How different technique and fixation devices influence bone tunnel enlargement. *Eur Rev Med Pharmacol Sci* 17:2956–2961
81. Iorio R, Vadalà A, Argento G, Di Sanzo V, Ferretti A (2007) Bone tunnel enlargement after ACL reconstruction using autologous hamstring tendons: a CT study. *Int Orthop* 31:49–55
82. Jagodzinski M, Foerstemann T, Mall G, Krettek C, Bosch U, Paessler HH (2005) Analysis of forces of ACL reconstructions at the tunnel entrance: is tunnel enlargement a biomechanical problem? *J Biomech* 38:23–31
83. Jansson KA, Harilainen A, Sandelin J, Karjalainen PT, Aronen HJ, Tallroth K (1999) Bone tunnel enlargement after anterior cruciate ligament reconstruction with the hamstring autograft and endobutton fixation technique. *Knee Surgery, Sport Traumatol Arthrosc Springer-Verlag* 7:290–295
84. Jørgensen U, Thomsen HS (2000) Behavior of the graft within the bone tunnels following anterior cruciate ligament reconstruction, studied by cinematic magnetic resonance imaging. *Knee Surgery, Sport Traumatol Arthrosc Springer-Verlag* 8:32–35
85. van Kampen A (1998) The effect of different graft tensioning in anterior cruciate ligament reconstruction: A prospective randomized study. *Arthrosc J Arthrosc Relat Surg W.B. Saunders* 14:845–850
86. Kato N, Koshino T, Saito T, Takeuchi R (1998) Estimation of Young's modulus in swine cortical bone using quantitative computed tomography. *Bull Hosp Jt Dis* 57:183–6
87. Kato Y, Ingham SJM, Kramer S, Smolinski P, Saito A, Fu FH (2009) Effect of tunnel position for anatomic single-bundle ACL reconstruction on knee biomechanics in a porcine model. *Knee Surgery, Sport Traumatol Arthrosc* 18:2–10

88. Kato Y, Maeyama A, Lertwanich P, Wang JH, Ingham SJM, Kramer S, Martins CQA, Smolinski P, Fu FH (2013) Biomechanical comparison of different graft positions for single-bundle anterior cruciate ligament reconstruction. *Knee Surg Sports Traumatol Arthrosc* 21:816–23
89. Kawaguchi Y, Kondo E, Takeda R, Akita K, Yasuda K, Amis A a. (2015) The Role of Fibers in the Femoral Attachment of the Anterior Cruciate Ligament in Resisting Tibial Displacement. *Arthrosc J Arthrosc Relat Surg The Authors* 31:435–444
90. Keklikci K, Yapici C, Kim D, Linde-Rosen M, Smolinski P, Fu FH (2013) The effect of notchplasty in anterior cruciate ligament reconstruction: a biomechanical study in the porcine knee. *Knee Surg Sports Traumatol Arthrosc* 21:1915–21
91. Keyak JH, Meagher JM, Skinner HB, Mote CD (1990) Automated three-dimensional finite element modelling of bone: a new method. *J Biomed Eng Elsevier* 12:389–397
92. Kiapour A, Kiapour AM, Kaul V, Quatman CE, Wordeman SC, Hewett TE, Demetropoulos CK, Goel VK (2013) Finite Element Model of the Knee for Investigation of Injury Mechanisms: Development and Validation. *J Biomech Eng* 136:11002
93. Kiapour AM (2013) Non-Contact ACL Injuries during Landing: Risk Factors and Mechanisms. *Vasa* 312
94. Kiapour AM, Kaul V, Kiapour A, Quatman CE, Wordeman SC, Hewett TE, Demetropoulos CK, Goel VK (2014) The Effect of Ligament Modeling Technique on Knee Joint Kinematics: A Finite Element Study. *Appl Math* 4:91–97
95. Kim HY, Seo YJ, Kim HJ, Nguyenn T, Shetty NS, Yoo YS (2011) Tension changes within the bundles of anatomic double-bundle anterior cruciate ligament reconstruction at different knee flexion angles: A study using a 3-dimensional finite element model. *Arthrosc - J Arthrosc Relat Surg* 27:1400–1408
96. Krosshaug T, Bahr R (2005) A model-based image-matching technique for three-dimensional reconstruction of human motion from uncalibrated video sequences. *J Biomech* 38:919–929
97. Kühne JH, Dürr HR, Steinborn M, Jansson V, Refior HJ (1998) Magnetic resonance imaging and knee stability following ACL reconstruction. *Orthopedics* 21:39–43
98. Kweon C, Lederman ES, Chhabra A (2013) Anatomy and Biomechanics of the Cruciate Ligaments and Their Surgical Implications. *Mult Ligament Inj Knee Springer New York, New York, NY*, pp 17–27
99. L-Y Woo S, Wu C, Dede O, Vercillo F, Noorani S Biomechanics and anterior cruciate ligament reconstruction.

100. L. Markolf K, Hame S, Monte Hunter D, A. Oakes D, Zoric B, Gause P, A.M. Finerman G (2002) Effects of femoral tunnel placement on knee laxity and forces in an anterior cruciate ligament graft. *J Orthop Res* 20:1016–1024
101. L’Insalata JC, Klatt B, Fu FH, Harner CD (1997) Tunnel expansion following anterior cruciate ligament reconstruction: a comparison of hamstring and patellar tendon autografts. *Knee Surg Sports Traumatol Arthrosc* 5:234–8
102. Lecompte D, Smits A, Bossuyt S, Sol H, Vantomme J, Van Hemelrijck D, Habraken AM (2006) Quality assessment of speckle patterns for digital image correlation. *Opt Lasers Eng* 44:1132–1145
103. Lee BH oon, Seo DY eon, Bansal S, Kim JH o, Ahn JH wan, Wang JH o (2016) Comparative Magnetic Resonance Imaging Study of Cross-Sectional Area of Anatomic Double Bundle Anterior Cruciate Ligament Reconstruction Grafts and the Contralateral Uninjured Knee. *Arthroscopy* 32:321–329
104. Lewis JL, Lew WD, Hill JA, Hanley P, Ohland K, Kirstukas S, Hunter RE (1989) Knee joint motion and ligament forces before and after ACL reconstruction. *J Biomech Eng* 111:97–106
105. Li G, Gil J, Kanamori A, Woo SL (1999) A validated three-dimensional computational model of a human knee joint. *J Biomech Eng* 121:657–662
106. Li G, Suggs J, Gill T (2002) The Effect of Anterior Cruciate Ligament Injury on Knee Joint Function under a Simulated Muscle Load: A Three-Dimensional Computational Simulation. *Ann Biomed Eng Kluwer Academic Publishers-Plenum Publishers* 30:713–720
107. Limbert G, Taylor M, Middleton J (2004) Three-dimensional finite element modelling of the human ACL: simulation of passive knee flexion with a stressed and stress-free ACL. *J Biomech Elsevier* 37:1723–31
108. Lionello G, Cristofolini L (2014) A practical approach to optimizing the preparation of speckle patterns for digital-image correlation. *Meas Sci Technol IOP Publishing* 25:107001
109. Loh JC, Fukuda Y, Tsuda E, Steadman RJ, Fu FH, Woo SL-Y (2003) Knee stability and graft function following anterior cruciate ligament reconstruction: Comparison between 11 o’clock and 10 o’clock femoral tunnel placement. *Arthrosc J Arthrosc Relat Surg* 19:297–304
110. Lu H, Cary PD (2000) Deformation measurements by digital image correlation: Implementation of a second-order displacement gradient. *Exp Mech* 40:393–400
111. Luyckx T, Verstraete M, De Roo K, Van Der Straeten C, Victor J (2016) High strains near femoral insertion site of the superficial medial collateral ligament of the Knee can explain the clinical failure pattern. *J Orthop Res* 34:2016–2024

112. Mae T, Shino K, Miyama T, Shinjo H, Ochi T, Yoshikawa H, Fujie H (2001) Single-versus two-femoral socket anterior cruciate ligament reconstruction technique: Biomechanical analysis using a robotic simulator. *Arthroscopy* 17:708–16
113. Mark Melhorn J, Henning CE The relationship of the femoral attachment site to the isometric tracking of the anterior cruciate ligament graft.
114. Markatos K, Kaseta MK, Lалos SN, Korres DS, Efstathopoulos N (2013) The anatomy of the ACL and its importance in ACL reconstruction. *Eur J Orthop Surg Traumatol Springer Paris* 23:747–752
115. Martens M, Van Audekercke R, De Meester P, Mulier JC (1981) The geometrical properties of human femur and tibia and their importance for the mechanical behaviour of these bone structures. *Arch Orthop Trauma Surg Springer-Verlag* 98:113–120
116. Melby A, Noble JS, Askew MJ, Boom AA, Hurst FW (1991) The effects of graft tensioning on the laxity and kinematics of the anterior cruciate ligament reconstructed knee. *Arthrosc J Arthrosc Relat Surg W.B. Saunders* 7:257–266
117. Middleton KK, Hamilton T, Irrgang JJ, Karlsson J, Harner CD, Fu FH (2014) Anatomic anterior cruciate ligament (ACL) reconstruction: a global perspective. Part 1. *Knee Surgery, Sport Traumatol Arthrosc Springer Berlin Heidelberg* 22:1467–1482
118. Moglo KE, Shirazi-Adl A (2003) On the coupling between anterior and posterior cruciate ligaments, and knee joint response under anterior femoral drawer in flexion: A finite element study. *Clin Biomech* 18:751–759
119. Muneta T, Sekiya I, Yagishita K, Ogiuchi T, Yamamoto H, Shinomiya K (1999) Two-Bundle Reconstruction of the Anterior Cruciate Ligament Using Semitendinosus Tendon With Endobuttons: Operative Technique and Preliminary Results. *Arthrosc J Arthrosc Relat Surg* 15:618–624
120. Musahl V, Burkart A, Debski RE, Van Scyoc A, Fu FH, Woo SL-Y (2003) Anterior cruciate ligament tunnel placement: Comparison of insertion site anatomy with the guidelines of a computer-assisted surgical system. *Arthrosc J Arthrosc Relat Surg* 19:154–160
121. Natsu-ume T, Shino K, Nakata K, Nakamura N, Toritsuka Y, Mae T (2001) Endoscopic reconstruction of the anterior cruciate ligament with quadrupled hamstring tendons. A correlation between MRI changes and restored stability of the knee. *J Bone Joint Surg Br Bone and Joint Journal* 83:834–7
122. Nawabi DH, Orth F, Imhauser C, Tucker SM, Wickiewicz T, Pearle AD ACL Fibers Inserting on the Lateral Intercondylar Ridge Carry the Greatest Loads - Are Modern Anatomic Femoral Tunnel Positions Too Low ?

123. Nebelung W, Becker R, Merkel M, Röpke M Bone Tunnel Enlargement After Anterior Cruciate Ligament Reconstruction With Semitendinosus Tendon Using Endobutton Fixation on the Femoral Side.
124. Nishimoto K, Kuroda R, Mizuno K, Hoshino Y, Nagamune K, Kubo S, Yagi M, Yamaguchi M, Yoshiya S, Kurosaka M (2009) Analysis of the graft bending angle at the femoral tunnel aperture in anatomic double bundle anterior cruciate ligament reconstruction: a comparison of the transtibial and the far anteromedial portal technique. *Knee Surgery, Sport Traumatol Arthrosc Springer-Verlag* 17:270–276
125. Noyes FR, Grood ES, Butler DL, Malek M (1980) Clinical laxity tests and functional stability of the knee: biomechanical concepts. *Clin Orthop Relat Res* 84–89
126. Nyland J, Caborn DN, Rothbauer J, Kocabey Y, Couch J (2003) Two-year outcomes following ACL reconstruction with allograft tibialis anterior tendons: a retrospective study. *Knee Surg Sport Traumatol Arthrosc* 11:212–218
127. Odensten M, Gillquist J (1985) Functional anatomy of the anterior cruciate ligament and a rationale for reconstruction. *J Bone Jt Surg* 67
128. Odensten M, Gillquist J (1986) A modified technique for anterior cruciate ligament (ACL) surgery using a new drill guide for isometric positioning of the ACL. *Clin Orthop Relat Res* 154–8
129. Odensten M, Hamberg P, Nordin M, Lysholm J, Gillquist J (1985) Surgical or conservative treatment of the acutely torn anterior cruciate ligament. A randomized study with short-term follow-up observations. *Clin Orthop Relat Res* 87–93
130. Onodera J, Yasuda K, Masuda T, Tanabe Y, Kitamura N, Yagi T, Kondo E (2017) Is the Grafted Tendon Shifted Anteriorly in the Femoral Tunnel at the Postremodeling Phase After Anterior Cruciate Ligament Reconstruction? A Clinical MRI Study. *Orthop J Sport Med* 5:232596711771112
131. Palanca M, Tozzi G, Cristofolini L (2015) The use of digital image correlation in the biomechanical area: a review. *Int Biomech Taylor & Francis* 3:1–21
132. Pan B, Li K (2011) A fast digital image correlation method for deformation measurement. *Opt Lasers Eng Elsevier* 49:841–847
133. Pan B, Xie H, Wang Z, Qian K, Wang Z (2000) Study on subset size selection in digital image correlation for speckle patterns. *Top Appl Phys Opt EXPRESS Springer Springer* 16
134. Park H-S, Ahn C, Fung DT, Ren Y, Zhang L-Q (2010) A knee-specific finite element analysis of the human anterior cruciate ligament impingement against the femoral intercondylar notch. *J Biomech Elsevier* 43:2039–2042

135. Peña E, Calvo B, Martínez M a., Doblaré M (2006) A three-dimensional finite element analysis of the combined behavior of ligaments and menisci in the healthy human knee joint. *J Biomech* 39:1686–1701
136. Peña E, Martínez M a., Calvo B, Palanca D, Doblaré M (2005) A finite element simulation of the effect of graft stiffness and graft tensioning in ACL reconstruction. *Clin Biomech* 20:636–644
137. Peña E, Martinez MA, Calvo B, Doblaré M (2006) On the numerical treatment of initial strains in biological soft tissues. *Int J Numer Methods Eng* 68:836–860
138. Penner DA, Daniel DM, Wood P An in vitro study of anterior cruciate ligament graft placement and isometry.
139. Petersen W, Zantop T (2007) Anatomy of the Anterior Cruciate Ligament with Regard to Its Two Bundles. *Clin Orthop Relat Res* 454:35–47
140. Petersen W, Zantop T (2006) Partial Rupture of the Anterior Cruciate Ligament. *Arthrosc. J. Arthrosc. Relat. Surg.*
141. Phatak NS, Sun Q, Kim SE, Parker DL, Kent Sanders R, Veress AI, Ellis BJ, Weiss J a. (2007) Noninvasive determination of ligament strain with deformable image registration. *Ann Biomed Eng* 35:1175–1187
142. Pioletti D, Rakotomanana L (1998) Finite Element Model of the Human Anterior Cruciate Ligament. ... *Biomech Biomed Eng*
143. Pioletti DP (1997) Viscoelastic properties of soft tissues.
144. Pioletti DP, Rakotomanana LR, Benvenuti J-F, Leyvraz P-F (1998) Viscoelastic constitutive law in large deformations: application to human knee ligaments and tendons. *J. Biomech.*
145. Race A, Amis AA (1994) The mechanical properties of the two bundles of the human posterior cruciate ligament. *J Biomech* 27:13–24
146. Radford WJ, Amis AA, Kempson SA, Stead AC, Camburn M (1994) A comparative study of single- and double-bundle ACL reconstructions in sheep. *Knee Surg Sports Traumatol Arthrosc* 2:94–9
147. Rahnama-Azar AA, Sabzevari S, Irrarázaval S, Chao T, Fu FH (2016) CURRENT CONCEPTS REVIEW Anatomical Individualized ACL Reconstruction. *Arch Bone Jt Surg* 4:291–291
148. Ramaniraka NA, Saunier P, Siegrist O, Pioletti DP (2007) Biomechanical evaluation of intra-articular and extra-articular procedures in anterior cruciate ligament reconstruction: A finite element analysis. *Clin Biomech* 22:336–343

149. Ramaniraka NA, Terrier A, Theumann N, Siegrist O (2005) Effects of the posterior cruciate ligament reconstruction on the biomechanics of the knee joint: A finite element analysis. *Clin Biomech* 20:434–442
150. Rangger C, Daniel DM, Stone ML, Kaufman K (1993) Diagnosis of an ACL disruption with KT-1000 arthrometer measurements. *Knee Surg Sport Traumatol Arthrosc* 1:60–66
151. Ren Y, Ahn C, Park HS, Fung DT, Zhang L-Q (2010) Testing for Material Properties of the Human Anterior Cruciate Ligament. *American Soc Biomechanics*
152. Renström P, Arms SW, Stanwyck TS, Johnson RJ, Pope MH (1986) Strain within the anterior cruciate ligament during hamstring and quadriceps activity*. *Am J Sports Med* SAGE Publications 14:83–87
153. Robi K, Jakob N, Matevz K, Matjaz V (2013) *The Physiology of Sports Injuries and Repair Processes. Curr Issues Sport Exerc Med InTech*
154. Ruff CB, Hayes WC (1982) Subperiosteal Expansion and Cortical Remodeling of the Human Femur and Tibia with Aging Subperiosteal Expansion and Cortical Remodeling of the Human Femur and Tibia with Aging. *Repl int Ser* 3:945–948
155. Sakane M, Fox RJ, Woo SLY, Livesay GA, Li G, Fu FH (1997) In situ forces in the anterior cruciate ligament and its bundles in response to anterior tibial loads. *J Orthop Res* 15:285–293
156. Sapega AA, Moyer RA, Schneck C, Komalahiranya N (1990) Testing for isometry during reconstruction of the anterior cruciate ligament. Anatomical and biomechanical considerations. *J Bone Joint Surg Am* 72:259–67
157. Sasaki Y, Chang S-S, Fujii M, Araki D, Zhu J, Marshall B, Linde-Rosen M, Smolinski P, Fu FH (2016) Effect of fixation angle and graft tension in double-bundle anterior cruciate ligament reconstruction on knee biomechanics. *Knee Surgery, Sport Traumatol Arthrosc* 24:2892–2898
158. Schiavone Panni A, Denti M, Franzese S, Monteleone M (1993) The bone-ligament junction: a comparison between biological and artificial ACL reconstruction. *Knee Surg Sports Traumatol Arthrosc* 1:9–12
159. Schmidt T, Tyson J, Galanulis K (2003) Full Field Dynamic Displacement and Strain Measurement Using Advanced 3D Image Correlation Photometry : Part I. *Exp Tech* 47–50
160. Schreier H, Orteu J-J, Sutton MA (2009) *Image Correlation for Shape, Motion and Deformation Measurements. Springer US, Boston, MA*
161. Screen HRC, Bader DL, Lee DA, Shelton JC (2004) Local strain measurement within tendon. *Strain* 40:157–163

162. Segawa H, Koga Y, Omori G, Sakamoto M, Hara T (2003) Influence of the femoral tunnel location and angle on the contact pressure in the femoral tunnel in anterior cruciate ligament reconstruction. *Am J Sports Med* 31:444–448
163. Shelbourne KD, Klootwyk TE, Wilckens JH, De Carlo MS (1995) Ligament stability two to six years after anterior cruciate ligament reconstruction with autogenous patellar tendon graft and participation in accelerated rehabilitation program. *Am J Sports Med American Orthopaedic Society for Sports Medicine* 23:575–9
164. Shi D, Wang D, Wang C, Liu A (2012) A novel, inexpensive and easy to use tendon clamp for in vitro biomechanical testing. *Med Eng Phys Institute of Physics and Engineering in Medicine* 34:516–520
165. Siegel L, Vandenakker-Albanese C, Siegel D (2012) Anterior Cruciate Ligament Injuries. *Clin J Sport Med* 22:349–355
166. Silva A, Sampaio R, Pinto E (2010) Femoral tunnel enlargement after anatomic ACL reconstruction: a biological problem? *Knee Surgery, Sport Traumatol Arthrosc* 18:1189–1194
167. Simon D, Mascarenhas R, Saltzman BM, Rollins M, Bach BR, MacDonald P (2015) The Relationship between Anterior Cruciate Ligament Injury and Osteoarthritis of the Knee. *Adv Orthop Hindawi Publishing Corporation* 2015:928301
168. Smith BA, Livesay GA, Woo SL (1993) Biology and biomechanics of the anterior cruciate ligament. *Clin Sports Med* 12:637–70
169. Song Y, Debski RE, Musahl V, Thomas M, Woo SLY (2004) A three-dimensional finite element model of the human anterior cruciate ligament: A computational analysis with experimental validation. *J Biomech* 37:383–390
170. Steckel H, Vadala G, Davis D, Fu FH (2006) 2D and 3D 3-tesla magnetic resonance imaging of the double bundle structure in anterior cruciate ligament anatomy. *Knee Surgery, Sport Traumatol Arthrosc Springer-Verlag* 14:1151–1158
171. Suggs J, Wang C, Li G (2003) The effect of graft stiffness on knee joint biomechanics after ACL reconstruction - A 3D computational simulation. *Clin Biomech* 18:35–43
172. Suzuki T, Shino K, Otsubo H, Suzuki D, Mae T, Fujimiya M, Yamashita T, Fujie H (2014) Biomechanical comparison between the rectangular-tunnel and the round-tunnel anterior cruciate ligament reconstruction procedures with a bone-patellar tendon-bone graft. *Arthroscopy* 30:1294–1302
173. Tsuda E, Fukuda Y, Loh JC, Debski RE, Fu FH, L-Y Woo S The Effect of Soft-Tissue Graft Fixation in Anterior Cruciate Ligament Reconstruction on Graft-Tunnel Motion Under Anterior Tibial Loading.

174. Veronda DR, Westmann RA (1970) Mechanical characterization of skin—Finite deformations. *J Biomech Elsevier* 3:111–124
175. Victor J, Bellemans J, Witvrouw E, Govaers K, Fabry G (1997) Graft selection in anterior cruciate ligament reconstruction—prospective analysis of patellar tendon autografts compared with allografts. *Int Orthop Springer* 21:93–7
176. Webster KE, Feller JA, Hameister KA (2001) Bone tunnel enlargement following anterior cruciate ligament reconstruction: a randomised comparison of hamstring and patellar tendon grafts with 2-year follow-up. *Knee Surg, Sport Traumatol, Arthrosc* 9:86–91
177. Weiss JA, Maker BN, Govindjee S (1996) Finite element implementation of incompressible, transversely isotropic hyperelasticity. *Comput Methods Appl Mech Eng* 135:107–128
178. Westermann RW, Wolf BR, Elkins JM (2013) Effect of ACL reconstruction graft size on simulated Lachman testing: a finite element analysis. *Iowa Orthop J* 33:70–7
179. Wilson TC, Kantaras A, Atay A, Johnson DL (2004) Tunnel Enlargement after Anterior Cruciate Ligament Surgery. *Am J Sports Med* 32:543–549
180. Woo SL-Y, Kanamori A, Zeminski J, Yagi M, Papageorgiou C, Fu FH (2002) The Effectiveness of Reconstruction of the Anterior Cruciate Ligament with Hamstrings and Patellar Tendon. *J Bone Jt Surg Am* 84 A:907–914
181. Woo SL, Hollis JM, Adams DJ, Lyon RM, Takai S (1991) Tensile properties of the human femur-anterior cruciate ligament-tibia complex. The effects of specimen age and orientation. *Am J Sports Med American Orthopaedic Society for Sports Medicine* 19:217–25
182. Wren T a, Yerby S a, Beaupré GS, Carter DR (2001) Mechanical properties of the human achilles tendon. *Clin Biomech (Bristol, Avon)* 16:245–251
183. Wu C, Noorani S, Vercillo F, Woo SL-Y (2009) Tension patterns of the anteromedial and posterolateral grafts in a double-bundle anterior cruciate ligament reconstruction. *J Orthop Res Wiley Subscription Services, Inc., A Wiley Company* 27:879–884
184. Xie F, Yang L, Guo L, Wang Z, Dai G (2009) A study on construction three-dimensional nonlinear finite element model and stress distribution analysis of anterior cruciate ligament. *J Biomech Eng* 131:121007
185. Xu Y, Md Y, Liu J, Md Z, Kramer S, Martins C, Kato Y, Linde-Rosen M, Smolinski P, Fu FH Comparison of In Situ Forces and Knee Kinematics in Anteromedial and High Anteromedial Bundle Augmentation for Partially Ruptured Anterior Cruciate Ligament.
186. Yagi M, Wong EK, Kanamori A, Debski RE, Fu FH, Woo SL-Y (2002) Biomechanical analysis of an anatomic anterior cruciate ligament reconstruction. *Am J Sports Med American Orthopaedic Society for Sports Medicine* 30:660–6

187. Yasuda K, Kondo E, Ichiyama H, Kitamura N, Tanabe Y, Tohyama H, Minami A (2004) Anatomic reconstruction of the anteromedial and posterolateral bundles of the anterior cruciate ligament using hamstring tendon grafts. *Arthrosc J Arthrosc Relat Surg* 20:1015–1025
188. Yeni YN, Brown CU, Wang Z, Norman TL (1997) The influence of bone morphology on fracture toughness of the human femur and tibia. *Bone* 21:453–459
189. Yoshiya S, Andrish JT, Manley MT, Bauer TW (1987) Graft tension in anterior cruciate ligament reconstruction. An in vivo study in dogs. *Am J Sports Med American Orthopaedic Society for Sports Medicine* 15:464–70
190. Zantop T, Herbort M, Raschke MJ, Fu FH, Petersen W (2007) The role of the anteromedial and posterolateral bundles of the anterior cruciate ligament in anterior tibial translation and internal rotation. *Am J Sports Med* 35:223–227
191. Zantop T, Petersen W, Sekiya JK, Musahl V, Fu FH (2006) Anterior cruciate ligament anatomy and function relating to anatomical reconstruction. *Knee Surgery, Sport Traumatol Arthrosc Springer-Verlag* 14:982–992
192. Zavras TD, Race A, Bull AMJ, Amis AA (2001) A comparative study of 'isometric' points for anterior cruciate ligament graft attachment. *Knee Surgery, Sport Traumatol Arthrosc Springer-Verlag* 9:28–33
193. Zhang X, Jiang G, Wu C, Woo SL-Y (2008) A subject-specific finite element model of the anterior cruciate ligament. *Conf Proc IEEE Eng Med Biol Soc* 2008:891–894
194. Zhou Y, Pan B, Chen YQ (2012) Large deformation measurement using digital image correlation: a fully automated approach. *Appl Opt Optical Society of America* 51:7674
195. Ziegler CG, Pietrini SD, Westerhaus BD, Anderson CJ, Wijdicks CA, Johansen S, Engebretsen L, LaPrade RF Arthroscopically Pertinent Landmarks for Tunnel Positioning in Single-Bundle and Double-Bundle Anterior Cruciate Ligament Reconstructions.
196. Zysset PK, Guo XE, Hofer CE, Moore KE, Goldstein SA (1999) Elastic modulus and hardness of cortical and trabecular bone lamellae measured by nanoindentation in the human femur. *J Biomech* 32:1005–1012